

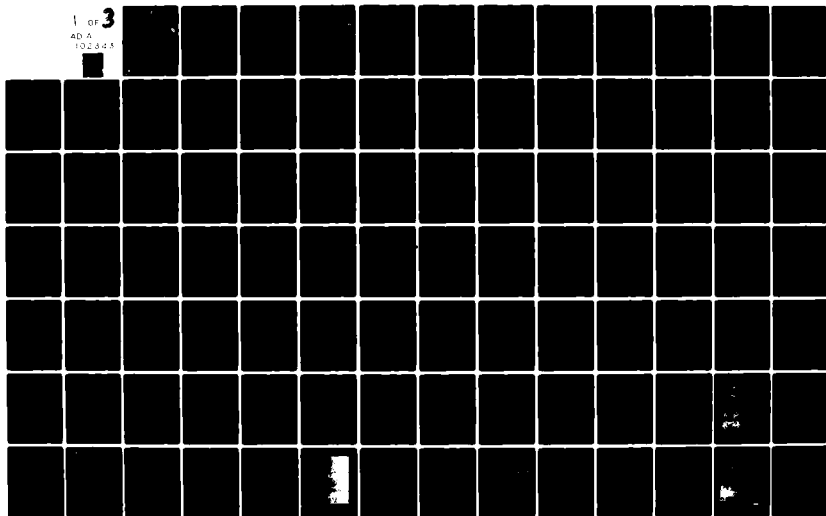
AD-A102 343

DEFENSE MAPPING AGENCY HYDROGRAPHIC/ TOPOGRAPHIC CENT--ETC F/G 8/10
INTERPRETATION OF HYDROGRAPHIC FEATURES SEEN IN THE WATERS OFF --ETC(U)
MAY 81 C L REED

UNCLASSIFIED

NL

1 OF 3
AD-A
102 343



LEVEL

(12)

AD A102343

INTERPRETATION OF HYDROGRAPHIC FEATURES
IN THE WATERS OFF CAPE COD

by
Charles Leonard Reed

DTIC
ELECTED
AUG 3 1981
C

A thesis submitted in partial fulfillment
of the requirements for the degree of
Master of Science
(Remote Sensing)

May 1981

Committee:

Professor Charles E. Olson, Jr., Chairman
Fabian C. Polcyn

DISTRIBUTION STATEMENT A

Approved for public release;
Distribution Unlimited

81 8 03 003

2345

DTIC FILE COPY

REPORT DOCUMENTATION PAGE		READ INSTRUCTIONS BEFORE COMPLETING FORM
1. REPORT NUMBER	2. GOVT ACCESSION NO.	3. RECIPIENT'S CATALOG NUMBER
	AD-A202 343	
4. TITLE (and Subtitle)	5. TYPE OF REPORT & PERIOD COVERED	
Interpretation of Hydrographic Features Seen in the Waters Off Cape Cod	Final repts Technical thesis May 1981	
6. PERFORMING ORG. REPORT NUMBER	8. CONTRACT OR GRANT NUMBER(s)	
7. AUTHOR(s)	10. PROGRAM ELEMENT, PROJECT, TASK AREA & WORK UNIT NUMBERS	
Charles Leonard/Reed	13) 211	
9. PERFORMING ORGANIZATION NAME AND ADDRESS	11. CONTROLLING OFFICE NAME AND ADDRESS	
DMAHTC 6500 Brookes Lane Washington, DC 20315	Defense Mapping Agency Building 56, US Naval Observatory Washington, DC 20305	
14. MONITORING AGENCY NAME & ADDRESS (if different from Controlling Office)	12. REPORT DATE	
N/A	May 1981	
	13. NUMBER OF PAGES	
	137	
	15. SECURITY CLASS. (of this report)	
	UNCLASSIFIED	
	15a. DECLASSIFICATION/DOWNGRADING SCHEDULE	
16. DISTRIBUTION STATEMENT (of this Report)		
Open publication		
17. DISTRIBUTION STATEMENT (of the abstract entered in Block 20, if different from Report)		
N/A		
18. SUPPLEMENTARY NOTES		
N/A		
19. KEY WORDS (Continue on reverse side if necessary and identify by block number)		
Remote Sensing Reflectance LANDSAT Multi Sensoral Hydrography Spectral		
20. ABSTRACT (Continue on reverse side if necessary and identify by block number)		
A study was conducted to determine the origin of features appearing in a Landsat image (1724-14472; 17 July 1974) of the waters off Cape Cod by multi-temporal and multispectral analysis techniques. Acquisition of ancillary data supplemented imagery from five different sensors, including visible, near infrared, and microwave, representing fifteen discrete times over a five-year period. Digital data for the Landsat image was evaluated multispectrally. Various water reflectance models were applied to the digital data to determine		

UNCLASSIFIED

SECURITY CLASSIFICATION OF THIS PAGE(When Data Entered)

Continued from block 20.

✓ whether features related to reflected light from the ocean bottom, turbidity, or surface reflectance. Parameters were estimated from historical data. Results of model calculations were compared with the observed radiances at several locations in the scene. Multitemporal analysis affirmed that the following detailed information can be determined from space imagery: Rapid rates of coastal change, possible uncharted shoals, and theorized surface manifestations of internal waves. In all cases multisensor imagery increased the reliability of the derived information. Multispectral analysis provided additional evidence for attributing variations of reflectance in deep ocean to the effects of surface reflection and also appears to be the primary cause of reflectivity of patterns over the shoal areas around Nantucket Island. ↗

UNCLASSIFIED

SECURITY CLASSIFICATION OF THIS PAGE(When Data Entered)

1
2
3
4
5
6
7
8
9
10
11
12
13
14
15
16
17
18
19
20
21
22
23
24
25
26
27
28
29
30
31
32
33
34
35
36
37
38
39
40
41
42
43
44
45
46
47
48
49
50
51
52
53
54
55
56
57
58
59
60
61
62
63
64
65
66
67
68
69
70
71
72
73
74
75
76
77
78
79
80
81
82
83
84
85
86
87
88
89
90
91
92
93
94
95
96
97
98
99
100

INTERPRETATION OF HYDROGRAPHIC FEATURES
IN THE WATERS OFF CAPE COD

by
Charles Leonard Reed

A thesis submitted in partial fulfillment
of the requirements for the degree of
Master of Science
(Remote Sensing)

May 1981

Committee:

Professor Charles E. Olson, Jr., Chairman
Fabian C. Polcyn

DISTRIBUTION STATEMENT A

Approved for public release;
Distribution Unlimited

ABSTRACT

A study was conducted to determine the origin of features appearing in a Landsat image (1724-14472; 17 July 1974) of the waters off Cape Cod by multitemporal and multispectral analysis techniques. Acquisition of ancillary data supplemented imagery from five different sensors, including visible, near infrared, and microwave, representing fifteen discrete times over a five-year period. Digital data for the Landsat image was evaluated multispectrally. Various water reflectance models were applied to the digital data to determine whether the features related to reflected light from the ocean bottom, turbidity, or surface reflectance. Parameters were estimated from historical data. Results of model calculations were compared with the observed radiances at several locations in the scene. Multitemporal analysis affirmed that the following detailed information can be determined from space imagery: Rapid rates of coastal change, possible uncharted shoals, and theorized surface manifestations of internal waves. In all cases multisensor imagery increased the reliability of the derived information. Multispectral analysis provided additional evidence for attributing variations of reflectance in deep ocean to the effects of surface reflection and also appears to be the primary cause of reflectivity of patterns over the shoal areas around Nantucket Island.

Accession For	<input checked="" type="checkbox"/>	<input type="checkbox"/>	<input type="checkbox"/>
DTIC 63-41			
DTIC 1-5			
Unannounced			
Justification			
by			
Distribution/			
Availability Codes			
Avail and/or			
Special			

A

DEDICATION

This study is lovingly dedicated to my wife, Judy, and daughter, Lisa, for their patience, understanding, and encouragement.

ACKNOWLEDGEMENTS

My thanks go to all those who helped make this study possible: James C. Hammack, of the Acquisition Systems Division, Defense Mapping Agency Hydrographic/Topographic Center, who brought the image in question to my attention. The Environmental Research Institute of Michigan, for the use of their equipment, computer software, and photo lab service. Keith A. Francis, fellow student, for excerpts from a joint paper for a class project. Dr. Gwynn H. Suits, Professor of Remote Sensing at the University of Michigan, for assistance in the use of the Bendix DK-2A Spectroreflectometer at the Environmental Research Institute of Michigan. Dr. David R. Lyzenga, of the Environmental Research Institute of Michigan, for technical advice throughout the study. Dr. Richard S. Williams, Jr., Research Geologist, U.S. Geological Survey, for comments and editing of the manuscript. Ms. Nancy Moon and Ms. Sandy Lawson for typing the manuscript. Dr. Charles E. Olson, Jr., and Fabian C. Polcyn, for aid and guidance in both this study and my graduate program.

TABLE OF CONTENTS

	PAGE
TITLE PAGE	
ABSTRACT	
DEDICATION	ii.
ACKNOWLEDGEMENTS	iii
TABLE OF CONTENTS	iv
LIST OF FIGURES	vi
LIST OF TABLES	xi
LIST OF ACRONYMS	xi
OBJECTIVES OF THIS STUDY	1
RATIONALE FOR STUDY	2
CHARACTERISTICS OF THE STUDY SITE	4
Glacial Origins	5
Erosion and Accretion	6
Sand Shoals	8
Currents	9
CHARACTERISTICS OF THE DATA SET	10
The Landsat Sensor System	13
MULTITEMPORAL ANALYSIS	15
Shoal Detection	17
Sea State	20
Blizzard and Landform Changes	22
Littoral Drift	23

Turbidity	24
Biological Factors	26
Clouds, Haze, and Fog	27
Sea Foam	27
Surface Manifestations of Internal Waves	29
Tidal Overfalls on the Shoals	32
Sunglint	34
Summary of Multitemporal Study	36
MULTISPECTRAL ANALYSES	38
Procedures	40
Water Reflectance Model and Estimation of Parameters	40
Solar Irradiance at Sea Level	41
Deep Water Signal	42
Sand and Foam Reflectivity	43
Water Attenuation Coefficient	46
Experimental Displays of Tests	48
Effects of Sunglint	51
Turbidity Effects	55
Sea Foam Consideration	57
Surface Manifestations of Internal Waves	57
Summary of the Multispectral Analyses	58
SUMMARY AND CONCLUSION	61
REFERENCES CITED	131

LIST OF FIGURES

FIGURE	TITLE	PAGE
1.	Cape Cod, Massachusetts and Environs.....	64
2.	Glacial Lobes and Deposition Lines (from Strahler, 1966).....	65
3.	Color Print from Transparency Taken by Skylab S-190B Showing Shoals of Nantucket.....	66
4.	Index Map of Cape Cod, Nantucket, and Martha's Vineyard (from Tisdall and El-Baz, 1979).....	67
5.	Portion of Landsat-3 RBV Image Showing Details of Cuspate Shoreline in Nantucket Harbor and Subaqueous Hydrographic Features.....	68
6.	Enlarged Portion of MSS Band 5 of Landsat Scene 1724-14472 of 17 July 1974. Bathymetry Chart Overlay Reveals Similarity in Patterns Over Shoals.....	69
7.	Landsat MSS Band 4 Image Showing Edge Definition of Pattern Related to Direction of Wind.....	70
8.	Landsat MSS Band 4 Image Showing Patterns of Sea State.....	71
9.	Landsat MSS Band 4 Image Showing Few Visible Patterns in the Ocean due to Calm Sea State, High Tide, and Low Sun Angle. Difference in Brightness of Land Surfaces is Attributed to Snow Accumulation.....	72
10.	Water Mass Boundaries that are Possibly due to Biological Activity are Recorded in this Image which also Illustrates the Effects of Radio- metric "Clipping".....	73
11.	Coastal Changes of Cape Cod Monitored by Landsat (from U.S. Geological Survey).....	74

FIGURE	TITLE	PAGE
12.	Landsat MSS Band 7 Image Showing Breach of Monomoy Island Resulting from the Blizzards of 1978, Deposition from Littoral Drift Currents, and Variations of Land Brightness Attributed to Snow Accumulation.....	75
13.	Map Showing Littoral Drift Directions Around Cape Cod, Massachusetts (from Strahler, 1966).....	76
14.	Landsat MSS Band 4 Image Showing Small Plume at the End of Cape Cod Canal.....	77
15.	Image Showing Sediment Plumes Resulting from Convergence of Longshore Currents.....	78
16.	Image Showing Shadow of Contrail on the Water Which May Indicate Presence of Turbidity.....	79
17.	Image Showing Two Distinct Cloud Types.....	80
18.	Landsat MSS Image Showing Major Patterns in Band 7.....	81
19.	Seasat Synthetic Aperture Radar (SAR) Image Showing "Shoal Pattern" Visible in Microwave.....	82
20.	First of Two Sequential Skylab-3 S-190A Photographs Illustrating the Directional Characteristic of Surficial Specular Reflection (Sunglint)...	83
21.	Second Sequential Skylab-3 S-190A Photograph Illustrating the Directional Characteristic of Surficial Specular Reflection (Sunglint).....	84
22.	First of Three Sequential Landsat MSS Band 5 Scenes Showing No Change of Pattern with Change in View Angle.....	85
23.	Second of Three Sequential Landsat MSS Band 5 Scenes Showing No Change of Pattern with Change in View Angle.....	86
24.	Third of Three Sequential Landsat MSS Band 5 Scenes Showing No Change of Pattern with Change in View Angle.....	87
25.	"Grey-Map" MSS4 Old Man Shoal.....	88
26.	"Grey-Map" MSS5 Old Man Shoal.....	89

FIGURE	TITLE	PAGE
27.	"Grey-Map" MSS6 Old Man Shoal.....	90
28.	"Grey-Map" MSS7 Old Man Shoal.....	91
29.	Turner Model of Solar Irradiance.....	92
30.	Nova Scotia to New Jersey Map Showing Relation of Land and Submarine Topography, Nova Scotia to Florida.....	93
31.	Reflectivity Graphs Showing Relation of Deep Water Signal to Other Areas.....	94
32.	Reflectivity Spectrums of Massachusetts Beach Sand and Simulated Sea Foam.....	95
33.	Billingsgate Shoal.....	96
34.	Regression of the Log Digital Number vs. Plotted Depth in MSS Band 4.....	97
35.	Regression of the Log Digital Number vs. Plotted Depth in MSS Band 5.....	98
36.	Calculated Depths for Billingsgate Shoal.....	99
37.	Actual vs. Computed Theoretical Reflectivity.....	100
38.	Calculated Depths for Pollock Rip.....	101
39.	MSS4 "Grey-Map" of Pollock Rip.....	102
40.	Pollock Rip Channel.....	103
41.	Calculated Depths for Old Man Shoal.....	104
42.	Old Man Shoal.....	105
43.	MSS Band 4 Reflectivity Actual vs. Computed Theoretical Relevant to Bottom Profile by Pixel Position.....	106
44.	Comparison of Actual vs. Computed Theoretical Signals for Old Man Shoal.....	107
45.	Reflectivity $V-V_s$ Old Man Shoal.....	108
46.	Comparison of Actual Reflectivity to Calculated Theoretical Reflectivity for Shoals "A".....	109

FIGURE	TITLE	PAGE
47.	Comparison of Reflectivities $V-V_s$ for Shoals "A"...	110
48.	Comparison for Reflectivities for Shoal "A".....	111
49.	MSS7 "Grey-Map" of Monomoy.....	112
50.	MSS7 "Grey-Map" of Nantucket.....	113
51.	"Grey-Water" $V-V_s$ Reflectivity.....	114
52.	Illustrating Estimate of Wave Slope Necessary for Specular Reflection.....	115
53.	Scan Line Orientation to Geographic Directions.....	116
54.	Three Dimensional Illustration of Unit Vector Solution.....	117
55.	Upwelling Spectral Radiance from Phytoplankton.....	118
56.	"Grey-Map" MSS5 Nantucket Sound.....	119
57.	Comparison of Actual $V-V_s$ Water Reflectance and QSS Modeled Water Reflectance.....	120
58.	Water Reflectance Model of Old Man Shoal Showing Effects of External Bias and Attenuation Curves....	121
59.	"Grey-Map" MSS5 Surface Manifestation of Internal Waves.....	122
60.	Digital Number in Each MSS Band Across a Surface Manifestation of Internal Wave (Line 1031, Points 625-654).....	123

LIST OF TABLES

TABLE	TITLE	PAGE
1.	Characteristics of Imagery Utilized in Studying Hydrographic Features off Cape Cod.....	124
2.	Selected Weather Data for Dates of Image Acquisition.....	126
3.	Tidal Summary for Nantucket on Dates of Image Acquisition.....	127
4.	Tidal Current Data at Pollock Rip Channel on Dates of Image Acquisition.....	128
5.	Percentage of Increased Radiance Compared to Solar Irradiance.....	129
6.	Slope of Digital Number to Linear Pixel Position for Surface Manifestations of Internal Wave.....	130

1

ACRONYMS

CCT - Computer Compatible Tape

DMA - Defense Mapping Agency (Department of Defense)

DMAHTC - Defense Mapping Agency Hydrographic/Topographic Center

DMSP - Defense Meteorological Satellite Program

ERIM - Environmental Research Institute of Michigan

ETC - Earth Terrain Camera

IFOV - Instantaneous-field-of-view

MIDAS - Michigan Interactive Data Analysis System

MSS - Multispectral Scanner (Landsat)

MTS - Michigan Terminal System

NASA - National Aeronautics and Space Administration

NESS - National Environmental Satellite Service

NOAA - National Oceanic and Atmospheric Administration

NOS - National Ocean Survey (NOAA)

NYBERSEX - New York to Bermuda Satellite Experiment

ONR - Office of Naval Research (Department of the Navy)

QSS - Quasi-Single-Scattering (Model)

PIXEL - Picture Element

RBV - Return-Beam Vidicon

SAR - Synthetic Aperture Radar

INTERPRETATION OF HYDROGRAPHIC FEATURES IN THE WATERS OFF CAPE COD

by

Charles Leonard Reed

On 13 December 1976, the tanker Argo Merchant was stranded on Fishing Rip in the Shoals of Nantucket. Its cargo of 3×10^7 liters of crude oil spilled into the sea, focusing American attention on an environmental disaster of unprecedented magnitude. Available charts, aerial photographs, satellite imagery, and environmental background information were reviewed to help assess the potential damage. Among the available data was Landsat image 1724-14472 of 17 July 1974, showing the area from Gloucester, Massachusetts, to Block Island, Rhode Island, including the intervening coastal waters and the Shoals of Nantucket (Figure 1) (Short, et al., 1976). Recorded in this image are several patterns suggestive of bottom features. If such patterns can be linked to bottom features, Landsat imagery may have important applications in nautical charting.

OBJECTIVES OF THIS STUDY

The study described in this report was conducted to determine the origin of several features appearing in Landsat image 1724-14472 of 17 July 1974, showing the Cape Cod area. Specific attention was given to four questions:

1. Are the features detected in the image related to water depth?

2. Can depth information be derived from Landsat data?
3. Do the features detected represent hazards to navigation?
4. If not related to water depth, could these features obscure or mask hazards to navigation?

RATIONALE FOR THIS STUDY

The compilation of charts for coastal areas and shallow waters is perhaps the most difficult task facing the hydrographic charting community. Conventional precision bathymetric surveys are costly, both in terms of time and money. The coastline and bathymetry are continually changing from both natural forces and man-made modifications. Available charts are usually inaccurate due to dynamic changes which occur during the time it takes to create the chart product. All marine charts issued by the Defense Mapping Agency Hydrographic/Topographic Center (DMAHTC) have an edition date, and should be continually corrected from information disseminated through the weekly Notice to Mariners. Such chart corrections must be manually entered on the charts and many civilian users are unaware of the numerous changes making their charts obsolete, especially if their chart is an old edition.

Shipboard bathymetric coverage of most ocean areas is minimal because ships are only capable of linear coverage, requiring a grid of transects to cover the survey area. Modern multi-beam sonar systems are of little help in shallow waters, for they do not provide data for much more of the ocean bottom than do conventional, single beam echo sounders. In addition, ships conducting hydrographic surveys in

uncharted shallow waters are subjected to greater hazards of grounding on unexpected shoals or reefs. The use of traditional aerial surveys is hampered by adverse weather in many coastal areas, and may be additionally limited by aircraft range, political considerations, and the limited availability of support facilities. If shipboard survey data and chart compilation resources could be augmented by use of Landsat data, better charts could be produced faster, and at less cost, than is now possible.

While the ultimate benefit of spacecraft imagery might be actual determination of ocean depth, especially in shallow waters, early detection of hazards to navigation would be a major benefit. Information on location and changes in underwater obstacles such as shoals could be used to alert mariners and revise existing charts.

Modern nautical chart products are basically concentrated in areas of potential military interest, and along major shipping lanes. Because survey resources are allocated by priority, charts of many areas of the world are so out of date or non-existent as to be unresponsive to the changing requirements of the 1980's (Dawson, 1980). Most charts of the world's oceans are based on surveys of the 1800's (Hammack, 1977). These charts were adequate during their day because vessels did not exceed 6 meter draft and sailed upon fairly well established trade routes. Today, our industrial society's appetite for raw materials has led to development of super tankers and deep draft cargo ships to carry increased exports from developing countries. Modern vessels include the largest bulk carriers ever devised by men, with some over 360 meters

in length and drawing over 28 meters (Cramer, 1975). Former marine charting standards are not adequate to meet the needs of these new vessels, and the number and cost of marine accidents is increasing. In an economy of ever rising costs and inflation, navigators must also seek shorter routes, more favorable sailing weather, and take advantage of any favorable currents to minimize fuel cost and avoid delays in transit (Dawson, 1980).

The combined elements of new vessels, new ports, and new trade routes require the production of new charts. This is an expensive undertaking and interest in satellite technology to assist in this undertaking is high. The shortfall in chart production is so large that new technology must be utilized. To meet long-term requirements for precise charting, sensor systems such as Landsat must be coupled with limited ship surveys to find a feasible solution to the current charting problem at a reasonable cost.

CHARACTERISTICS OF THE STUDY SITE

The waters around Cape Cod represent a highly dynamic and complex environment, in which the combined forces of wind and water act upon the surface of the earth. The geologically rapid changes in land forms due to erosion and aggradation are significant to topographic and bathymetric mapping, and represent a difficult and continuing task of map revision. The task of hydrographic charting which includes both shorelines and bathymetry, is more difficult than mapping of the land surface.

The waters around Cape Cod provide a textbook example of multiple use problems, and a wide variety of marine charting applications are uniquely represented by this multiplicity of uses. Oil leases have now been sold on the Georges Bank. To pump oil to the mainland requires routing of pipelines and cables. Problems of oil drilling and pipeline construction are compounded because the area is one of the most productive fishing areas in the world. Frequent dredging is required to allow the fishing fleet from Chatham to sail past the barrier island, Nauset Spit, and Monomoy Island to fishing grounds. The waters off Cape Cod and Nantucket Shoals represent one of the busiest commercial shipping lanes of the Atlantic Ocean, and the area is one of the major maritime graveyards of the world. More than 145 shipwrecks have been recorded in the area since World War II (Green, 1979), with perhaps 2,000 since colonization (Melham, 1975).

Glacial Origins

The unique land form that is called Cape Cod began to develop at the end of the last Ice Age, during the final, or Wisconsin stage of the Pleistocene Epoch (from about 50 to 70 thousand years ago until 10 thousand years ago). As the glaciers grew, sea level declined about 90 meters below present sea level and the area we now know as Cape Cod was a coastal plain. The ice spread southward with three separate lobes converging over the area leaving the basic deposits which formed Cape Cod. Deposition occurred in two stages. At their furthest advance southward, the three lobes of the ice sheet left end moraine deposits which formed Martha's Vineyard and Nantucket Island (Figure 2).

The ice then retreated, but during a temporary delay in this retreat formed the south shore of Cape Cod Bay. Two secondary interlobate moraines were formed between these two periods of glacial equilibrium with the climate. Both were somewhat smaller in size and trend north-south from the northernmost point of Martha's Vineyard to the west side of Cape Cod Bay, and from Nantucket Island along the east side of Cape Cod. No remnant of the latter moraine persists due to erosion from the sea, but its existence can be inferred from the generally smooth appearance of the sediment from the ocean to Cape Cod Bay. The "forearm" of Cape Cod was an outwash plain from a glacier and moraine deposit on the Atlantic side (Strahler, 1966).

Erosion and Accretion

After the major glacial deposits were laid down and the glaciers retreated, sea level began to rise to the present level and a second great shaping of the land commenced. Rough edges of the topography were smoothed by wave action to the more mature shoreline of today.

Erosion and accretion are very rapid in unconsolidated glacial sediments, such as those of Cape Cod. The high energy expended on these easily eroded deposits by wind, tide, and sea state can produce dramatic changes. Winds are normally from the northwest or southwest, but severe storm winds are often from the northeast; colloquially called "nor' easters." Winds from the northeast encounter no obstructions across the entire breadth of the North Atlantic, and large swell waves generated from the large fetch of the ocean batter the shoreline and shoal areas. The waves strike the land at an angle,

setting up littoral currents that transport sediment along the shore, adding sediment to offshore spits, and sometimes actually closing off estuaries. Normal tidal range is between 3 and 4 meters (Strahler, 1966), but Cape Cod often has very high tides associated with storms. Effects of tidal surges upon the land form are pronounced due to the wide and shallow continental shelf. Intensely rippled, broad tidal flats characteristically result from the strength of the tides.

The coastal zone is a dynamic system in which sediment is continuously in motion due to sea state, tides, and littoral drift; therefore, Cape Cod's shoreline is continuously changing. An example of long term coastal processes can be found in the account of the first recorded shipwreck in the New World at Nauset Beach, Cape Cod, Massachusetts, in 1626. The Sparrow-Hawk, a 12 meter (40-feet) shallow draft vessel set sail from England for Virginia. During the crossing of the Atlantic the captain became ill with scurvy, and provisions ran low. After six weeks without water, "... the immigrants forced the crew to steer between southwest and northeast in hope of finding some land, what so ever, and caring not" (Anonymous, 1865; Onysko, 1978).

The ship first ran aground on an offshore sand bar late one evening. Rising tides the following morning freed it to sail safely through an inlet into what is now known as Pleasant Bay. A violent storm (perhaps a "nor' easter") subsequently grounded and wrecked the Sparrow-Hawk, engulfing it in sand. After the storm, the inlet migrated to the south and coastal processes completely buried the ship.

In 1863, 237 years after it was wrecked, the Sparrow-Hawk was uncovered by yet another storm. Since 1863, the inlet has again migrated away from the wreck site.

Short term affects of wind, tide, and sea state upon the shoreline of Nantucket Island have been described by Gutman, et al., (1979). The island can lose as much as 11 meters to the sea per year, depending upon wind and wave direction, and on the amount of energy dissipated from storm waves by the sand shoals which lie to the north and east of the island.

Sand Shoals

The Nantucket Shoals represent a remarkable depositional topography. The ridges and trenches of the shoals trend northwest-southeast, and rise to within 4 meters (2 fathoms) of the surface. The Nantucket Shoals deposition has been compared "... to the Norfolk Banks of the southern bight of the North Sea, or the Syrtis Major section of Mars" (Swift, 1978). The shoals are overprinted by a second pattern of sand "waves" up to seven meters high and spaced hundreds of meters apart. These features are clearly visible on Skylab-3 S-190B color photography (Figure 3). Similar sand ridges on Georges Bank, 120 miles east of Cape Cod, were studied by Stewart and Jordan (1964) after the shoals were attributed to reshaping of glacial deposits by strong current action (Shepard, et al., 1934). Three interesting phenomena were observed. The shoals were found to have migrated up to 310 meters over a period of 25 years; the tidal pattern was found to move rotationally, 360° in 12 hours, rather than reciprocally; and a change in level of

the water surface was found above the ridges of the shoals. The rise in water level was attributed to an overfall created when tidal currents move normal to the trend of the ridges. An actual rise in the sea surface can be detected at the confluence of the currents.

Swift (1978) described the area as follows:

"The development and migration of the shoals are a response of the cohesionless sand substrate to the intense tidal flow. The ridge channels are not exact replicas of each other; some shoal north and some shoal south; depending on whether they service primarily the south moving ebb tidal stream or the north moving flood tidal stream. Sand wave crests are not truly orthogonal to the ridge set; sand wave crests tend to approach ridge crests asymetrically, so that sand waves are convex toward the direction from which the dominant tidal stream approaches, and the residual flow moves alternately clockwise and counterclockwise around successive ridges."

McCave (1971) studied similar sand shoaling and tidal currents in the North Sea to attempt to learn more about the depositional mechanism of sand transported by tidal currents. Knowledge of the growth and migration of shoaling could be very useful in reducing the danger to shipping and the potential environmental dangers inherent in transport of oil by ships or pipelines across such rich fishing grounds.

Currents

Major currents contribute to the unique marine climate of Cape Cod. The Gulf Stream, which carries warm water from the tropics, turns eastward as its northward flow meets the cold Labrador Current flowing southward from the Arctic. The upwelling of nutrients caused by the meeting of the currents promotes the growth of phytoplankton, the primary link in the food chain for the fishing grounds. Approximately 1.3×10^7 kilograms of commercial fish with a value of \$78

million are taken annually from waters off the coast of Massachusetts (Fricke and Maiolo, 1978).

Fog and marine haze are characteristic of Cape Cod in the warmer months, when cold waters from tidal currents are warmed over shallows, such as the ridges of the shoals (Ryder, 1979). Fog patches up to 10 kilometers across are common.

Very strong tidal currents, with velocities up to three knots, occurring in the Cape Cod area are frequently called rip tides. Charts of the area designate many sites as "rips," such as Fishing Rip, the site of the Argo Merchant grounding. The along-shore, or littoral-drift, current resulting from the oblique angle at which waves strike the shore, is a dominant force in the transport of sediment from land erosion and subsequent accretion.

CHARACTERISTICS OF THE DATA SET

This study was stimulated by observations of potential bottom features in Landsat image 1724-14472 of 17 July 1974, but several additional images were also studied. The full image set included records from 14 dates, representing several sensors and spectral bands (Table 1). These remote sensor data were supplemented with data on weather at the times the images were obtained (Table 2), tidal data for Nantucket (Table 3), and tidal currents at Pollock Rip Channel (Table 4).

Most of the remote sensor data originated with a sensor on one of the Landsat series of satellites, but data from Skylab-3 and Seasat-1 were also utilized. In each case the record represents the

spatial distribution of intensities of electro-magnetic energy in specific spectral bands determined by sensor configuration. To provide a record of underwater phenomena, this energy must travel from its source -- the sun except for the Seasat-1 radar data -- to the surface of the water, travel downwards through the water column to the bottom, be reflected off of the bottom, travel upwards from the bottom through the water column to the surface, and travel from the water surface to the sensor. Thus, each record represents the integrated result of a large number of variable factors affecting the "energy-flow-profile" from source to sensor (Olson, 1962; Colwell, et al., 1963). Solar energy recorded by the Landsat and Skylab sensors included two components: direct solar irradiation and indirect irradiation from atmospheric scattering in what is assumed to be a uniform Lambertian sky (Francis and Reed, 1979). Scattering of energy in the atmosphere, reflectance from the sea surface, and scattering of energy in the water column all tend to increase the amount of energy reaching the sensor and, therefore, tend to reduce the contrast between deep water and bottom signals received at the sensor. The final response of the sensor is a product of the sensitivity of the sensor and the radiance received:

$$V_i = c(\lambda)_i L(\lambda)_i$$

where, V_i = the sensor response
 $c(\lambda)$ = the spectral sensitivity of the sensor
 $L(\lambda)$ = the spectral radiance received
 i = the spectral band of operation of the sensor.

The spectral radiance received at the sensor includes several components, only one of which originates from bottom reflectance. Specular reflections from water surfaces are common, but are more limited in Landsat data than in conventional photography because of the narrow acceptance angle (field-of-view) of the Landsat sensors. What specular reflections do occur are usually the result of sloping water surfaces of waves or currents, and appear as "glitter" in image forms of the data. Within the water column of the ocean, scattering is minimal and little of the scattered energy exits the water. Thus, the volume scattering of the water column is usually ignored. The signal reflected from the bottom is strongly affected by attenuation in the water column. This attenuation is proportional to the clarity and type of water, and to the length of the water column. Scattering in the atmosphere adds a non-directional radiance to the total signal reaching the sensor. Thus, the total radiance recorded by a sensor over water is composed of three primary components, and can be expressed as follows:

$$L_{\text{total}} = L_p + L_s + L_b$$

where, L_p = the atmospheric path radiance due to scattering

L_s = the surface-reflected radiance

L_b = the bottom-reflected radiance

both L_p and L_s are assumed to be homogeneous for a scene. L_b is a result of bottom reflectance and water attenuation. The atmospheric path radiance, L_p , and surface-reflected radiance, L_s , contain no information regarding water depth, and are therefore considered "background" radiance which must be subtracted from the total radiance for

water depth calculations. The sum of these two factors is the radiance of deep ocean water, L_d . Unfortunately, there is nothing in the signal itself to identify what part of the signal reaching the sensor originated as path radiance, as surface-reflected radiance, or as bottom reflectance. Accuracy of bathymetry extracted from Landsat would be degraded by erroneous interpretation of signals received from haze over the water, foam on the water, or vegetation in the water as bottom reflectance. Some way must be found to eliminate these potential erroneous interpretations if Landsat is to be effective in nautical charting applications. Since most of the factors leading to erroneous interpretations are transient, comparison of images from different dates can often reveal their transient nature and permit correct classification of the image patterns.

The Landsat Sensor System

Characteristics of the Landsat sensor systems have been well described by Taranik (1978). The sensor of primary interest in this study was the multispectral scanner (MSS) recording reflected solar energy in four wavelength bands, with the return-beam vidicon sensors (RBV) of secondary interest. The spectral bands associated with each of these sensors are:

Landsat-3 (2 cameras)	RBV	0.505 to 0.0750 micrometers
Landsat (-1, -2, -3)	MSS Band 4	0.500 to 0.600 micrometers
	MSS Band 5	0.600 to 0.700 micrometers
	MSS Band 6	0.700 to 0.800 micrometers
	MSS Band 7	0.800 to 0.900 micrometers

Energy received at the sensor in each of these bands is telemetered to ground receiving stations. Data from the four channels of the MSS are converted to digital values, each representing the average brightness of the scene within the instantaneous-field-of-view (IFOV) of the scanner in a particular spectral band, at a particular moment in time. These digital values can be processed in digital form or converted to an image form for analysis by conventional image interpretation. Each digital value represents an area in the scene, called a picture element (pixel), with an assigned brightness value ranging from 0 through 127 in Bands 4, 5, and 6, and from 0 through 63 in Band 7. Since image products cannot show more than about 20 detectably different shades of grey, the full information content of the record can seldom be extracted from the image form alone. At the present state of the art in digital analysis of Landsat data human interpreters can do a better job of interpreting contextual information than can computers, and joint-human machine interpretations are frequently required to maximize information extraction. In this study, human interpretation of multitemporal data was used to identify image patterns associated with non-bottom features so that these patterns would not be erroneously interpreted as shoals or shallow water areas. Computer processing of the digital data to obtain relative depth information was conducted in association with the human interpretation of the images. Computer processing was performed at The University of Michigan Computer Center through the Michigan Terminal System (MTS). Image histograms, statistics, direct

output of signal values (digital numbers), and line-printer "grey-maps" were produced with the 11 LINE software package developed at the Environmental Research Institute of Michigan (ERIM). Statistical programs designed for the Michigan Interactive Data Analysis System (MIDAS) were used to establish parameters for transforming geographic positions from a Mercator chart to Landsat column (line) row (point) pixel coordinates, and for other statistical operations required in depth calculation.

MULTITEMPORAL ANALYSES

When confronted with a variety of images, the interpreter should first look for known features, or known characteristics before proceeding with the interpretation of unknown features. Initial orientation can be achieved by associating features seen in Figure 1 with the index map of the area (Figure 4). Figure 4 shows the Cape Cod peninsula and the surrounding bodies of water. The Atlantic Ocean is to the east, Cape Cod Bay to the north, Nantucket Sound to the south separates the ten-kilometer wide peninsula from the two large islands of Martha's Vineyard and Nantucket. Highly reflective quartz-sand dunes, created from detrital wind blown sand appear to the north and northeast of Provincetown and on Sandy Neck, the spit which partly enclosed Barnstable Harbor. Smooth mature coastlines surround the Cape Cod peninsula and the associated islands. Recurved spits such as Monomoy and Race Point have grown from the deposition of sediment by littoral drift. Baymouth bars and spits have grown across the mouths of estuaries, often sealing them off from the open sea.

A feature which appears in the waters directly above Great Point on Nantucket Island is not a spit. It is called Point Rip, is subaqueous, and is curved toward the Atlantic Ocean not the mainland. It marks the location of the remnants of a glacial kame deposit, which originally provided the sediments for Coskata Beach and Great Point (Tisdall and El-Baz, 1979).

A most distinctive feature is the cusped shoreline within the harbor of Nantucket. The origin and mode of formation of these cusps have been disputed for some time. Farouk El-Baz and Tracey Tisdall (1979) suggest the following model as most plausible: (1) The shore was modified by the wind system particular to the area; (2) The harbor is oriented parallel to the prevailing winds from the southwest; (3) The dominant storm wind direction is from the northeast; and (4) It is primarily the action of the opposing winds at high angles to the beach that has produced the cusped configuration. Leonard and others (1976) felt that "longshore processes acting in both directions erode sediment from the centers of the concavities and transport it to the spit ends where it is deposited as subaqueous bars, the upwind spit preventing longshore drift in the center of the concavity." This process creates the symmetry of the cusps and the lengths of the points are determined by the relative strength of currents. The distance between the cusps is thought to depend upon the harbor width. Equilibrium of processes is necessary for the stability of the beach morphology. Although the beach has been stable for some time, there is some evidence that an inlet formerly

existed at Haulover Beach, causing decreased tidal flow in the harbor. This caused an imbalance between accretion on the spits and erosion by the tidal currents. The spits then grew long enough to reach the opposite shore. Now that the inlet is closed, equilibrium has again been regained. The remnant bars crossing the harbor can be seen in Figure 5.

Shoal Detection

Light-toned areas in the waters around Cape Cod may represent bottom features due to upwelling reflectance through the water; or, on the other hand, they may represent only temporal "shoal apparitions" of phytoplankton concentrations, sediment-laden water, clouds and haze, or other surface effects, such as sea state and sun-glint. The prudent navigator would not be in danger from interpretation errors of light-toned water; however, errors in interpretation of darker-toned water due to light absorbing vegetation and sediments could be a real danger in shallow seas because these factors can make water appear deeper than it really is. Several features are consistently represented on multitemporal images and are also designated as bathymetric shallows on published charts.

Shoal areas around Nantucket can be detected in the waters to the north and to the east of the island. An enlargement of the 17 July 1974 Landsat image of Cape Cod (Figure 6), overlaid by a portion of the National Oceanic and Atmospheric Administration (NOAA) National Ocean Survey (NOS) bathymetry chart No. 13237 (26th Ed., 27 January 1979, from 1957 survey data), illustrates how closely the lighter-toned

patterns in the image correspond to the bathymetric highs of the shoal areas.

When the attention of the reader is focused upon Figure 1, other light-toned areas, matching other areas of shallow bathymetry, can be detected. The gently sloping Billingsgate Shoal, for example, can be seen west of Jeremy Point, a southern extension of Great Island in Wellfleet. The channel leading into Wellfleet Harbor is also evident. Bars and channels of ebb tidal deltas can be seen outside Nantucket Harbor, Barnstable Harbor, and Chatham Harbor. Within Barnstable Harbor are flood tidal deltas. These features are also detectable but are less apparent within Pleasant Bay. The area of Brewster Flats east of Barnstable Harbor and extending further eastward to Eastham is also highly visible. The area is rather regular in appearance when contrasted to the sinuous patterns of shoals around Nantucket and within Nantucket Sound north of Tuckernuck and Muskeget Islands. This is a result of the lower energy of wave turbulence due to shorter wind fetch within Cape Cod Bay compared to the coast towards the Atlantic Ocean. To the south of, and adjoining Nantucket Island at its midsection, is another remnant of a glacial kame called Miacomet Rip. Within Nantucket Sound, on the west side of Monomoy Island, is the Commons, an old tidal delta. This bathymetric feature will be discussed from another point of view later in this thesis.

The offshore bar called Peaked Hill Bar can be detected north of Provincetown with aid of magnification. The resolution of the Landsat MSS (79 meters) is simply not adequate to discern smaller offshore

bars without additional knowledge and ancillary data. It can be shown that smaller features in the water can be detected with digital data, but the features may be just too difficult to recognize. The narrow-band multispectral quality of Landsat imagery was found to be of significant benefit over broad-band panchromatic imaging systems.

The higher resolution of Landsat-3 RBV (40 meters) images have significant advantage over the MSS for recognition of submarine features. By comparing Figure 1 to Figure 5 it is evident that much greater detail in submarine morphology can be more easily delineated. In the Landsat-3 RBV image, breaking waves can be seen approximately over the location of the shoals. Offshore bars are exposed along the southern shore of Nantucket. Much more detail of under water channels and shoals can be seen near the islands of Tuckernuck and Muskeget, west of Nantucket. Features appear in the Commons which may be parallel bars oblique to the shoreline of Monomoy. The tidal flats parallel to the shoreline north of Nantucket appear cross-hatched and may indicate the presence of bars, although these features do not appear on the latest edition of NOAA's (NOS) chart No. 13237 (26th Ed., 27 January 1979).

The resolution of the S-190B Earth Terrain Camera (ETC) "high-resolution" color photograph (SL-3-86-314) in Figure 3 is 21 meters at a scale of 1:250,000 (enlarged from an original scale of 1:950,000). The photographs taken over Cape Cod are superior in clarity and resolution to Landsat MSS or Landsat-3 RBV imagery. Ship wakes, exposed bars, breaking waves, and even subaqueous sand waves lying above the Nantucket Shoals are clearly visible in the original transparency.

Sea State

The extreme variety of patterns of light and dark tones are represented by multi-date band 4 Landsat MSS images in Figures 7-10. Careful analysis of the patterns to the east of Nantucket revealed a clue that the patterns were related to sea state. The edges of the pattern in the 28 May 1975 Landsat image (Figure 7) are very different from the 17 July 1974 Landsat image (Figure 1). In Figure 1 the eastern edge is sharp and the western edge is diffuse. The edges of the same pattern in Figure 7 are just the opposite, indicating a change of wind direction upon the sea surface. A dramatic change is apparent in the 9 March 1978 image (Figure 9), where distinct patterns of tone are barely detectable. The wind direction was from the north-northeast (20°) for the 17 July 1974 image; north-northwest (330°) for the 28 May 1975 image; and no wind was present at Nantucket Tower Weather Station at the time of the 9 March 1978 image. Other patterns in Figures 7-10 generally seem to correlate to charted bathymetric highs, with variations due to wind direction, wind speed, and wave swell. Sea state conditions could cause sediment to be entrained directly above the higher points of the shoals. The amount of sediment suspended is a function of wave height to water depth. Therefore, the height of the tide is also important.

The 9 March 1978 MSS image is exceptional for many reasons. It is one of only a few, cloud-free, wind-free images obtained by Landsat over Cape Cod in the five-year sampling period. The absence of wind generated surface effects leaves the water areas in the image devoid

of the striking multitude of patterns that characterize the other images; however, some patterns are visible. They are the shoals, whose upwelling reflectance is not masked by water turbulence. They are less prominent because proportionally less direct sunlight illuminates and reflects from them to the sensor. This is due to the low sun elevation (above the horizon) and increased path radiance, than would be the case for images with higher sun elevations. The light reaching the bottom features and subsequently reflected is also attenuated by the level of water (2.4 meters) above mean low tide.

The reader will note that the mainland and Martha's Vineyard are much brighter than Nantucket. The difference in brightness is not a result of special processing, or of radiometric discrepancies, because the Landsat-3 RBV images from the same day and time also contain the striking difference in brightness between the land surfaces. Both the MSS and RBV images were taken in late winter, when Nantucket had apparently escaped a snow fall which covered the mainland and Martha's Vineyard.

Radiometric discrepancies do occur in the Landsat-2 images created in the period between 22 January to 16 July 1975 (Figures 7 and 10). The preflight calibration data used did not fully utilize the dynamic range capabilities of the sensor and, therefore, had a different response compared to other Landsat responses (Colvocoresses, 1977).

The images appear lighter and do not have as much contrast. They were electronically "clipped;" e.g., the digital number values were

adjusted by about three digital numbers at the high end and one digital number at the low end of the 128 discrete grey-levels for MSS Bands 4, 5, and 6 and 64 discrete grey-levels for MSS Band 7. This was done partly to reduce striping caused by differences in the output of the individual detectors.

Blizzard and Landform Changes

Another hypothesis that was considered in the interpretation of the 9 March 1980 image was the possibility that the shoal formations might have been altered and made less visible by the catastrophic blizzards of 1978. Damage from that series of blizzards (especially the 6-7 February 1978 storm) has been estimated at over one billion dollars. Piers, jetties, breakwaters, and beach-front homes were destroyed by the nine meter waves, generated by 50 knot winds that blew for up to 33 hours.

The storm severely impacted the coastal areas from Rhode Island to Maine. On York Beach, Maine, an ancient wreck was uncovered by the storm--reminiscent of the story of the Sparrow-Hawk. The exposed hull of the small ship was fifty feet long and between 300-600 (sic.) years old (Phaneuf, 1978). At Provincetown, the sea separated the northern tip of Cape Cod from Herring Cove Beach. Some residents lost as much as 600 feet of shoreline to the ocean (Phaneuf, 1978). The fishing fleet of Scituate was stranded and a tanker ship was grounded at Marblehead (Anonymous, 1978). Monomoy Island, which had been a single island for many years was breached by the sea and is now separated into two islands (Figures 11 and 12). The Commons, the tidal

delta mentioned earlier, is a result of a break in Monomoy Island approximately 150 years ago (Tisdall and El-Baz, 1979). The separation of Monomoy Island from the mainland is reported to have occurred in 1960. The separation was triggered by the construction of a causeway between Morris Island and Chatham proper (Tisdall and El-Baz, 1979). A new tidal delta has already begun to form. It is more complex than the Commons delta, because it has both an ebb and a flood component.

Littoral Drift

Significant changes were noticed in the subaerial land forms that were not recorded on the charts. Several spits have an altered shape or join small islands. Jeremy Point has now joined Billingsgate Island by extending its length 500 meters since 1967 (Tisdall and El-Baz, 1979). These changes were not due to change in tide level on different Landsat images. Nauset Spit migrates southward at a rate of about 90 meters per year (Strahler, 1966). Sediment has been removed from the midsection of Monomoy by wave refraction and transported southwards by littoral drift resulting in an increase in its length (Williams, 1979; Odale, et al., 1971). The growth can be seen in the trend of sequential arcs which mark past changes in the deposition process. Another indicator of current direction is the accumulation of sediment on the updrift side of jetties, groins, and similar barriers as seen on (Figure 12) the northern boundary of Nantucket Sound and verified by Strahler's (1966) published longshore drift current map (Figure 13). Sediment transport in the area of Cape

Cod is primarily accomplished by littoral drift, except in the dune areas at Provincetown and at Sandy Neck.

Turbidity

Turbidity is defined as the suspension in the water of fine silt sized minerals biological particulate matter, and "yellow substance" (from the German, "gelbstoffe"), (a strong blue-absorbing complex of decomposing vegetative matter that resembles tannic acid). Better bathymetric data can be obtained if areas of suspected turbidity can be detected and then edited for alternative processing by use of more appropriate attenuation coefficients. It is difficult to visually detect changes of water turbidity, but general guidelines can help Landsat users evaluate areas where water clarity change is suspected.

Very fine-grain sediment can remain suspended for extremely long periods of time. "Yellow substance" is a complex product of decay, and is more prevalent in waters with a land source. In low wave energy environments, such as the Amazon continental margin, fine-grain sediment deposition can occur near the source. A similar deposition would generally occur in an estuarine environment. In high wave energy areas, such as around Cape Cod, fine-grain sediment is transported further from the coast to the continental shelf or deep ocean before deposition occurs.

The highly turbulent waters caused by strong currents and breakers over the shoals usually carries entrained sediment. However, the sediments of this relict beach have been reworked for two millenia (6000 years), and are relatively coarse (Rea, 1979). Sediments measured by

Stewart and Jordan (1964) on Georges Bank measured 0.68 millimeters in mean-grain size on the ridges. Recent studies of suspended matter in the vicinity of Nantucket inspired by the Argo Merchant oil spill, indicate that in surface waters the particulate count is 1 miligram/liter and at the bottom 2 miligram/liter. After severe winter storms under conditions of high sea state in the area south of Nantucket Island, the surface waters contained 3 miligram/liter, the bottom 15 miligram/liter. Non-mineral material is combustible, therefore, to determine how much particulate matter is biological in origin, samples are burned and weighed. Combustibles represent 50 percent of the total particulate weight. Turbidity was also measured with a transmissometer and was found to be negligible over the shoals (Bothner, et al., 1980).

It is reasonable to expect that heavy particles would settle out as a minimum threshold of turbulence is reached. Sediment transport occurs within one meter of the shoal surface (Stewart and Jordan, 1964). Local fishermen and boat operators report that the water is clear enough to see the bottom (Ryder, 1979).

Sediment plumes can usually be found in the Landsat images near the mouths of estuaries, rivers, channels, and along spits where areas of turbulence are occurring. A small plume is visible at the northern end of Cape Cod Canal (Figure 14). Sediment plumes occur at the point where longshore currents moving in opposite directions converge, such as midway along the southern coast of Martha's Vineyard (Figure 15) and midway along the Atlantic coast of Cape Cod (Figure 15).

The contrail seen in Figure 16 is a relative measure of the turbidity in the water. Contrail shadows would not be visible over deep, clear water (theoretically), because only skylight is reflected, and direct solar irradiation is completely attenuated in deep water. The image suggests, therefore, that there is either turbidity present in the water to reflect direct solar illumination from the suspended particles or that there is a surface effect. The shadow represents the difference between strong solar illumination which has been interrupted and skylight illumination which is always present.

Biological Factors

The fishing grounds off Cape Cod and Georges Bank are some of the most productive in the world. Plankton is the primary link in the food chain. Plankton are not distributed evenly, rather they appear on the surface in patches with concentrations accounting for about 10 percent of the particulate matter. Plankton blooms occur most commonly in March and September oftentimes causing substantial fish kills (Bush, 1979). No plankton communities could be detected with certainty in the images, although the water mass boundary seen in Figure 10 may be of biological origin. A further discussion of the detection of phytoplankton's chlorophyll-A will follow later in the paper.

No marine vegetation could be detected in the water, although it may be present. Typically, there is none visible on or near the surface (such as kelp), although marine plants foul bottom planted scientific instruments with up to six inches of growth in less than three years (Bothner, et al., 1980). Vegetation in the channels between

the shallower shoal areas is unlikely because of the strong currents of the rips.

Clouds, Haze, and Fog

Images selected for this study were "cloud free;" that is, with less than 10 percent cloud cover. Still, two distinct types of clouds are visible. The lower level cumulus clouds are dense, rounded, and bright (usually the brightest reflectance in the scene) with shadows on the land or water surface below them. High altitude cirrus clouds are usually thin and wispy, with patterns oriented in the direction of the wind. Both types are visible on the 13 December 1973 image (Figure 17).

Fog is reported to be very common on and around Cape Cod during the summer months, because of the upwelling of colder currents which then flow across sun-warmed shallows (Limeburner, 1979). The fog patches are described as being 5 to 10 kilometers across. No fog was detectable on any of the images, nor was there a marked decrease in visibility noted on the weather logs (Table 2). One plume of haze or smoke is visible on the 17 July 1974 image (Figure 1) oriented NE-SW from Block Island, Rhode Island, the small island in the lower left hand corner of the image.

Sea Foam

Sea foam is a factor that should be considered in the interpretation of the imagery. Quantitative data of the coverage and thickness of foam does not exist. Its distribution is dependent upon the water

chemistry, wind and wave interaction, spray, and bathymetry. Spilling waves seem to generate more foam than breaking waves. Sea foam is observed at the breakers and is common to shallows (Limeburner, 1979), where it may be extensive depending upon the wind speed. The percentage of area covered has been roughly estimated to be: 0 percent up to 15 knot winds; 10 percent at 15 knot or higher; 40 percent at 20 knot winds by Richard Limeburner (1979). This estimate may be very high at the top end but it is significant that up to 15 knot winds that there is little foam observable. This appears to agree with photographs and sea state description data examples in the Bowditch (U.S. Defense Mapping Agency Hydrographic/Topographic Center). It also shows agreement with low altitude aerial photographs of the stranded Argo Merchant on Fishers Rip (Milgram, 1977) where few white-caps and foam are seen even at wind speeds greater than 20 knots.

An interesting phenomenon is that the observed major pattern which is seen over the shoals appears in all four spectral bands of Landsat. Figure 18 of 17 July 1974 shows the patterns in MSS Band 7 (800-1100 nanometers). Landsat MSS Band 7 has such a high attenuation coefficient that its water penetration is negligible ($4.66 \cdot 10^{-12}$ meters) (Wolf and Zissis, 1978). In addition, Seasat Synthetic Aperture Radar (SAR) backscatter images (Figure 19) show patterns over the shoals that are very similar to those from Landsat (Figure 18). The L-band wavelength (23 centimeters) of the Seasat Radar does not penetrate the water. Therefore, patterns observed must be due to surface effects, perhaps a modulation of the surface wave structure, rather

than (or in addition to) turbidity within the water. This phenomenon appearing over the shoals may be very promising for charting if shallow bathymetry is directly linked to observable surface effects. Hazards to shipping could be detected in spite of turbidity. It may be of great value for navigation of muddy rivers. These radar applications are currently being investigated by Robert Shuchman at ERIM (1980, pers. comm.).

Surface Manifestations of Internal Waves

Perhaps one of the more remarkable, more easily recognized, yet not absolutely understood phenomenon is seen in Figure 1B. The long periodic wavelike features have been observed on spacecraft imagery, including Landsats 1 and 2, Defense Meteorological Satellite Program (DMSP) satellite; National Oceanic and Atmospheric Administration (NOAA) weather satellites, Skylab; Apollo-Soyuz; and high flying U-2 aircraft, since 1972. Such features usually appear on continental shelves of the world and are generally oriented parallel to the continental slope, although sometimes with variations which are apparently influenced by topographic and bathymetric features (Sawyer and Apel, 1976). The circular feature on Figure 1 is one result of such influence. The morphology below this visible phenomenon is a basin which has one prominence on its southern edge as indicated on Figure 30 of the following section. They have also been observed in deep ocean areas (Apel, et al., 1976) and off the North American, African East and West coasts, in the Baltic Sea, in the Sulu Seas, in the Gulf of Mexico, and in the Caribbean Sea (Apel, et al., 1975).

They are theorized to be the visible surface manifestations of internal gravity waves. These internal wave structures result from stratification within the water body of two different densities of water. The density difference can result from variations in temperature and/or salinity. These surface manifestations are distinguished by their large scale (Apel, et al., 1976) and are most frequently seen during the summer months.

Observed from the surface they appear as long, narrow quasi-parallel, smooth streaks on the water when the wind is light. "They move slowly toward the coastline, one after the other, each locating below it the point on the internal wave halfway between a crest and the following trough, as this is the region where the currents at the surface, due to the internal wave below, converge. The natural oils damp the capillary waves and produce a smooth, slick appearance." (Neumann and Pierson, 1966).

This action is thought to increase specular reflection and to decrease the diffuse scattering over the convergence region. "A second theory predicts that the small waves are concentrated in the convergence regions due to the wave-current stresses, thereby decreasing the specular reflection and increasing the diffuse scattering over the convergence region" (Apel, et al., 1976).

The qualitative characteristics of the surface manifestations of internal waves when studied on spacecraft images are summarized by Apel, et al., (1976):

- (1) The waves occur in groups or packets of 3 to 5 kilometers usually landward of the continental slope and separated by distances which are on the order of either 15 or 30 kilometers; taken together with both the observed and calculated phase

velocities, these facts suggest a semidiurnal or a diurnal origin;

- (2) The crests are nearly always oriented parallel to the bottom topography or can be loosely associated with some topographic feature seaward of their observed position, or both;
- (3) The wavelengths fall between 200 and 10,000 meters, depending on the geographical area; within a given packet, there is a monotone decrease in wavelength, varying from λ at the front to λ_0 at the back of the group;
- (4) The lengths of the crests fall between a very few and perhaps 100 kilometers with a decrease in crest length occurring from front to back of the group;
- (5) The widths of the slicks are often small compared to the lead wavelength;
- (6) The crests are curved in a horizontal plane with their convex sides pointed in the direction of propagation; the radii of curvature range from essentially infinity to a few kilometers.
- (7) As the packet progresses up on the continental shelf, there is some evidence of a continued increase in the wavelengths throughout; an accounting for this may be had by a combination of linear dispersion and nonlinear effects akin to solitary wave behavior.

Unfortunately, simultaneous identification of internal waves on spacecraft images and from on-site ship observation has not yet been completely successful; however, all data gathered from shipboard

thermistors and sonar in the New York-to-Bermuda Remote Sensing Experiment (NYBERSEX) by Apel, et al., (1976) are consistent with the characteristics as seen in associated imagery.

Internal waves can affect ships. The density discontinuity between water strata can be quite sharp under certain circumstances. "An internal wave motion at the interface is easily excited as very little energy is needed to cause a large internal oscillation that has at the same time, very little kinetic and potential energy. The currents are slow and work done in displacing the denser mass of water is small as it displaces only a slightly less dense mass of water. If the density discontinuity is near the keel of a ship, it is observed that large amounts of power are needed to get the ship underway and to maintain speed if the ship is going slowly. This is the phenomenon of 'dead water.' For the same power, the ship moves more slowly as, in addition to making bow waves and a wake and overcoming friction, she must also generate internal waves" (Neumann and Pierson, 1966).

Internal waves pose no threat to the safety of surface vessels, but are considered a potential hazard to submarines. Submarines maintain their underwater vertical position by ballasting. If a submerged vessel over-ballasted upon encountering an upward acceleration due to an internal wave, and was subsequently caught in the downward acceleration phase of the wave cycle, it could conceivably exceed the ship's maximum depth limit or strike bottom before compensation of the over-ballast could be accomplished. This scenario has been suggested as a possible cause of the sinking of the American submarine Scorpion and the subsequent loss of all her crew (Naval Environmental Prediction Research Facility, 1979).

Tidal Overfalls on the Shoals

Another factor that should be tested for detectability by multi-temporal Landsat data is the phenomenon of water motion variously called

"intermittent tide rip," "a moving wave," and "a confluence of ocean currents," which has been reported as a peculiarity of the area by Stewart and Jordan (1964). Stewart and Jordan (1964) found that there is a visible tidal overfall that occurs when a large volume of fast moving water when it is forced upward and over the crests of the sand shoals when the tidal current flow direction is perpendicular to the orientation of the shoal, as at the time of the Landsat image of 17 July 1974. Perhaps this phenomenon of water motion, which has such a striking visual impact on ground observers (compared to the impact on surface observers of manifestations of internal waves), might contribute to the patterns seen above the shoals on Landsat and other satellite images.

Pollock Rip Channel was chosen as the site of this investigation, because tidal current information was readily available and highly accurate, because it is the location of a NOAA observation station, whereas Nantucket Shoals has no stations which could provide direct observations.

Table 4 lists the results of the study of image prints, currents, and winds. This part of the study was inconclusive in regard to the detection of tidal overfall, because the factors of windspeed, wind direction, and radiometric rendition of the printed photographs far outweighed any detectable visual contribution to the brightness of the patterns. Fifteen knot winds from the north and northeast generated the brightest patterns over Pollock Rip than any of the other images, with the exception of one influenced by errors of image processing.

Future studies should be pursued, especially with regard to SAR radar imagery, because of the documented alteration of the surface wave structure. A larger sample of digital data should also be analyzed and correlated with tidal current flow direction and with wind velocity and direction, so that a quantitative relationship might be determined.

Sunglint

Interpretation of what might be the cause of the lighter grey-toned water areas (Figure 1C) in the upper right portion of the image as contrasted with the dark areas (Figure 1) proved to be difficult with the available multitemporal data. Changes detected could not conclusively be linked positively or negatively to the three most likely variables of: (1) white caps due to sea state, (2) haze, or (3) sunglint, when comparing the same nominal Landsat scene.

Haze as a contributor to the "grey-water" areas could be safely eliminated on the 17 July 1974 image under study, because details of the internal wave manifestations could be seen clearly. Details of features on land also could be seen clearly; and the absence of fog or haze for land areas is supported by weather logs which show clear visibility.

Sea state due to wind waves and swell was shown to be higher at Chatham Coast Guard Station, where areas of "grey-water" are visible in the scene; then at the "dark water" location of Nantucket Lightship, where calm was reported (Table 2). It is probable that the grey areas in the upper right portion of the image also have rougher waters.

Sunglint is a result of specular reflection of direct solar irradiance upon the water. It occurs when the angle of incidence is equal to the angle of view of the sensor. Sunglint in photometric photographs appears as a round blob of light with a bright core (Cox and Munk, 1954). The pattern spreads over more area when the sea state is higher (Naval Environmental Prediction Research Facility, 1979). Reflectance is a function of the index of refraction, the viewing angle, and, because wind affects the statistics of wave slopes on the ocean surface, it is also a function of windspeed (Duntley, et al., 1974). Sunglint pattern on optical-mechanical scanner images is usually seen as a lighter-toned strip the length of the image on the side in the direction of the sun; good examples of which can be found in the manuals of the Defense Meteorological Satellite Program (Naval Environmental Prediction Research Facility, 1979).

On Landsat images, because of the satellite's selective view angles and sun synchronous orbit, sunglint is minimized. Therefore, sunglint's likelihood as a causative agent of the "grey-water" patterns was not obvious, until sequential frames of two photographs (panchromatic; 0.5-0.6 micrometers) from the S190-A camera of Skylab-3, taken on 12 September 1973, were reviewed (Figures 20 and 21). The six-lens multispectral camera produced photographs with an original scale of 1:2,850,000. These figures are enlarged to a scale of 1:500,000. The sequence illustrates how the pattern changes with the angle of view. This change would not occur with a Lambertian reflector, such

as haze or sea foam. The effects of sunglint should therefore, be conclusively determined by the change of view angle as the sensor platform traverses its orbital path; however, with sequential Landsat-1 scenes (Figure 22-24) the anticipated evidence of sunglint pattern did not appear. Because Landsat is an optical-mechanical scanner system, it does not take an instantaneous image as does a camera system. The imaged pixel areas are in a state of flux, and each water surface facet variously reflects specularly or "twinkles and glitters." The rise in signal received, therefore, may be attributed to either specular reflection or to sea state. The range of sun azimuths of the images was not sufficient to notice any difference in pattern. The RBV sensor which does capture an instantaneous image was not used for this same sequence of scene coverage.

Summary of Multitemporal Study

This portion of the paper illustrates the value of interpretations of multitemporal Landsat data. Highly detailed information can be gathered from orbital space sensors about offshore features, some of which do not appear on charts. These results indicate that rapid change in coastal and submarine landforms can be monitored by satellite. Catastrophic changes, such as those caused by a "100-year storm," can be assessed quickly, and areas of survey priority can be determined. Trends of regional changes can also be predicted. Space imagery is particularly well suited to the monitoring of coastal environments because of the large areal coverage which can be captured by a single frame. Space imagery can amplify studies done during periods of

limited areal coverage from either photographs taken by low flying survey aircraft or from observations from surface ships.

A great deal of information has been obtained from evaluation of surface manifestations of internal waves on Landsat imagery, some of which was not previously known. Significant information has been acquired from multisensor data. The patterns seen over the shoals are created by a significant contribution from surface effects, such as sea state, which are detectable by Seasat radar as well as by the sensors on Landsat. The hypothesis that the patterns seen in the Landsat image of 17 July 1974 are caused by "muddy water" is unlikely to be correct, because: (1) The shoals are composed of coarse sediments which were of glacial outwash plain deposition; (2) The sediments were sorted by glacial runoff water; (3) The sediments were reworked by several subsequent periods of wave action when the sea level rose and fell; and (4) Because the fine grained sediments were transported by wave and current action to deeper, calmer, water for deposition. Sunlint is not easily detected from analysis of single nominal Landsat scenes but detection of sunlint improves when sequential scenes are studied. The amount of information gathered without aid of surface observations is significant.

MULTISPECTRAL ANALYSES

The human interpretations of remote sensor images described in the preceding section provided important insights into hydrographic features of the Cape Cod area. Edge definition of some image patterns indicates breaking waves over submarine features. Some image patterns were found to correlate, at least approximately, with charted bathymetry, while others were apparently due to sea state. Sea state was found to be a contributing factor to the phenomenon of "grey-water" areas (Figure 1C), and also to the visibility of the surface manifestation of internal waves (Figure 1B).

Based on these human interpretations it appears clear that the Landsat MSS sensor can be used to assist in locating possible shoal areas, and to determine if the observed phenomena are due to bottom reflectance, turbidity, or surface effects. For hydrographic charting purposes, it is important to know when patterns observed in the image are due to bottom reflectance or other factors. When an observed pattern is not related to water depth, it is important to determine what other factor(s) could account for the image appearance.

Since sea water has negligible water penetration in the infrared portion of the spectrum (Wolfe and Zissis, 1978), patterns seen in all four Landsat bands should not be due to bottom reflectance. Image patterns visible in Band 6 (0.7 to 0.8 micrometers) or Band 7 (0.8 to 1.1 micrometers) are almost certainly due to surface conditions such as sunglint, foam on the water, or turbidity at the surface. Figures

25, 26, 27, and 28 show similar image patterns in all four spectral bands. These computer generated "grey-maps" were produced from the Landsat computer compatible tape (CCT) for scene (1724-14472 of 17 July 1974).

When image patterns are determined to be the result of bottom reflection, it is usually desirable to determine the depth of water at that location. Methods of water depth determination from Landsat data have been under investigation for nearly ten years. Work at the Environmental Research Institute of Michigan (ERIM) for the National Aeronautics and Space Administration (NASA), the Defense Mapping Agency (DMA), and the Office of Naval Research (ONR), is encouraging. Remote mapping of water depth from multispectral scanner data was first demonstrated with aircraft data collected over Lake Michigan (Brown, et al., 1971). The model developed during that study was successfully tested during the NASA/Cousteau Ocean Bathymetry Experiment when depths determined from Landsat MSS data agreed within 10 percent of charted depth in waters to 42 meters deep (Polcyn, 1976). Color-coded maps of the Little and Great Bahama Banks were generated with high gain Landsat multispectral scanner data showing variations in water depth to demonstrate the feasibility of satellite bathymetric mapping (Polcyn, Lyzenga, and Tanis, 1977). Further progress was reported by Lyzenga and Polcyn in 1979, and Denoyer reported successful use of the depth determination algorithm by the U.S. Geological Survey in analysis of the Palau Islands (1979).

Procedures

Multispectral analysis techniques were used to determine if patterns seen over the shoals were related to depth. This was accomplished by using a water reflectance model which accounts for reflection of light from the ocean bottom developed at the Environmental Research Institute of Michigan (ERIM) (Polcyn, 1976). Digital numbers calculated from the model were compared with actual digital numbers produced by the Landsat MSS to test whether patterns seen in the image were due to bottom reflectance or to surficial phenomena. The water-reflectance model used has been tested and proved useful for measuring water depths within 10 percent accuracy to depths of 20 meters in clear ocean water (Doak, et al., 1979). The environment of Cape Cod does not meet all the assumptions of the model, however, and results of the model are of limited accuracy. Despite this, use of this model was expected to aid in establishing whether or not features seen in the images can be correlated with reflected light from the sea bottom.

Water Reflectance Model and Estimation of Parameters

The energy received by the Landsat MSS sensors in band (i) over clear shallow water can be computed from:

$$V_i = V_{si} + K_{si} \frac{T_1 T_2}{\pi n^2} E_{oi} T_i R_{bi} e^{-2k_i Z}$$

$$\text{or, } (V_i - V_{si}) = V_{oi} e^{-2k_i Z}$$

where:

V_i = Landsat MSS signal value in volts

$*V_{si}$ = Signal over deep water

K_{si} = Landsat-1 low gain sensitivity constant (Taranik, 1978)
= (127/2.48) centimeters² steradian/milliwatt for MSS Band 4
= (127/2.00) centimeters² steradian/milliwatt for MSS Band 5
= (127/1.76) centimeters² steradian/milliwatt for MSS Band 6
= (63/4.60) centimeters² steradian/milliwatt for MSS Band 7

$T_1 = T_2 = 0.98$ = Air-water boundary transmittance

$n = 1.33$ = index of refraction of water

$*E_{oi}$ = Total irradiance in the spectral band (i) at the
water surface

T_i = Atmospheric radiance transmittance = 0.8

$*R_{bi}$ = Bottom reflectance

k_i = Water attenuation coefficient

Z = Depth of ocean bottom

$*V_{oi}$ = Signal as depth goes to 0, after subtraction of deep
water signal

The five variables indicated by * are those for which data needed to be derived or estimated from other information to use the model without field observations in the study area.

Solar Irradiance at Sea Level

Initially, the value for E_{oi} was calculated for all Landsat MSS bands from tables of solar irradiance at sea level for an air mass of two (Wolfe and Zissis, 1978). The Turner atmospheric model (Turner, 1974) was used to improve results of initial calculations from tabular data (Wolfe and Zissis, 1978) by more accurately modeling the shorter wavelength content of the solar spectrum for a sun elevation of 57°,

23 kilometers visibility, and an air mass of one at sea level. The computer printout for the solar irradiance is shown in Figure 29.

Improved values used were:

$E_{04} = 9.6700$	milliwatts/centimeter ²	steradian	
$E_{05} = 9.0225$	milliwatts/centimeter ²	steradian	Sun elevation 57°
$E_{06} = 7.0125$	milliwatts/centimeter ²	steradian	Visibility 23 kilometers
$E_{07} = 16.06125$	milliwatts/centimeter ²	steradian	Air Mass of one

These values of irradiance (incident to the normal plane) were multiplied by cosine 33°, to correct for the angle of incidence of direct solar irradiance at the plane of the water surface.

Deep Water Signal

In order to use the water-reflectance model as written $(V_i - V_{si}) = V_{oi} e^{-2k_i Z}$, one must first determine the deep water signal (V_{si}) in all bands. The deep water signal (V_{si}) (the lowest MSS spectral signal) represents the signal when direct solar irradiance is completely attenuated.

Eight likely areas within the scene were evaluated. The lowest signals in all bands were found in the area of "dark water" east of Monomoy Island (Figures 1 and 30). Water depth at this location is charted as 32.4 meters (107 feet). Computer listings, showing digital numbers (signal strength) in all four MSS bands, were generated with the 11 LINE software program developed at ERIM. This program uses Landsat Computer Compatible tape (CCT) data as input for manipulating and processing the data into various statistical and visual hard copy formats. Histograms, statistics, direct output of wave band digital

numbers (signal values) and line printer "grey-maps" can be generated. Selected within "dark-water" areas, 6x6 pixel subareas were averaged to obtain the lowest deep water signal. The deep water signals, in digital numbers, were: MSS Band 4, 18.63888; MSS Band 5, 8.47222; MSS Band 6, 4.1666; MSS Band 7, 0.38888. The apparent radiance was calculated by dividing the digital number by the sensitivity coefficient for each MSS Band. Apparent reflectance was calculated using the formula

$$R = \frac{\pi L}{E_{oi}}, \text{ where: } R = \text{apparent reflectance}$$

π = factor to convert cone of radiance to point source

L = apparent radiance

E_{oi} = irradiance of direct sunlight upon the water surface.

These values were plotted on semilog graph paper, together with plots of other reflectance values from other areas within the scene (Figure 31). The deep water signal is the lowest obtained over all the water areas. It is very significant that the deep water signal was found in an area shown to be calm, from direct observation from the Nantucket Lightship.

Sand and Foam Reflectivity

The solar irradiance and deep water signal parameters for the water reflectance model were easily derived from data on hand. To estimate the reflectance of the sea bottom for a geographic area 800 miles away was more of a problem. Sand can be highly variable in reflectance, and studies of sea bottom reflectivity are uncommon. Aircraft imagery and photography over the study area, from which

values of reflectivity could be derived, are also scarce. A study of upwelling radiance in the area for NOAA's National Environmental Satellite Service (NESS) had been recently initiated (Wright, 1979), but did not appear useful to the specific problem of this thesis. John Portney volunteered to send the author a sample of beach sand from Cape Cod National Seashore (1979), from which the spectral reflectivity of the sand could be measured in the laboratory. While one sample may not be fully representative of an entire pixel, and sand from mainland Cape Cod may not be representative of Nantucket Shoals, measurements from this sample were believed better than no measurement at all. The Cape Cod sand sample came from a high berm formed by Hurricane Camille, and represents the larger grain-size sand normally found offshore in high energy wave environments. It was acquired on 30 September 1979, on the east coast of Cape Cod, near South Wellfleet. It is not an unreasonable assumption, considering the geology of the area, that quartz-rich sand eroded from Cape Cod would be carried by littoral drift currents and deposited upon the shoals. Mineral composition of the sample was probably similar to that of sediments near Nantucket. Indeed, Nantucket Island, itself, represents the glacial moraine sediments.

The effects of sea state, breakers (cresting waves) and resulting sea form should be a consideration when evaluating the upwelling reflectance to the sensor; therefore, to set a benchmark estimate of what sea foam may look like radiometrically, a sample of Gillette Foamy Shaving Cream was used as a test material to simulate sea foam.

Spectral reflectivity measurements of the sand and foam samples were made with a Beckman DK-2A Spectroreflectometer at ERIM on 19 October 1979. Samples of dry sand and foam were each placed in tinfoil-lined film container cups. Glad-Wrap clear, polyethylene film was used to cover the sand sample. Barium sulfate (BaSO_4) was used as the reflectance standard. Instrument output was a series of analog plots of total hemispherical reflectance over wavelength for the spectral band from (λ_1) to (λ_2) (Figure 32).

Reflectivity of the foam and the film was read directly from the analog plots. However, because the reflectivity of the film varies from one wavelength to another and because a portion of the radiant energy is reflected a second time at the film plane before exiting to be recorded, the reflectivity of the sand could not be read directly from the analog plots. Reflectivity of the combination of sand and film components is represented by the following formula:

$$\rho(\text{combination of sand and film}) = \rho(\text{film}) + \frac{\tau^2(\text{film}) \cdot \rho(\text{sand})}{1 - \rho(\text{film}) \rho(\text{sand})}$$

which was solved for the reflectivity of sand at each wavelength

where: ρ = reflectivity

τ = Transmittance

$$\rho(\text{film}) = 1 - \tau(\text{film}).$$

Reflectivity for each sample (and transmissivity of the film) was determined at the midpoints of the Landsat bands of operation with the following results:

<u>Band</u>	<u>Spectral Midpoint</u>	<u>ρ Sand</u>	<u>ρ Foam</u>	<u>τ film</u>
4	5.5 micrometers	0.28	0.96	0.905
5	6.5 micrometers	0.36	0.96	0.908
6	7.5 micrometers	0.40	0.967	0.916
7	9.5 micrometers	0.50	0.92	0.915

Reflectivity of the shaving cream was nearly as high as the barium sulfate calibration plate. The effect of sea foam covering a portion of a water area viewed by the sensor can be estimated from:

$$\rho = (1-F) \rho \text{ water} + (F) \rho \text{ (foam)}$$

where F is the fraction of the resolution element covered by foam. For example, using data from MSS Band 7, where the reflectivity of water equals 0.005, calculation shows that if foam covered 5 percent of the water area, the resulting signal would be increased by a factor of ten, assuming transmission through the foam is negligible and that real sea foam is as reflective as the shaving cream.

Water Attenuation Coefficient

To estimate, the water attenuation coefficient, the last required parameter of the water reflectance model, a calibration site was selected on the gently sloping Billingsgate Shoal, located on the east side of Cape Cod Bay where it is somewhat better protected from waves by the shorter fetch of Cape Cod Bay (Figures 1, 4, 30, and 33). The shoal has a long and distinctive triangular shape with a gentle slope towards the deeper water of Cape Cod Bay. Charted depths can be easily correlated with line printer "grey-maps" to obtain line and point coordinates of digital numbers (signal counts) for the Billingsgate Shoal area.

A least squares regression was carried out to find the best linear fit between the line and point coordinates of digital numbers (signal counts) and the geographic coordinates from the bathymetric charts (Mercator projection) for selected, distinctive control points, and yielded the following equations:

$$\text{Line} = 2132.00 - 22.4130 (\text{Latitude}) + 3.3988 (\text{Longitude})$$

$$\text{Point} = 774.51 - 8.3388 (\text{Latitude}) - 23.0160 (\text{Longitude})$$

Files of positioned depths without tidal correction were then regressed against files of the logs of digital numbers (signal counts) in MSS Bands 4 and 5. Tidal information, although requested, had not been received. The slope of the regression line in each MSS band represents the apparent water attenuation coefficient for that band of operation. Scatter plots of the two bands are shown in Figures 34 and 35. The values for V_o and k were calculated from:

$$V_i - V_{si} = V_{oi} e^{-2kZ}$$

or:

$$\ln (V_i - V_{si}) = \ln V_{oi} - 2kZ.$$

The computed values for V_{oi} and k are then:

$$\begin{aligned} \text{MSS Band 4: } V_o &= e^{1.7887} = 5.98; k = 0.01528 (\text{foot}^{-1}) = \\ &0.05015 (\text{meter}^{-1}) \end{aligned}$$

$$\begin{aligned} \text{MSS Band 5: } V_o &= e^{1.6455} = 5.18; k = 0.2215 (\text{foot}^{-1}) = \\ &0.07267 (\text{meter}^{-1}) \end{aligned}$$

Comparing these values for MSS Band 4 and MSS Band 5 attenuation to values obtained by Jerlov (1976), reveals that the MSS Band 4 value of $0.0515 (\text{meter}^{-1})$ is about the same as the attenuation coefficients reported for areas of deep ocean. A ratio of MSS Band 5/MSS Band 4

should yield a value of approximately 0.25 and values for MSS Band 4 should range between 0.1 - 0.2 (meters⁻¹) (Lyzenga, 1980). MSS Band 5 values should range between 0.35 - 0.45 (meters⁻¹). The value for MSS Band 5 seemed far too low to be considered reasonable, because 0.07 (meters⁻¹) is lower than the absorption coefficient for water at that wave length. Because of this, the two-band calculation of water depth was not used, but the single-band calculation seemed to hold some promise for successfully relating the observed phenomenon to depth. The maximum depth that can be mapped using the MSS Band 4 attenuation coefficient would be equivalent to one digital number above the deep water signal. That is:

maximum depth Z - depth corresponding to $V - V_s = 1$ count

or, $\ln (V - V_s) = 0$. In this example it would be

$$\ln (V - V_s) = (0.7887 - 0.030564Z)$$

$$Z = 52.624 - 28.652 \ln (V - V_s)$$

$$Z_{\text{maximum}} = 16 \text{ meters.}$$

Experimental Displays of Tests

A symbolic display of depths, by single band calculation, was generated on the computer for the calibration site (Figure 36). Manual calculations using averaged pixel values showed depth values to be within reason for the chart, last surveyed in 1957.

The values of calculated depths seemed to be within reasonable (that is to say tolerable) limits for the Billingsgate Shoal calibration site. The digital display indicated a depth of roughly 2.5 meters \pm 2.5 meters compared to a 3.4 meters plotted depth at the

computer display coordinates line 934, point 215. The actual 3 x 3 pixel values compared to calculated theoretical signal values are as follows:

<u>MSS Band</u>	<u>Actual Signal</u>	<u>Calculated Theoretical Signal</u>
4	27.8889	28.7163
5	14.0000	10.3689
6	7.8889	4.2003
7	1.7778	0.3889

The actual reflectivity plotted with the calculated theoretical reflectivity is shown in Figure 7.

A display of the Pollock Rip subarea is shown in Figure 38. This display may be compared to the MSS Band 4 "grey-map" in Figure 39, and to the portion of the chart of the same area shown in Figure 40.

A depth map generated for the Old Man Shoal area off Nantucket (Figure 41), proved less successful. While it appears to show the shoal patterns, depth ranges do not adequately agree with the charted depths (Figure 42). A graphic plot of Old Man Shoal showing the bottom profile scaled from the charted bathymetric contours is compared with the actual MSS Band 4 reflectivity along display line 1799 in Figure 43. The geographic position of this line is shown in Figure 42. Actual reflectivity was calculated using a "moving window" averaging 3 x 3 pixels along the display line, then plotting the averaged reflectance corresponding to the pixel position of the depth contour. Figure 44 shows the plot of the actual signal, the averaged signal, and the computed theoretical signal to be expected

for pixel 721 in line 1799. The $V-V_g$ reflectivity is plotted in Figure 45 and indicates higher reflectivity in MSS Band 4 and MSS Band 5.

These two graphs indicate that the actual signal received by the sensor over the shoal is not the same as the signal expected from theoretically calculated values related to reflection of light from the ocean bottom. The same calculations were performed many times for other areas in the Nantucket Shoals, and the pattern of the graphic plots was similar.

A typical result of the plot of actual $V-V_g$ reflectivity is shown for an area, (pixel coordinates line 1789, point 708), which the author called Shoals "A," where the water depth was 9 meters (Figure 46). The reflectivities of the actual signals for MSS Band 6 and MSS Band 7 are much higher than the calculated theoretical values for MSS Band 6 and MSS Band 7. Calculations indicate that the water attenuation coefficients for these bands are so large that there would be negligible penetration, thereby producing a signal of zero. $V-V_g$ reflectivity plots consistently show higher reflectance for MSS Band 4 than the other bands. Figures 47 and 48 are the linear and log scale plots of $V-V_g$ reflectivity. When computed theoretical values of V were subtracted from the actual signal values in each band, and reflectivity was plotted, the plotted line is flatter and higher than zero. This suggests a contributing factor independent of wavelength. The proportions of the direct solar irradiance spectrum (E_{oi}) are the same as the proportions of the increased radiance (L_1) of the V - theoretical V shown in Table 5,

therefore, surface specular reflection is the most probable contributing agent.

Another peculiarity of the data set for this image is that MSS Band 7 signals are higher than those usually encountered (normally the range of 0 to 1 digital numbers). This scene had occasional values as high as four digital counts. Landsat data gathered by ERIM for the Bahamas test range did not exhibit such high values (Lyzenga, 1980). Figures 49 and 50 show the MSS Band 7 "grey-map" for Monomoy and Nantucket Islands and environs, and show the distribution of digital numbers higher than one for water areas. The higher counts cluster in areas of shoals and rips.

Effects of Sunlint

The $V-V_s$ reflectivity for the "grey-water" areas in the image was calculated to see what the reflectance spectrum looked like. Sunlint was suspected as the cause of the "grey-water" areas. The familiar pattern of the spectral signature of the shoals reappeared (Figure 51).

The similar pattern of the $V-V_s$ reflectivity graphs was enough cause to suspect that sunlint was the primary factor in the "grey-water" reflectivity, but further evidence was necessary. Analysis of the wave slope required to specularly reflect incident solar irradiance into the view of the sensor also supports the hypothesis. Considering that the MSS angle of view is 5° and that the solar elevation at the time of imaging was 57° , an estimation of the wave slope necessary to reflect direct sunlight in the direction of the

sensor is shown in Figure 52. Also, the satellite's orbital path is approximately 10° east of north, and at that time of year the sun in the east (azimuth of 120°) is more in the direction (within 10°) of the line-scan direction of the MSS scanner (Figure 53). The probability of sunglint will increase as the direction of scan approaches the direction of the sun.

A much more rigorous solution to determine the wave slope necessary to reflect solar irradiation "down the throat" of the sensor uses unit vectors. Figure 54 illustrates this approach to the problem, where:

$$\vec{S} = \text{Solar direction unit vector} = (\sin 33^\circ \sin 120^\circ; \sin 33^\circ \cos 120^\circ; \cos 33^\circ)$$

$$\vec{V} = \text{View direction unit vector} = (\sin 5^\circ \sin 100^\circ; \sin 5^\circ \cos 100^\circ; \cos 5^\circ)$$

$$\vec{N} = \text{Wave normal } \frac{1}{2} \text{ unit vector} = \frac{(\vec{S} + \vec{V})}{(|\vec{S} + \vec{V}|)}$$

The result is a vector that has the coordinates:

$$X(0.278), Y(-0.144), \text{ and } Z(0.917)$$

The orientation of the wave is the arc tangent of $\frac{X}{Y} = 1.939 = 62.7^\circ$

The slope of the wave is the complement of the arc cosine of

$$X = 0.304 = (90^\circ - 72.30^\circ) = 17.69^\circ$$

Of the three wind directions recorded for the time of imaging (Table 2), both Chatham Coast Guard Station and Nantucket Lightship recorded a wind direction from the north-northeast, and Nantucket Lightship recorded a swell direction of 330° . The X axis for the computation is east, so 90° should be added to 62.7° to equal 152.7° , which

is nearly perpendicular to the direction of the wind. Therefore, because the orientation and slope of the wave necessary to specularly reflect irradiance to the sensor agrees with the known conditions, the chances of sunglint are nearly certain. The conclusive evidence of sunglint, that is a directional change due to a change of viewing angle recorded by an instantaneous sensor (the RBV sensor) is absent. The RBV was not used for the scenes imaged by the MSS sensor.

The reflectivity graph was approximately equal in all bands except MSS Band 4. Occasionally the reflectance in MSS Band 4 was as much as 1.6 times higher than the other three bands. Figure 51 is included to illustrate the pattern of the graphs. This phenomenon is very interesting, because if specular reflection (sunglint) is the cause of the "grey-water" areas, reflectivity in all four bands must be equal. Turner's atmospheric model was used to recalculate the reflectance to more accurately model the shorter wavelength portion of the spectrum for an air mass of one. The result of the calculations did not remove the MSS Band 4 "spike" in the graphs.

An error in radiometric calibration could cause such a variation between the spectral bands. Studies of calibration for Landsat-1 are currently in progress (Chance, 1980). Errors in radiometric calibration have been noted in the past for Landsat-2 for the period of 22 January to 15 July 1975 by Colvocoresses (1977), and corrections have been reported by NASA (Anonymous, 1977).

However, on the assumption that the radiometric calibration for Landsat-1 during the period in question is correct, there are other

possible explanations of this phenomenon. White caps may reflect an increased amount of skylight, in addition to direct sunlight, into the field of view of the sensor. The proportion of skylight is greater in MSS Band 4 and would add to the apparent reflectance. If such turbulence was present, MSS Band 4 would be more affected by the light scattered from submerged air bubbles because of its deeper water penetration, than in the other bands (Lyzenga, 1980). It is reasonable to assume, but cannot be proven from the data available, that wind speed may be higher in "grey-water" areas. A higher wind speed, acting in conjunction with the longer fetch of the ocean, could produce more whitecaps than were recorded at Chatham (Table 2). The phenomenon of variation of reflectance in the image is, in itself, perhaps the best evidence of higher sea state conditions when there is no other contrary evidence.

It should be emphasized that the water reflectance model used in this study deals with the reflectance of light from the ocean bottom, and does not include the phenomenon of variation in surface and near-surface reflectance (Polcyn, 1976). The signature used for Figure 51 came from an area which was charted to be 55 meters deep.

Another possible explanation which was only briefly considered as a cause of the additional upwelling radiance in MSS Band 4 was that of marine organisms, such as phytoplankton which might be a factor; however, any added contribution to upwelling reflectance caused by phytoplankton's Chlorophyll A would cancel in the equation used. The very small contribution (Figure 55) from phytoplankton would be difficult to detect with the Landsat MSS, even with a ship on-site to

verify the organism's presence (Hovis, 1980). It is also unlikely that they would have any correlation to the patterns in the image.

Turbidity Effects

An area (Figure 56) within Nantucket Sound, which was thought to contain turbid water (from Multitemporal Analyses), was evaluated multispectrally to see how the plotted signature differed from other plots (Figure 57). The slope increased from MSS Band 6 to MSS Band 7 for the $V-V_g$ plotted signal values (compare to Figure 48). The other three curves on Figure 57 represent the simulated $V-V_g$ curves computed from the Quasi-Single-Scattering (QSS) model of Gordon (1973) using different water attenuation coefficients for the Jerlov (1976) water types. Theoretical modeling studies by Maul and Gordon (1975) have shown that the water reflectance can be approximated by the equation:

$$R = K \frac{ab}{a + b}$$

where: R = reflectivity

K = geometric factor equal to 0.27

a = the absorption coefficient of water

(including dissolved and/or suspended material)

b = the backscattering coefficient (the fraction of the total scattering coefficient which results in scattering in the backward hemisphere)

For these computations \underline{R} was set equal to the reflectivity of MSS Band 4; \underline{a} was set equal to Jerlov's coefficient for water type 9 for coastal water; the equation was then solved for \underline{b} . The value for

b was then used for all other bands of operation, assuming that scattering was independent of wavelength. The same procedure was used for other water attenuation coefficients for each of the other water types.

The graphs on Figure 57 indicate that turbidity is present and that, as expected, the initial constants selected for use with the water-reflectance model would cause errors in depth measurement (Polcyn, 1976). In addition, there were probably surficial effects which would also cause errors, just as if there were a variation of turbidity density.

The Old Man Shoal $V-V_s$ reflectivity (Figures 45 and 58) was examined for turbidity, with the knowledge that evidence of sunglint had been demonstrated. The reflectivity bias at all four wavelengths was set at 2.3 percent, because the reflectivity in MSS Band 6 and MSS Band 7 was approximately flat and equal to 2.3 percent. The two main water-penetrating bands (MSS Bands 4 and 5) would therefore, have contributions not only from depth but also from suspected turbidity.

QSS-simulated reflectance curves were generated in the same manner as before, except that the bias had been subtracted from the MSS Band 4 reflectivity. The actual $V-V_s$ curve fell between the theoretical curves for 0.19 and 0.12 ($k_d \cdot \text{meter}^{-1}$) and may be more appropriate for water depth measurements over this local area of the Old Man Shoal, where turbidity and sunglint both are present.

Sea Foam Consideration

Sea foam as a Lambertian reflector could raise the signal value in the same manner as sunglint, except sea foam reflectance is not directional. When the transect across Old Man Shoal was mapped in Figure 43, it was noted that the highest signal values did not fall exactly on the peak of the charted shoal, but were offset in the westward direction by one pixel. This could be explained by the action of waves breaking over the shoal creating and spreading sea foam. Another explanation is that the shoal could have migrated or changed shape since it was last surveyed 23 years ago.

Surface Manifestations of Internal Waves

Figure 59 is a "grey-map" of the surface manifestation of internal waves. There are approximately seven waves across the display of 124 pixels from points 625-749. There is also some apparent refraction with other waves in the display. The leading wave is propagating westward in the convex direction of the arc. The period between successive waves diminishes from approximately 1,368 meters at the leading wave to approximately 625 meters at the eastern edge of the display. The wave is oriented about 10° east from north.

A plot of the digital numbers in each multispectral band across the leading wave in line 1031, points 625 through 654, is shown in Figure 60. The wave is sinusoidal in each band. The slopes of lines drawn from the highest signal in each band to the lowest signal in each band are different on each side of the wave form. Table 6 lists the approximate slope for each band of operation on the eastern and

western sides of the wave form. The rate of signal increase in each band on the eastern side of the wave form is approximately half that of the rate of signal increase on the western side of the wave form. The lowest digital numbers lie clustered on the eastern side of the plot. The lowest MSS Band 4 digital number is approximately five digital numbers higher than the deep water signal at 18.6, so there is some additional radiance other than diffuse radiance in the recorded signal. This observation of the surface manifestation of internal waves seems to match other observations in nearly every respect, even to the time of year, direction of propagation, and dark band trailing the leading edge of the wave form. The shape of the leading wave (the actual physical wave), is probably different than the shape of the trailing waves, as suggested by the pattern of the wave propagation of the internal wave itself. This fact is illustrated in the work of Neumann and Pierson ((1966) (Figure 38)) and in studies by LaFond and Cox ((1962) (Figure 57)) indicating that the leading wave has a higher amplitude than succeeding waves. Specular reflection from the leading wave surface may actually enter a water surface nearby, depending on the shape of the wave, and therefore be absorbed. This could explain the dark trailing band when propagating westward. If the surface was slightly rough, the reflection from small facets could explain the higher signal received at the sensor rather than the expected lower signal from diffuse deep water.

Summary of the Multispectral Analyses

The water-reflectance model developed by Polcyn (1976) at ERIM, was applied to the low-gain Landsat CCT for the 17 July 1974 image

(1724-14472) of Cape Cod in order to aid the interpretation of hydrographic features. The techniques used to extract bathymetry remotely from successful tests in clear ocean waters were applied to subareas in the scene whose characteristics were unknown. The purpose was not solely to map depths with high accuracy, but rather to determine if the signals received by the Landsat sensor were from bottom reflectance.

1

Estimates of the variable parameters of the water reflectance model were derived from existing data rather than through direct measurement. Transformation of pixel coordinates to geographic coordinates was accomplished by a least squares regression. Charted depths and positions were regressed to provide an apparent coefficient of attenuation for the water over Billingsgate Shoal. Estimates of the variable parameter of bottom reflectance and possible surficial sea foam were taken from reflectivity and transmission spectra measured from Cape Cod sand and simulated sea foam.

Computer-generated depth maps, using a single-band algorithm for depth measurement, and "grey-maps" were created for the initial calibration area and other areas within the image. The relationship to depth was judged by comparison with charted depths and comparison with theoretically computed depths and theoretical signals calculated from such depths.

The signals for image patterns over the area of Old Man Shoal did not correlate well with bottom reflected energy. The other areas tested were more accurate, when compared to charted depths and to theoretical signals calculated from such depth.

Several working hypotheses were tested to account for the cause of the errors. Sunlint (specular reflectance) was shown to be the primary cause of a significant bias in the signal and also the cause of variations of reflectivity in deep ocean water areas. An interesting variability of the reflectivity between the four MSS spectral bands of the MSS sensor was also observed. This phenomenon was attributed to surface turbulence of whitecaps, multiple scattering of submerged bubbles, or additional reflection of skylight in the field of view of the sensor.

The hypothesis that turbidity was present in the local water above Old Man Shoal was evaluated by comparing reflectances from the depth algorithm to the QSS model for turbid water and to graphs of calculated theoretical values. Techniques comparing simulated reflectivity curves to actual calculated reflectivities were used to estimate more appropriate water attenuation coefficients.

Sunlint and turbidity contribute to the increased visibility of the feature in question. Digital displays and observations on the identified surface manifestations agree with previous studies.

SUMMARY AND CONCLUSIONS

The Cape Cod study site represents a unique marine environment. It is subject to prevailing winds from the southwest in summer and to gales from the northeast in winter. The geologically young (Pleistocene) glacial deposits are subject to high rates of erosion and aggradation from the action of winds, waves, and currents. The physiography of the coast and continental shelf is the result of geologically recent innundation from melting glaciers. Offshore sediments represent relict beaches and the waters are relatively clear because areas of turbid water are contained within estuaries, or the turbid water is flushed into the deep ocean by the rapid action of wind, waves, and strong currents.

Space imagery can provide highly detailed information about the coastal and offshore features, some of which will never appear on standard nautical charts. Bottom areas in the near shore marine environment can change slowly over time and also change rapidly in response to catastrophic storms. In either event, the resulting ocean bottom changes can represent hazards to navigation. Charts of such areas will require frequent correction and, if resources are available, will require frequent revision. Detection of these hazards to navigation and their subsequent publication to the maritime community is the subject of great international concern.

Findings of this study support use of Landsat imagery to ascertain bottom changes, coastal changes and man made changes for the following

purposes: Initiation of appropriate marine warnings such as Notice to Mariners for hazards to navigation; and, when supported by ground truth data, chart revision.

Large areal coverage, repetitive coverage, and multispectral qualities of Landsat data can provide significant benefits to the hydrographic community. Information can be derived remotely which amplifies, complements, or supplements studies done from aircraft and ships. Information can be obtained that is beyond the capability of single band sensor systems or from conventional stereo-compilation methodology. Landsat MSS imagery provides additional information and furnishes evidence to support conclusions about observed phenomena. For example, one result of this study was to show that data significant to hydrographic mapping for the Cape Cod area was surprisingly difficult to obtain even though the water around Cape Cod is an active, offshore area for both economic and defense purposes. Most space imagery available is neither cloud free, nor without some sea state. Hydrographic survey data is out of date and oceanographic data is sparse because of data collection hazards posed by the shoals. With the significance of the Nantucket Shoals area to the maritime community, and its well established reputation as a grave yard for ships, the lack of a detailed environmental data base or even a plan to collect such data seemed peculiar.

To aid interpretation, relatively new techniques were applied to determine bathymetry from the image data. Some image patterns were identified as being the surface manifestation of internal waves.

Other patterns seen over the shoals and, Old Man Shoal in particular (Figure 1A), resulted from both surface phenomena and bottom reflectance. The Landsat signals received give erroneous depth measurements due to turbidity, and the signals appear to be primarily due to surface effects. From all evidence gathered, these surface effects include both sunglint and surface turbulence.

Analysis of "grey-water" patterns shows that their reflectance spectrum is similar to those for shoal areas. All evidence gathered suggests that the cause of the lighter patterns is sunglint and surface turbulence; but, because these patterns occur in deep water they would not endanger ships.

The author believes that this report demonstrates the need for and feasibility of extracting bathymetry data from Landsat records, and provides some guidance to other users of these same data analysis techniques. The study of the sea as a specular and diffuse reflector is a long term continuing process. Efforts should be started to determine the best way of estimating water turbidity on satellite images, including an analysis of shadows from clouds or contrails and their utility in accurately measuring turbidity. A second area of study should be directed at determining whether or not shoals can be detected from local turbidity densities, as suggested by the analysis of Old Man Shoal in this paper.

Figure 1. Cape Cod, Massachusetts and Environs.

(Note: Data for each image is provided and descriptors will not be repeated on succeeding caption pages. Data are as follows:

Image Identification Number = 1724-14472

Sensor and Spectral Band = Landsat-1 band 5

Acquisition Date = 17 July 1974

Scale = 1:1,000,000

Wind Speed, Direction and

Reporting Station = 14 knots 20° (Nantucket Tower)

Nantucket Tide Level above

Low Mean Sea Level (if

Available) = 2.3 meters

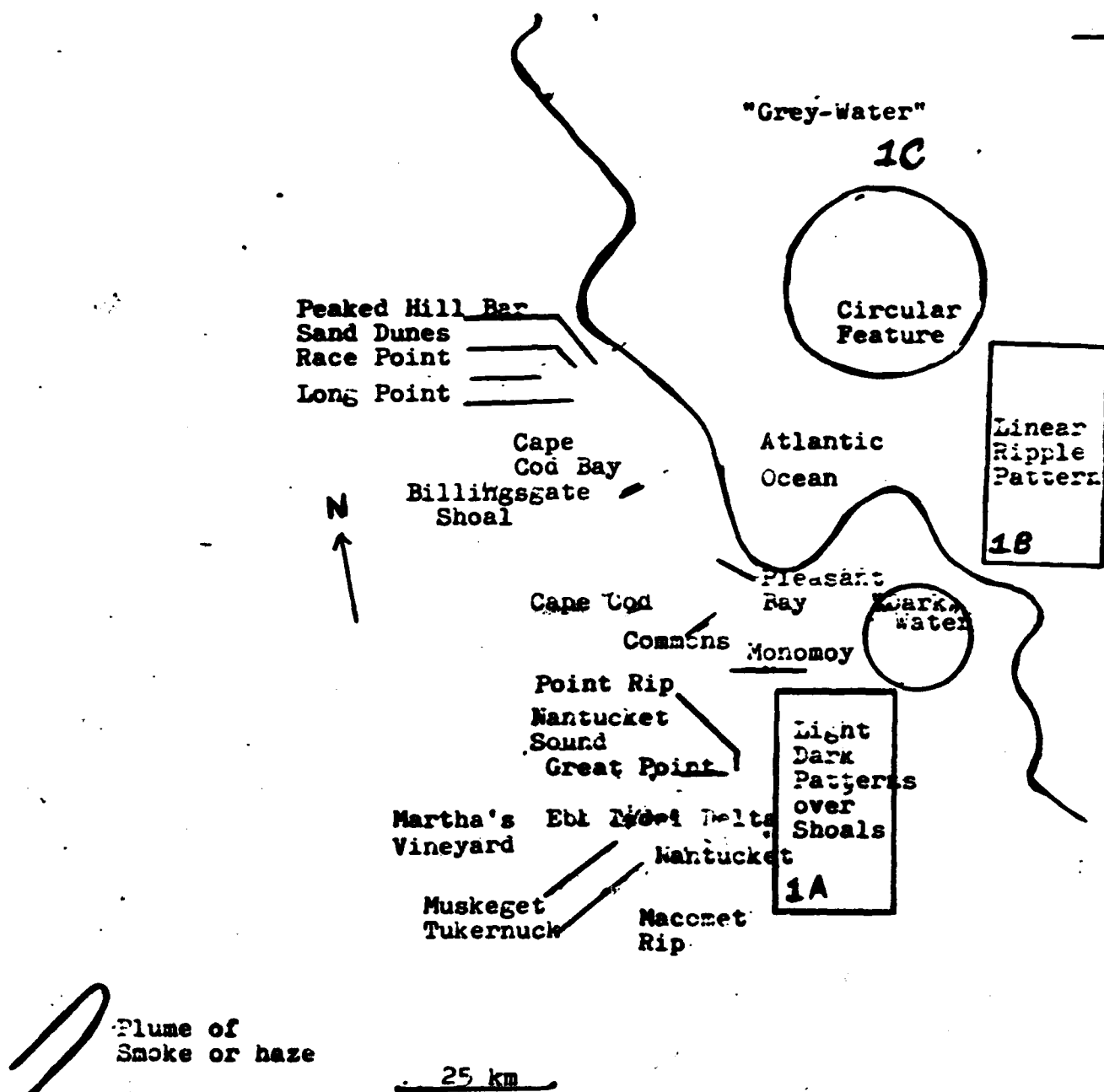
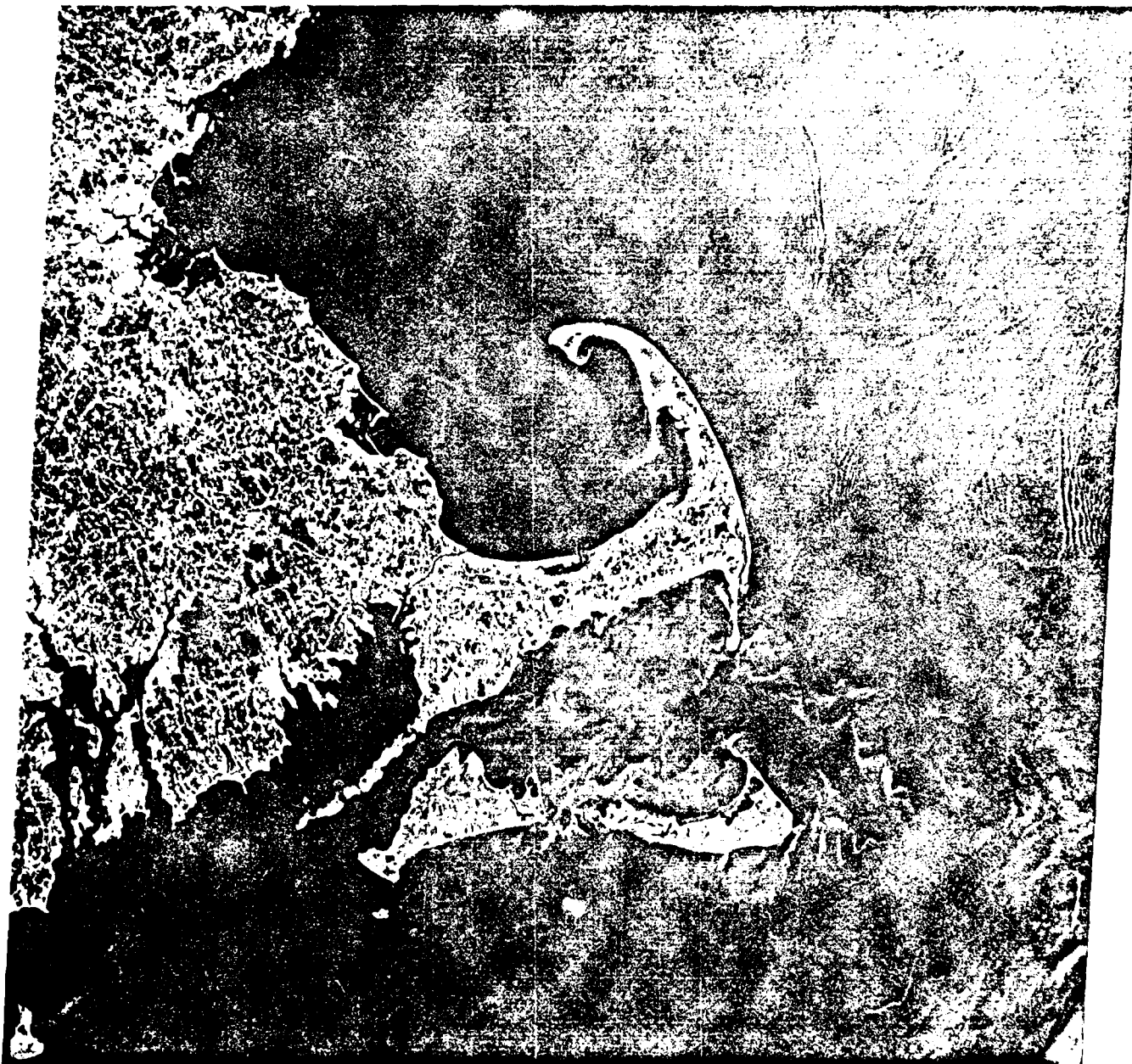


Figure 1. Cape Cod, Massachusetts and Environs:

1043-1-202



NR41-001

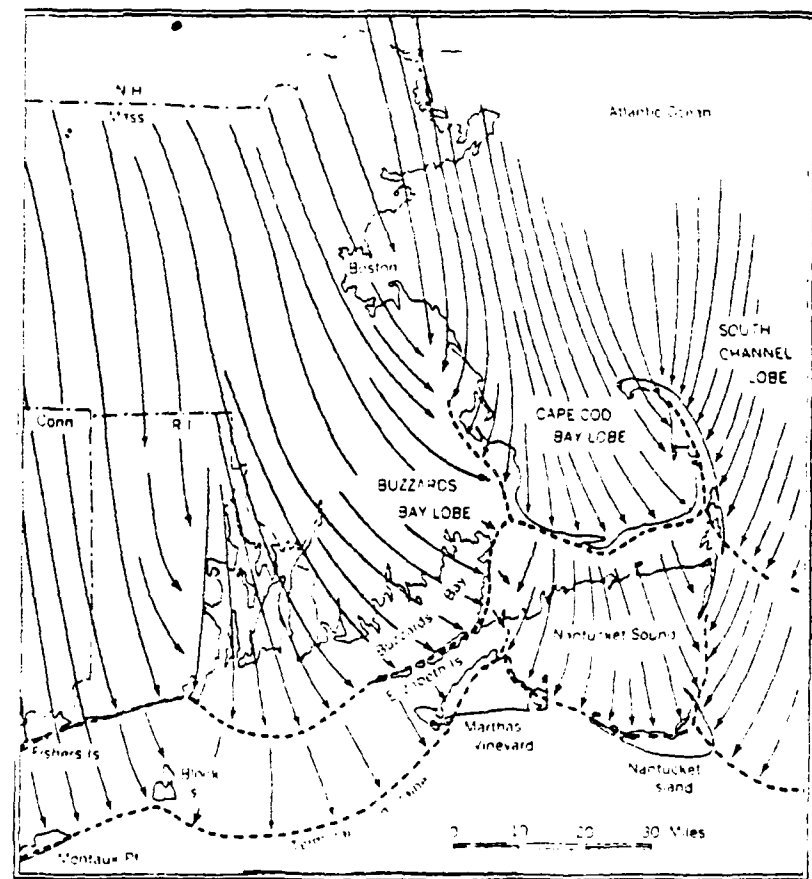


Figure 2. Glacial Lobes and Deposition Lines (from Strahler, 1966).

Cape Cod Peninsula

Martha's Vineyard

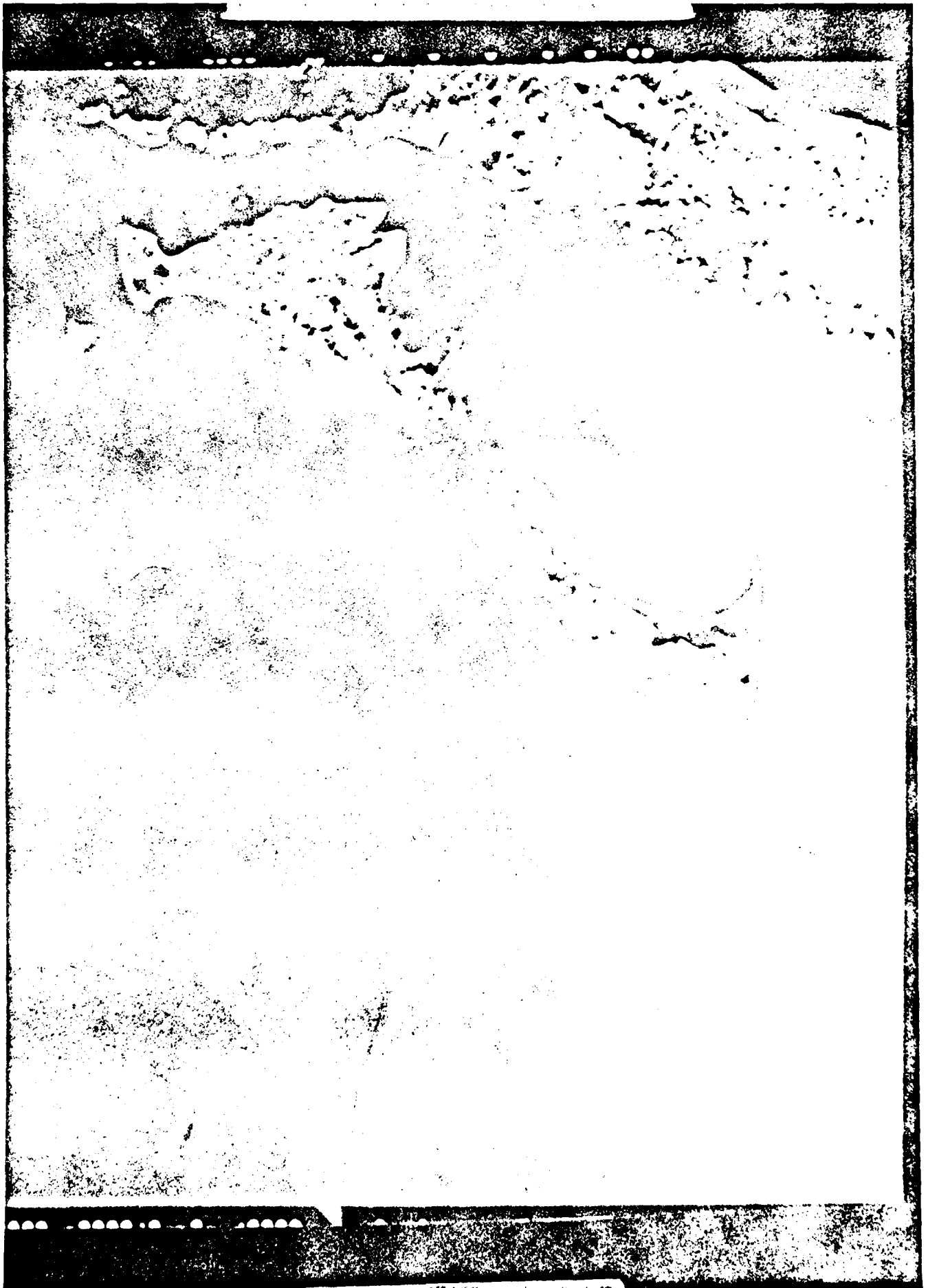


Nantucket

25 km

Nantucket Shoals

Figure 3. Color Print from Transparency Taken
by Skylab S-190B Showing Shoals of Nantucket.



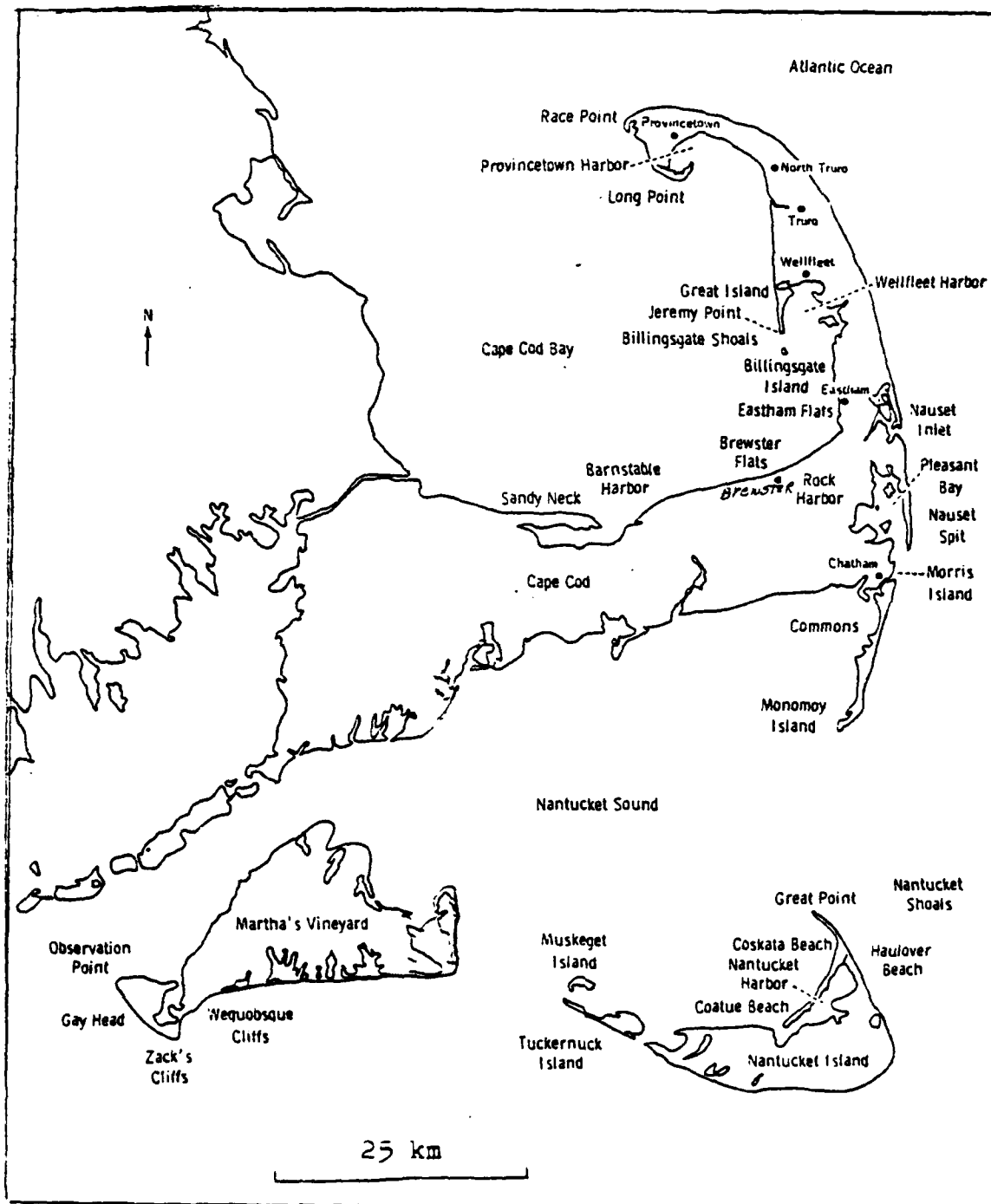


Figure 4. Index Map of Cape Cod, Nantucket, and Martha's Vineyard (from Tisdall and El-Baz, 1979).

Figure 5. Portion of Landsat-3 RBV Image Showing Details of
Cuspate Shoreline in Nantucket Harbor and Subaqueous
Hydrographic Features.

30041-14433

Landsat-3 RBV (0.505-0.750) micrometers

15 April 1978

1:500,000

20 knots NW (Chatham)

1.9 meters

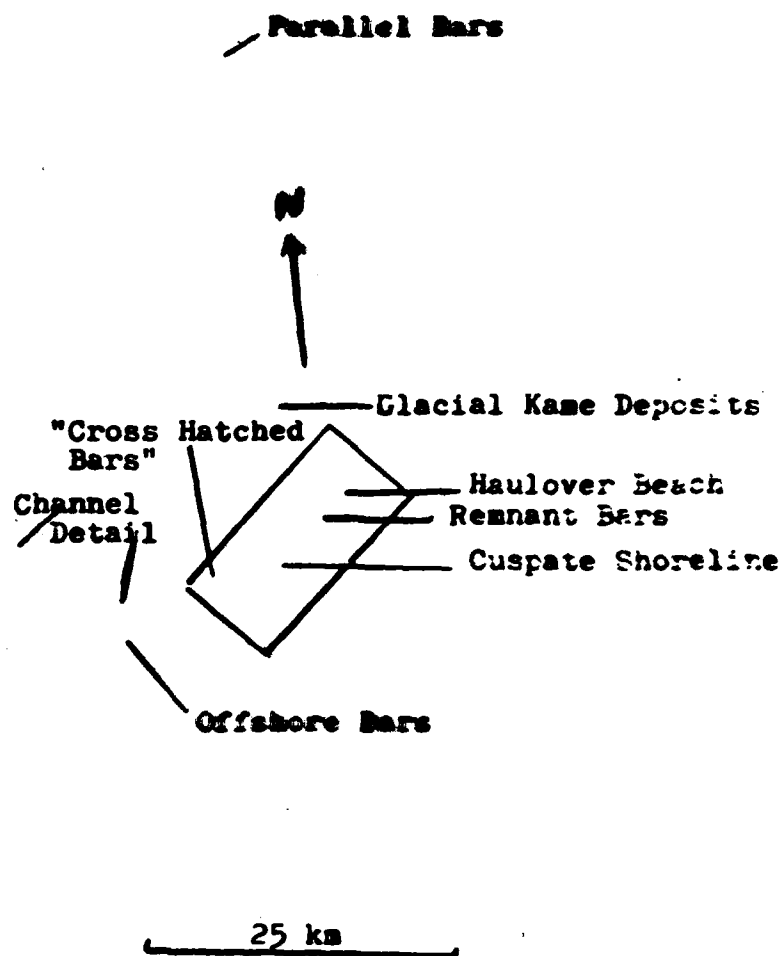


Figure 5. Portion of Landsat-3 RBV Image +
 Showing Details of Cusate Shoreline in
 Nantucket Harbor and Subaqueous Hydrographic
 Features.



15APR78 C N41-08/4069-45 D012-031 N N41-36/4070-06 R DDXBI SUN EL49 f

Exadix

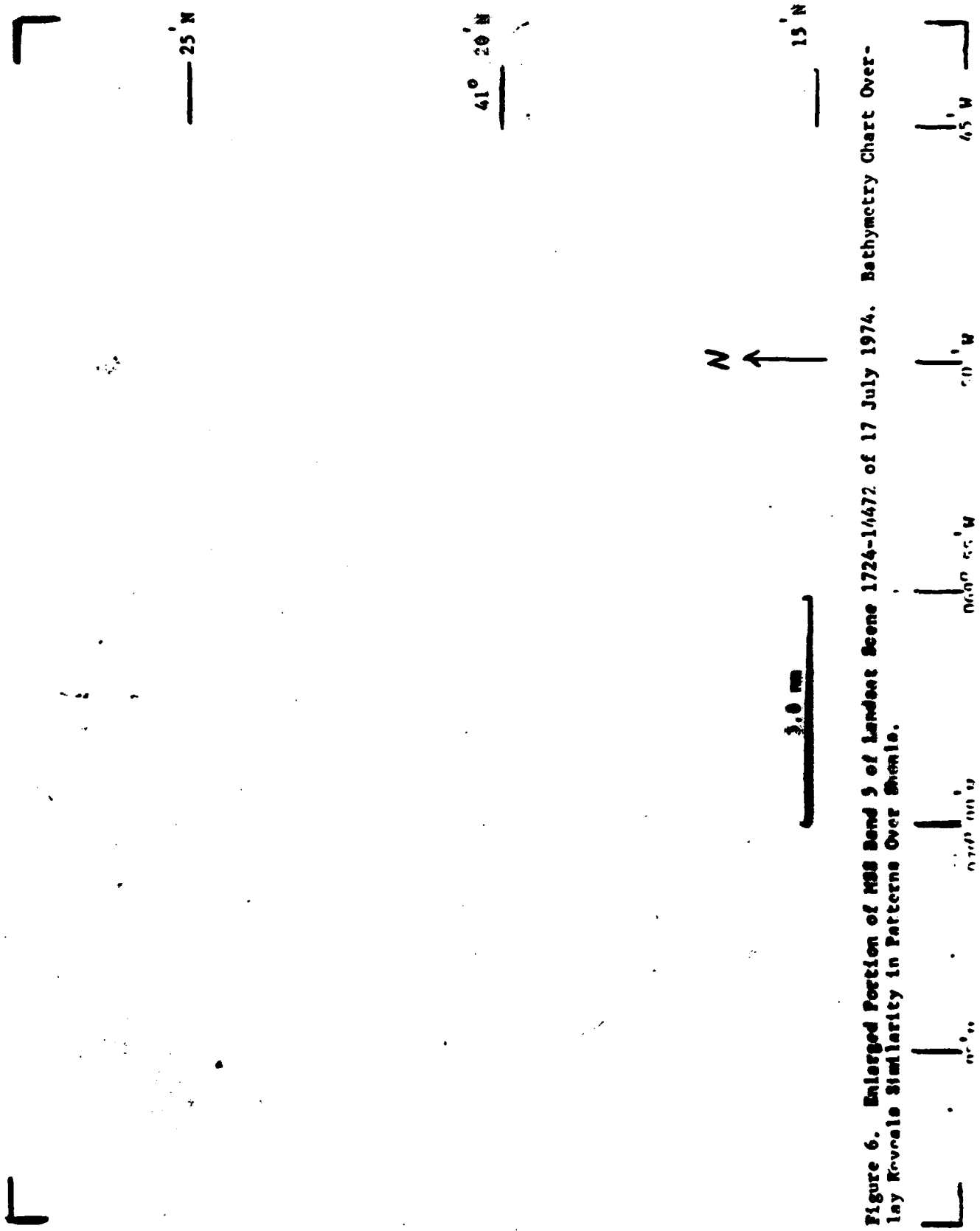
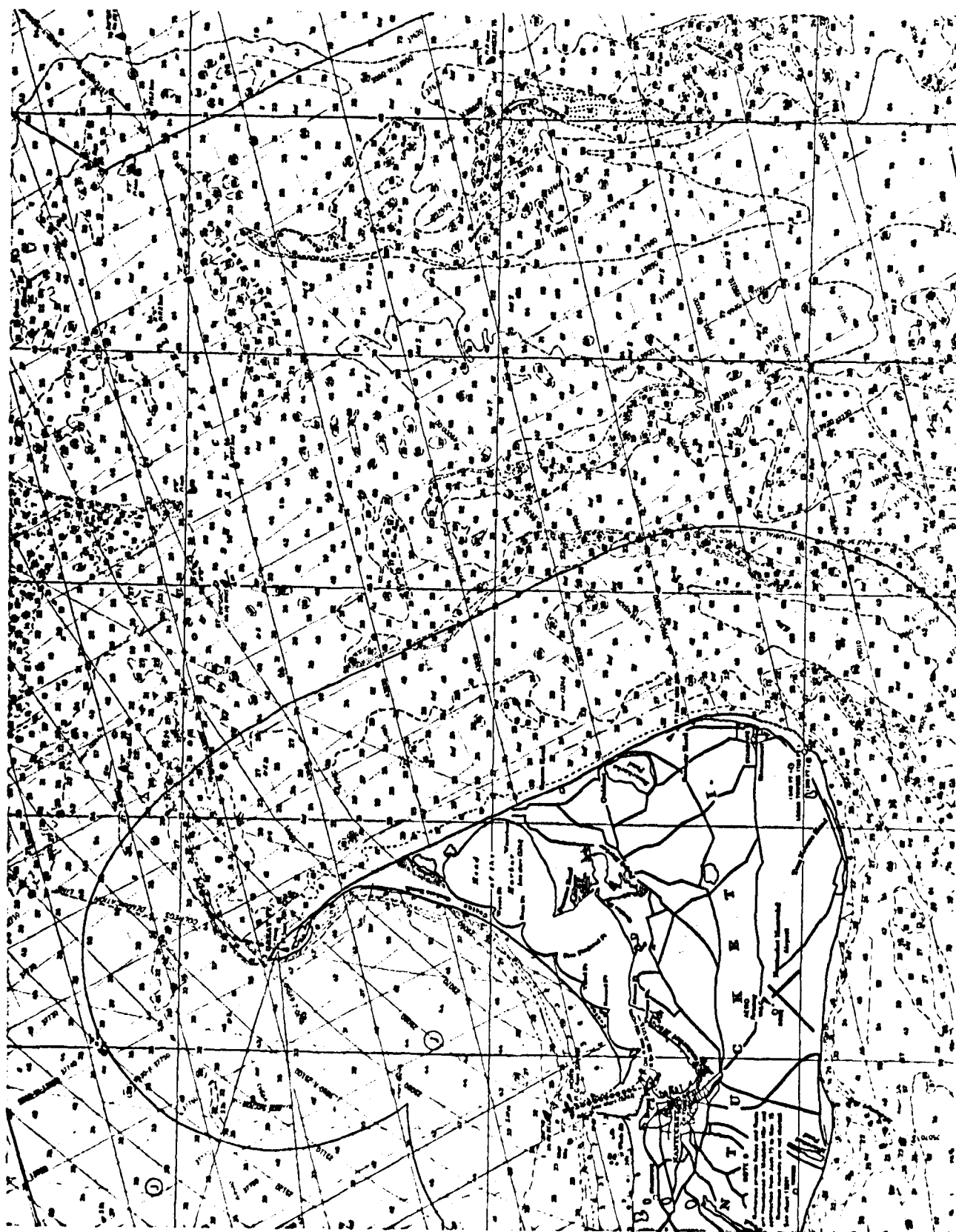


Figure 6. Enlarged Portion of MSS Band 3 of Landsat Scene 1724-1/472 of 17 July 1974. Bathymetry Chart Overlay Reveals Similarity in Patterns Over Shoals.



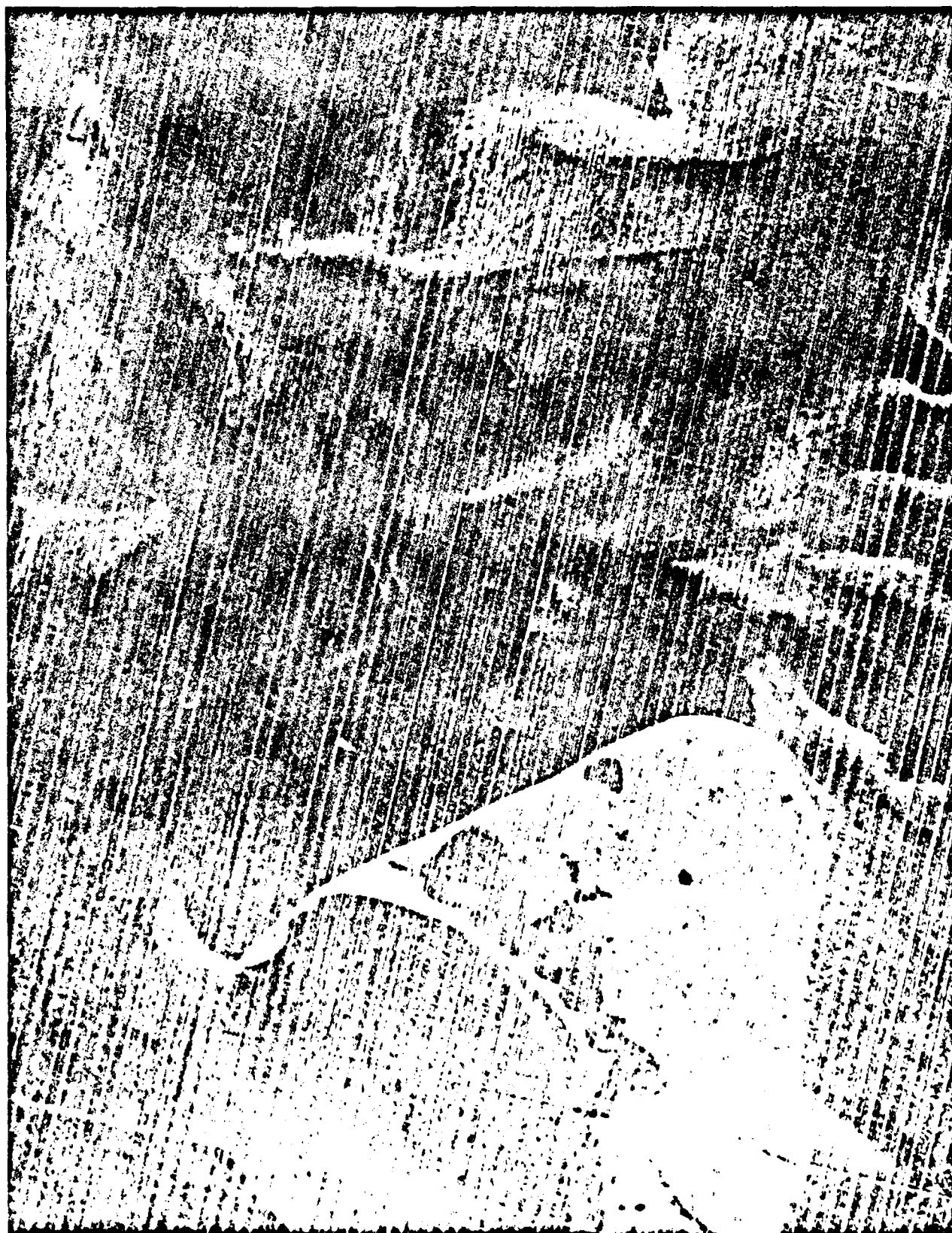


Figure 6. Enlarged Portion of MSS Band 5 of Landsat Scene 1724-14472 of 17 July 1974.
Bathymetry Chart Overlay Reveals Similarity in Patterns Over Shoals.

Figure 7. Landsat MSS Band 4 Image Showing Edge Definition of
Pattern Related to Direction of Wind.

2126-14440

Landsat-2 MSS Band 4

28 May 1975

1:1,000,000

6 knots 330° (Nantucket Lightship)

1.3 meters

+

N
↑

Direction of Wind
↘



Sharp and
Diffuse Edge
Definition
of Pattern.

20 km

+

Figure 7. Landsat MSS Band 4 Image Showing Edge
Definition of Pattern Related to Direction of Wind.

1001N50Z

1001N50Z

1001N50Z



W071-001 W070-301 W070-001 W069-301
28MAY75 C N41-32/W070-09 N N41-32/W070-05 MSS 4 D SUN EL58 AZ121 191-1755-N-1-N-D-2L NASA ERTS F-2126-14440-4 01

W071-001

N041-001

W070-301

W070-001

W069-301

T



25 km

L

+

+

Figure 8. Landsat MSS Band 4 Image showing patterns of Sea State. (Note: Compare water surface patterns to Figures 7-10.)

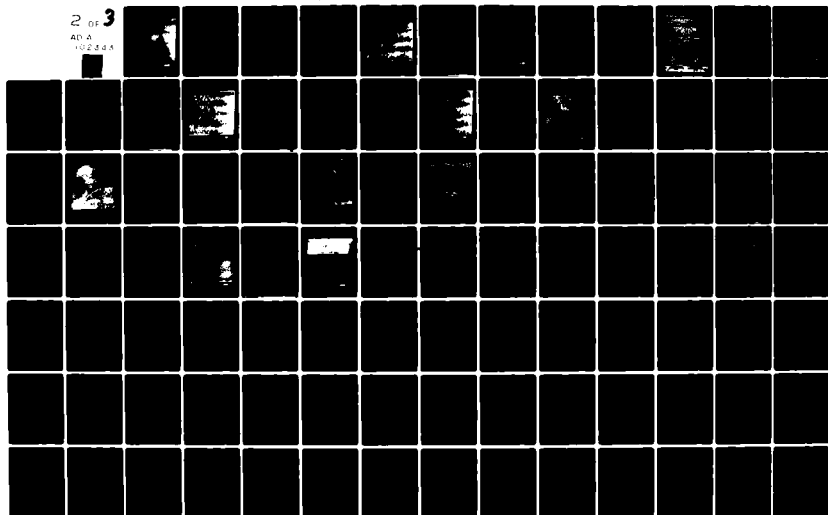
AD-A102 343

DEFENSE MAPPING AGENCY HYDROGRAPHIC/ TOPOGRAPHIC CENT--ETC F/6 8/10
INTERPRETATION OF HYDROGRAPHIC FEATURES SEEN IN THE WATERS OFF --ETC(U)
MAY 81 C L REED

UNCLASSIFIED

NL

2 of 3
AD-A
102343



W071-001

W070-301

W070-001

W071-301

W070-30

13 MAY 76

199 JAN 82

199 JAN 82



W071-301 N041-001 W071-00
13 MAY 76 C N41-46/W070-29 N N41-44/W070-18 HSS 4

W070-301 W070-001
D SUN EL51 AZ115 190-9381-N-1-N-P-2L NASA ERTS E-5390-14124-4 81

W071-301

W071-001

W070-301

W070-001

0000

Figure 8. Landsat MSS Band 4 Image Showing Patterns of Sea State.

(Note: Compare water surface patterns to Figures 7-10.)

5390-14124

Landsat-1 MSS Band 4

13 May 1976

1:1,000,000

12 knots W (Chatham)

1.9 meters

Figure 9. Landsat MSS Band 4 Image Showing Few Visible Patterns
in the Ocean due to Calm Sea State, High Tide, and
Low Sun Angle. Difference in Brightness of Land
Surfaces is Attributed to Snow Accumulation.

30004-14435

Landsat-3 MSS Band 4

9 March 1978

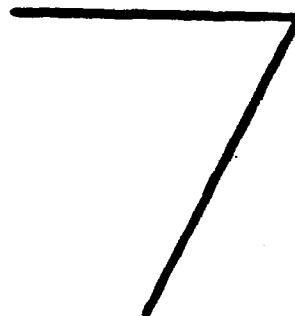
1:1,000,000

Calm (Nantucket Tower)

2.4 meters



Difference in
Brightness of
Land Surfaces



Few Patterns Visible
in Ocean

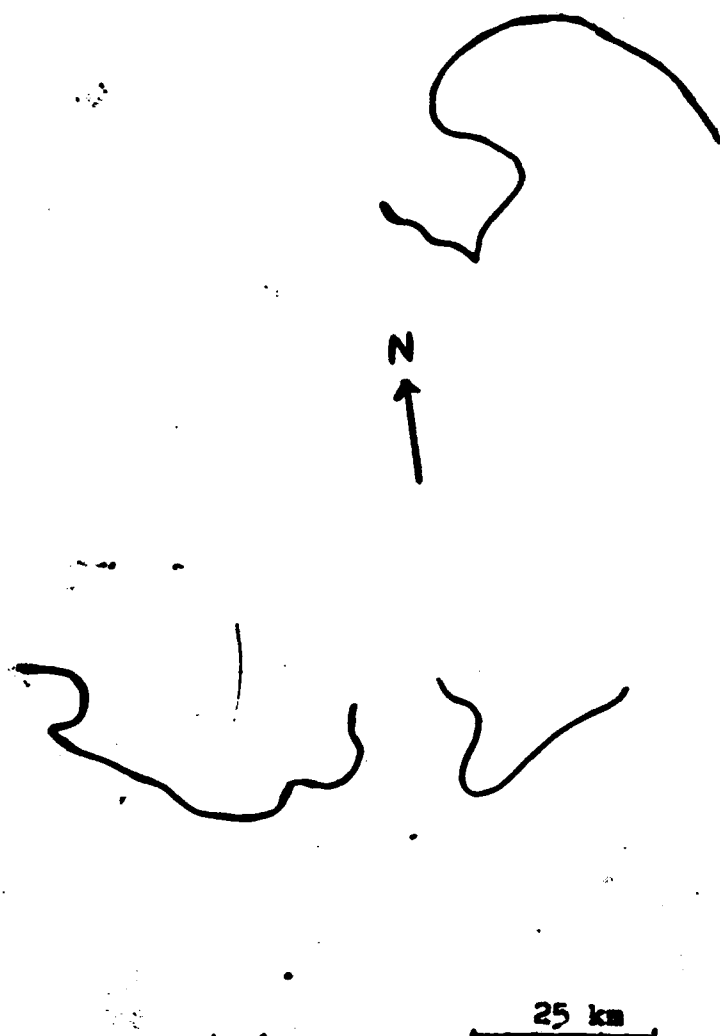
25 km

Figure 9. Landsat MSS Band 4 Image Showing Few Visible Patterns in the Ocean due to Calm Sea State High Tide, and Low Sun Angle. Difference in Brightness of Land Surfaces is Attributed to Snow Accumulation.



315-7 N 22 HIGH CAVIAR 2 0000

N041 - 001



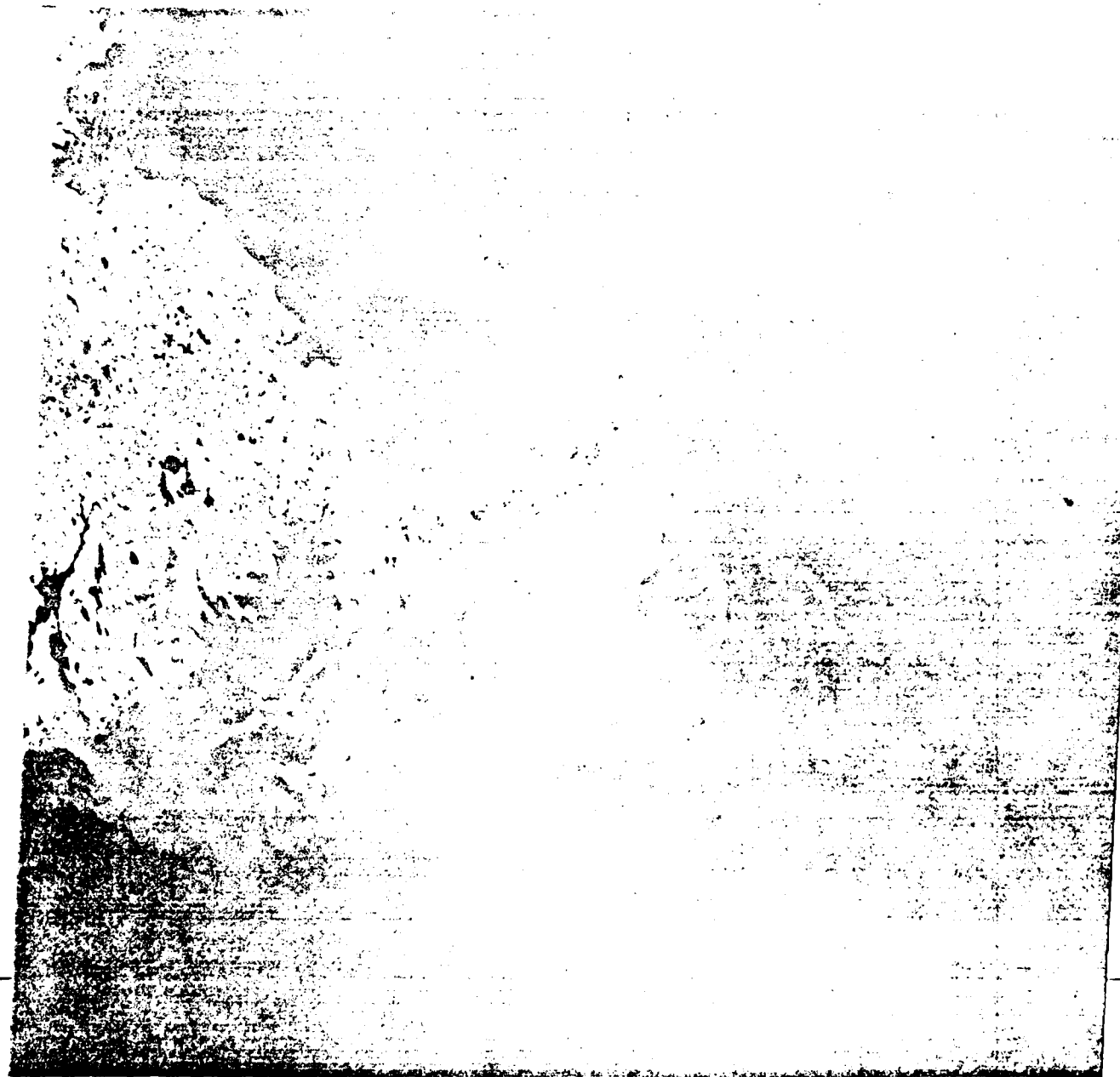
+

Figure 10. Water Mass Boundaries that are Possibly Due to Biological Activity are Recorded in this Image which also illustrates the Effects of Radiometric "Clipping."

100 IN AGZ

100 IN AGZ

100 IN AGZ



22 APR 75 C N41-37/4070-10 N N41-36/4070-04 MSS 4 D SUN EL51 RZ131 191-1253-N-1-N-D-2L NASA ERTS F-2090-14441-4 01

0000

Figure 10. Water Mass Boundaries that are Possibly due to
Biological Activity are Recorded in this Image which
also Illustrates the Effects of Radiometric "Clipping."

2090-14471

Landsat-2 MSS Band 4

22 April 1975

1:1,000,000

10 knots WSW (Chatham)

2.2 meters

Figure 11. Coastal Changes of Cape Cod Monitored by Landsat
(From U.S. Geological Survey).

COASTAL CHANGES OF CAPE COD MONITORED BY LANDSAT

Landsat-1 MSS



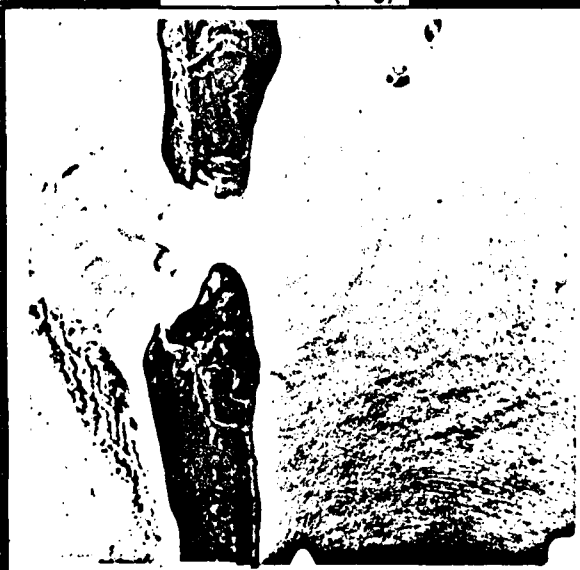
July 1974, 1:1,000,000 scale
Monomoy Island is continuous

Landsat-3 RBV



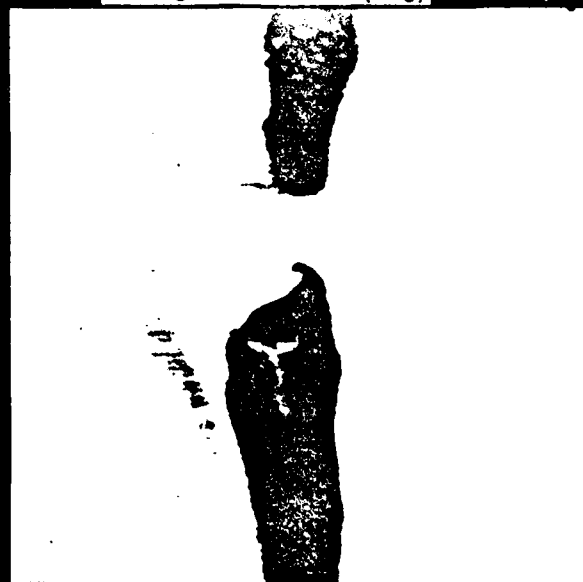
March 1978, 1:500,000 scale
500 meter rupture in Monomoy Island

Aerial Photo (Neg)



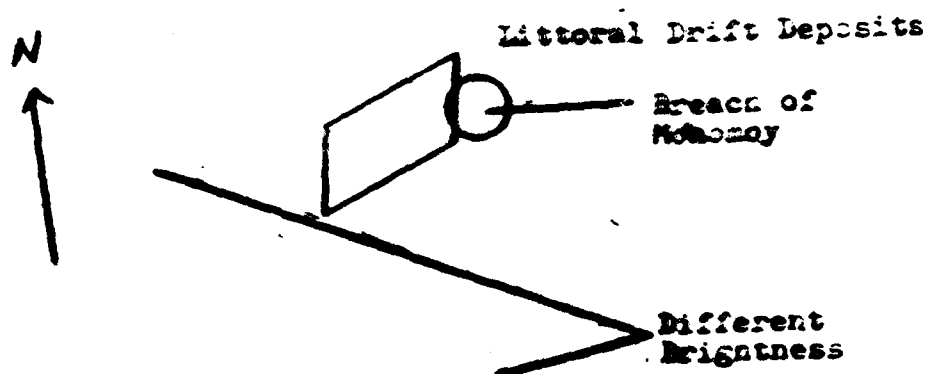
March 1978, 1:20,000 scale
Detail of Monomoy Island rupture
Low Tide

Enlarged Landsat 3 (Neg)



March 1978, 1:20,000 scale
Outline of Monomoy Island rupture
High Tide





25 km

Figure 12. Landsat MSS Band 7 Image Showing Breach of Monomoy Island resulting from the blizzards of 1978, Deposition from Littoral Drift Currents, and Variations of Land Brightness Attributed to Snow Accumulation.

A high-contrast, black and white photograph of a dark, textured surface, possibly a rock or metal, with a large, irregular, light-colored, jagged hole or crack running diagonally across the center. The texture is grainy and rough.

1973 (33) 1974 (34) 1975 (35) 1976 (36) 1977 (37) 1978 (38) 1979 (39) 1980 (40) 1981 (41) 1982 (42) 1983 (43) 1984 (44) 1985 (45) 1986 (46) 1987 (47) 1988 (48) 1989 (49) 1990 (50) 1991 (51) 1992 (52) 1993 (53) 1994 (54) 1995 (55) 1996 (56) 1997 (57) 1998 (58) 1999 (59) 2000 (60) 2001 (61) 2002 (62) 2003 (63) 2004 (64) 2005 (65) 2006 (66) 2007 (67) 2008 (68) 2009 (69) 2010 (70) 2011 (71) 2012 (72) 2013 (73) 2014 (74) 2015 (75) 2016 (76) 2017 (77) 2018 (78) 2019 (79) 2020 (80) 2021 (81) 2022 (82) 2023 (83) 2024 (84) 2025 (85) 2026 (86) 2027 (87) 2028 (88) 2029 (89) 2030 (90) 2031 (91) 2032 (92) 2033 (93) 2034 (94) 2035 (95) 2036 (96) 2037 (97) 2038 (98) 2039 (99) 2040 (100) 2041 (101) 2042 (102) 2043 (103) 2044 (104) 2045 (105) 2046 (106) 2047 (107) 2048 (108) 2049 (109) 2050 (110) 2051 (111) 2052 (112) 2053 (113) 2054 (114) 2055 (115) 2056 (116) 2057 (117) 2058 (118) 2059 (119) 2060 (120) 2061 (121) 2062 (122) 2063 (123) 2064 (124) 2065 (125) 2066 (126) 2067 (127) 2068 (128) 2069 (129) 2070 (130) 2071 (131) 2072 (132) 2073 (133) 2074 (134) 2075 (135) 2076 (136) 2077 (137) 2078 (138) 2079 (139) 2080 (140) 2081 (141) 2082 (142) 2083 (143) 2084 (144) 2085 (145) 2086 (146) 2087 (147) 2088 (148) 2089 (149) 2090 (150) 2091 (151) 2092 (152) 2093 (153) 2094 (154) 2095 (155) 2096 (156) 2097 (157) 2098 (158) 2099 (159) 2100 (160) 2101 (161) 2102 (162) 2103 (163) 2104 (164) 2105 (165) 2106 (166) 2107 (167) 2108 (168) 2109 (169) 2110 (170) 2111 (171) 2112 (172) 2113 (173) 2114 (174) 2115 (175) 2116 (176) 2117 (177) 2118 (178) 2119 (179) 2120 (180) 2121 (181) 2122 (182) 2123 (183) 2124 (184) 2125 (185) 2126 (186) 2127 (187) 2128 (188) 2129 (189) 2130 (190) 2131 (191) 2132 (192) 2133 (193) 2134 (194) 2135 (195) 2136 (196) 2137 (197) 2138 (198) 2139 (199) 2140 (200) 2141 (201) 2142 (202) 2143 (203) 2144 (204) 2145 (205) 2146 (206) 2147 (207) 2148 (208) 2149 (209) 2150 (210) 2151 (211) 2152 (212) 2153 (213) 2154 (214) 2155 (215) 2156 (216) 2157 (217) 2158 (218) 2159 (219) 2160 (220) 2161 (221) 2162 (222) 2163 (223) 2164 (224) 2165 (225) 2166 (226) 2167 (227) 2168 (228) 2169 (229) 2170 (230) 2171 (231) 2172 (232) 2173 (233) 2174 (234) 2175 (235) 2176 (236) 2177 (237) 2178 (238) 2179 (239) 2180 (240) 2181 (241) 2182 (242) 2183 (243) 2184 (244) 2185 (245) 2186 (246) 2187 (247) 2188 (248) 2189 (249) 2190 (250) 2191 (251) 2192 (252) 2193 (253) 2194 (254) 2195 (255) 2196 (256) 2197 (257) 2198 (258) 2199 (259) 2200 (260) 2201 (261) 2202 (262) 2203 (263) 2204 (264) 2205 (265) 2206 (266) 2207 (267) 2208 (268) 2209 (269) 2210 (270) 2211 (271) 2212 (272) 2213 (273) 2214 (274) 2215 (275) 2216 (276) 2217 (277) 2218 (278) 2219 (279) 2220 (280) 2221 (281) 2222 (282) 2223 (283) 2224 (284) 2225 (285) 2226 (286) 2227 (287) 2228 (288) 2229 (289) 2230 (290) 2231 (291) 2232 (292) 2233 (293) 2234 (294) 2235 (295) 2236 (296) 2237 (297) 2238 (298) 2239 (299) 2240 (300) 2241 (301) 2242 (302) 2243 (303) 2244 (304) 2245 (305) 2246 (306) 2247 (307) 2248 (308) 2249 (309) 2250 (310) 2251 (311) 2252 (312) 2253 (313) 2254 (314) 2255 (315) 2256 (316) 2257 (317) 2258 (318) 2259 (319) 2260 (320) 2261 (321) 2262 (322) 2263 (323) 2264 (324) 2265 (325) 2266 (326) 2267 (327) 2268 (328) 2269 (329) 2270 (330) 2271 (331) 2272 (332) 2273 (333) 2274 (334) 2275 (335) 2276 (336) 2277 (337) 2278 (338) 2279 (339) 2280 (340) 2281 (341) 2282 (342) 2283 (343) 2284 (344) 2285 (345) 2286 (346) 2287 (347) 2288 (348) 2289 (349) 2290 (350) 2291 (351) 2292 (352) 2293 (353) 2294 (354) 2295 (355) 2296 (356) 2297 (357) 2298 (358) 2299 (359) 2300 (360) 2301 (361) 2302 (362) 2303 (363) 2304 (364) 2305 (365) 2306 (366) 2307 (367) 2308 (368) 2309 (369) 2310 (370) 2311 (371) 2312 (372) 2313 (373) 2314 (374) 2315 (375) 2316 (376) 2317 (377) 2318 (378) 2319 (379) 2320 (380) 2321 (381) 2322 (382) 2323 (383) 2324 (384) 2325 (385) 2326 (386) 2327 (387) 2328 (388) 2329 (389) 2330 (390) 2331 (391) 2332 (392) 2333 (393) 2334 (394) 2335 (395) 2336 (396) 2337 (397) 2338 (398) 2339 (399) 2340 (400) 2341 (401) 2342 (402) 2343 (403) 2344 (404) 2345 (405) 2346 (406) 2347 (407) 2348 (408) 2349 (409) 2350 (410) 2351 (411) 2352 (412) 2353 (413) 2354 (414) 2355 (415) 2356 (416) 2357 (417) 2358 (418) 2359 (419) 2360 (420) 2361 (421) 2362 (422) 2363 (423) 2364 (424) 2365 (425) 2366 (426) 2367 (427) 2368 (428) 2369 (429) 2370 (430) 2371 (431) 2372 (432) 2373 (433) 2374 (434) 2375 (435) 2376 (436) 2377 (437) 2378 (438) 2379 (439) 2380 (440) 2381 (441) 2382 (442) 2383 (443) 2384 (444) 2385 (445) 2386 (446) 2387 (447) 2388 (448) 2

NYAC: 1,1



Figure 12. Landsat MSS Band 7 Image Showing Breach of Monomoy
Island Resulting from the Blizzards of 1978,
Deposition from Littoral Drift Currents, and
Variations of Land Brightness Attributed to Snow
Accumulation.

30004-14435

Landsat-3 MSS Band 7

9 March 1978

1:1,000,000

Calm (Nantucket Tower)

2.4 meters

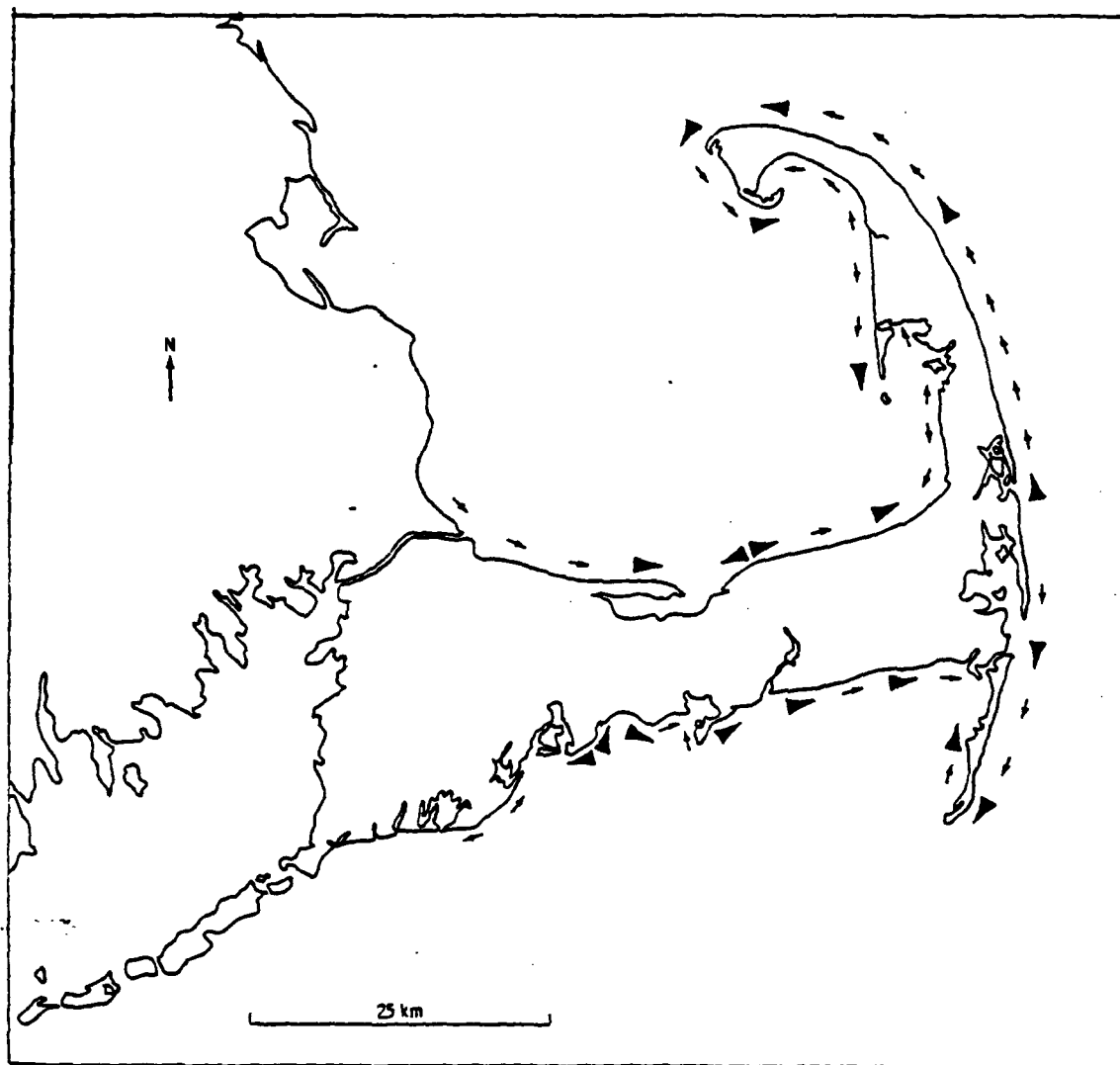


Figure 13. Map Showing Littoral Drift Directions Around Cape Cod, Massachusetts. (from Strahler, 1966). (Arrows indicate current flow directions).



25 km

Figure 14. Landsat MSS Band 4 Image Showing
a Small Plume at the End of Cape Cod Canal.

Figure 14. Landsat MSS Band 4 Image Showing Small Plume at the
End of Cape Cod Canal.

2288-14423

Landsat-1 MSS Band 4

6 November 1975

1:1,000,000

5 knots NNE (Chatham)

1.9 meters

Figure 15. Image Showing Sediment Plumes Resulting from Convergence of Longshore Currents.

21368-14275

Landsat-2 MSS Band 4

21 October 1978

1:1,000,000

12 knots WSW (Chatham)

1.7 meters

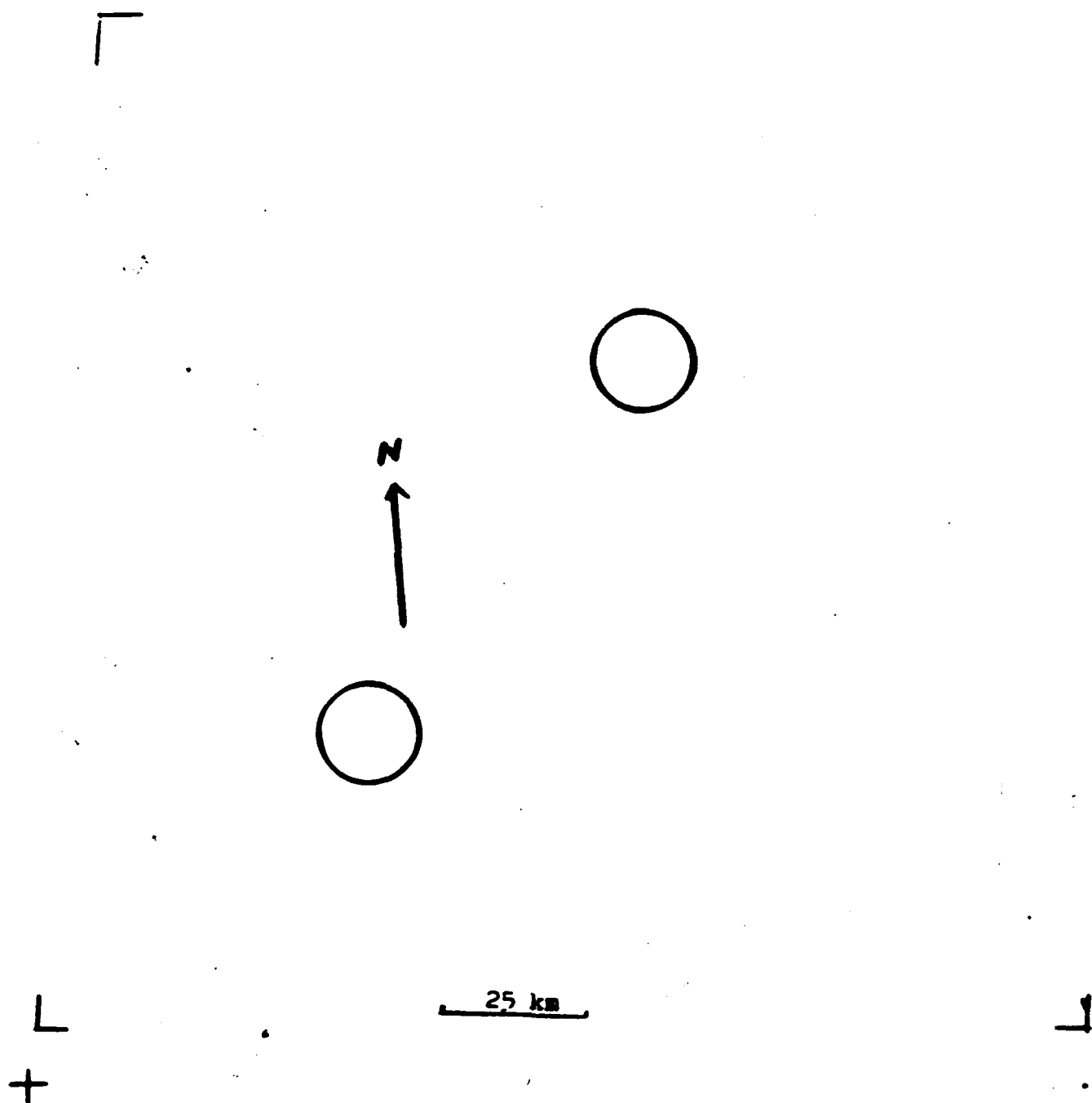


Figure 15. Image Showing Sediment Plumes Resulting from Convergence of Longshore Currents.

1000-2-1000

1000-2-1000



W071-001
21OCT78 C N41-35/W070-02 D012-031 N N41-36/W070-06 M 4

W070-001
D SUN EL31 R145 SIS- P-N L2 NASA LANDSAT F-21368-14275-4

W069-301

W071-001

W070-301

IN041-00

IN070-00

W069-301

121



Shadow
Contrail

25 km

Figure 16. Image Showing Shadow of Contrail on the water which may indicate the Presence of Turbidity.

Figure 16. Image Showing Shadow of Contrail on the Water Which
May Indicate Presence of Turbidity.

2810-14265

Landsat-2 MSS Band 4

11 April 1977

1:1,000,000

10 knots E (Chatham)

0.8 meters

Figure 17. Image Showing Two Distinct Cloud Types.

1508-14530

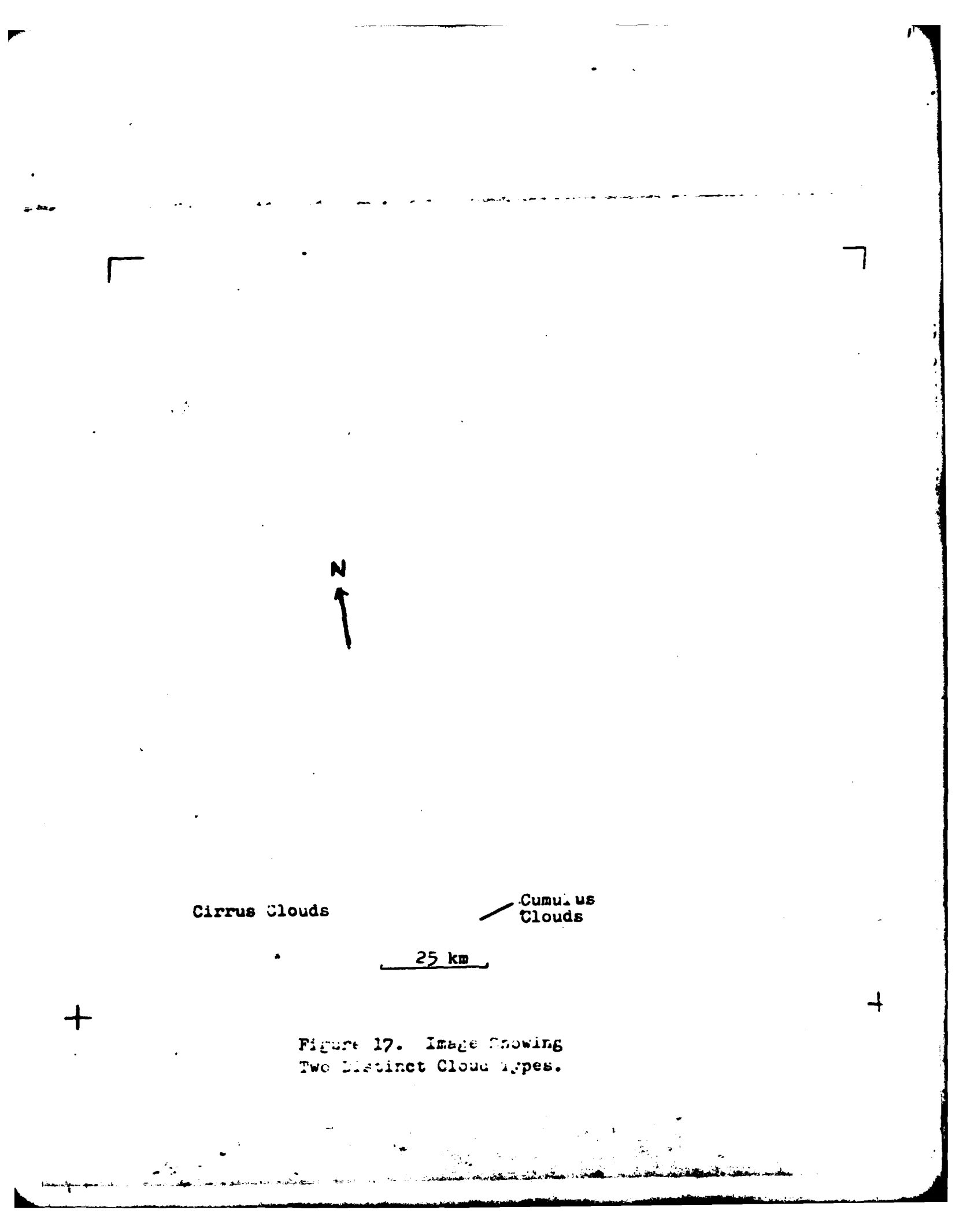
Landsat-1 MSS Band 4

13 December 1973

1:1,000,000

Calm (Chatham)

1.5 meters



Cirrus Clouds

Cumulus
Clouds

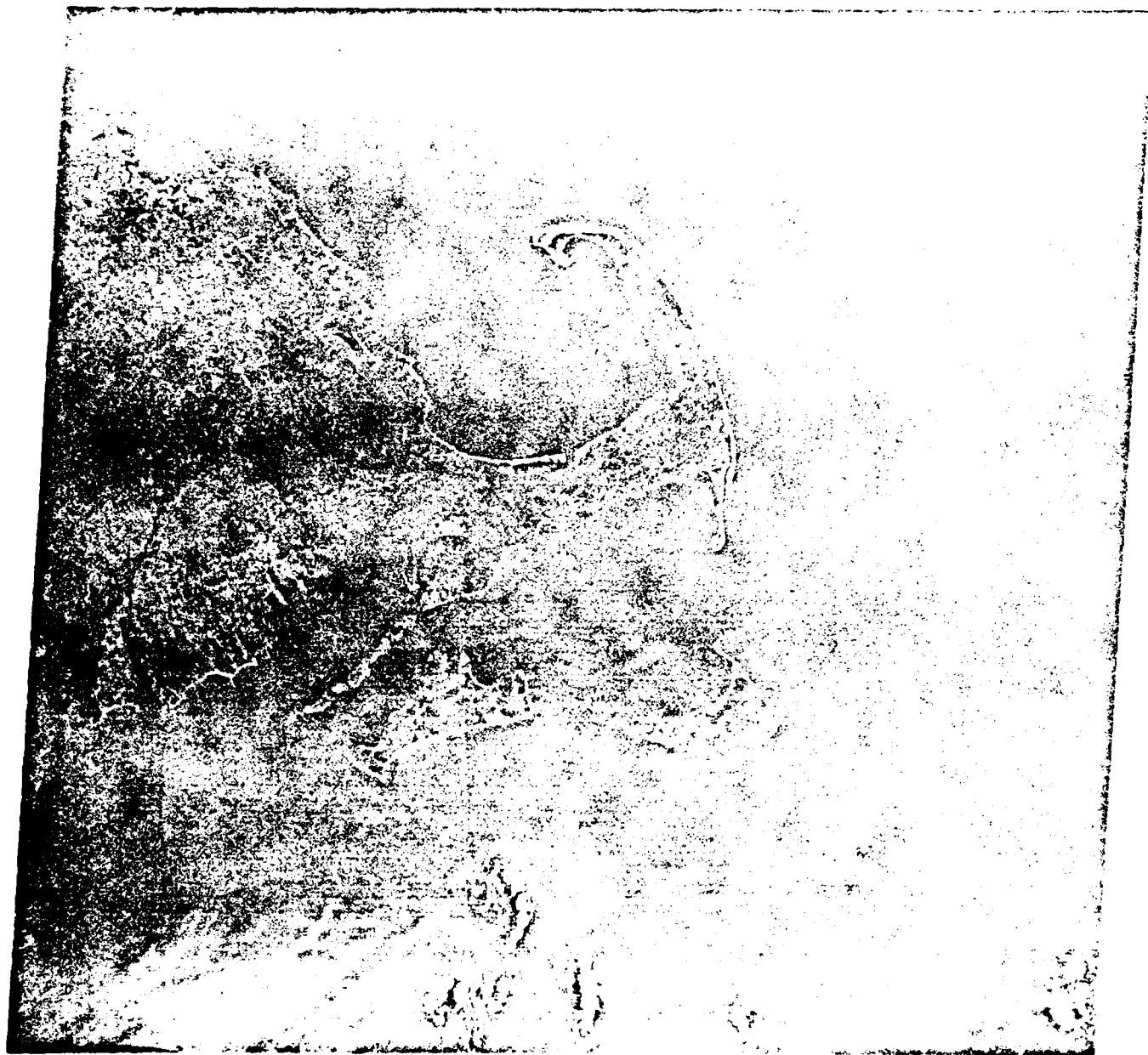
25 km

Figure 17. Image Showing
Two Distinct Cloud Types.

1900-1901

1901-1902

1902-1903



1903-1904

1904-1905



25 km

Figure 18. Landsat MSS Image Showing Major Patterns in Band 7. (Note: This indicates the patterns above are apparently surficial).



Figure 18. Landsat MSS Image Showing Major Patterns in Band 7.

(Note: This indicates the patterns above are
apparently surficial.)

1724-14472

Landsat-1 MSS Band 7

17 July 1974

1:1,000,000

14 knots 20° (Nantucket Tower)

2.3 meters

Figure 19. Seasat Synthetic Aperture Radar (SAR) Image Showing
"Shoal Pattern" Visible in Microwave.

(Note: L-Band wave length is (23 cm) and does not
penetrate water.)

(No image number)

Seasat (SAR) L-Band

27 August 1978

(No scale)

10 knots WSW (Chatham)

1.7 meters

N



1.7 nm

Figure 19. Seasat Synthetic Aperture Radar (SAR)
Image Showing "Snow Pattern" Visible in Microwave.
(Note: L-Band wave length is 23 cm and does not
penetrate water.)



N

25 km

Figure 20. First of Two Sequential Skylab-3 S-190A
Photographs Illustrating the Directional Characteristic
of Surficial Specular Reflection (Sunlight). (Note:
Compare pattern to second photograph-Figure 21)

133

NASA JSC SL3
RL 42 SEP 78



Figure 20. First of Two Sequential Skylab-3 S-190A Photographs
Illustrating the Directional Characteristic of
Surficial Specular Reflection (Sunglint).

(Note: Compare pattern to second photograph-Figure 21.)

SI-3-42-133

Skylab-3 S-190A (0.5-0.6) micrometers

12 September 1973

1:500,000

4 knots ESE (Chatham)

Figure 21. Second Sequential Skylab-3 S-190A Photograph
Illustrating the Directional Characteristic of
Surficial Specular Reflection (Sunglint).

(Note: The pattern changes with the angle of view.)

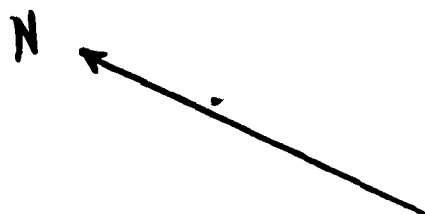
S1-3-42-134

Skylab-3 S-190A (0.5-0.6)micrometers

12 September 1973

1:500,000

4 knots ESE (Chatham)



25 km

Figure 21. Second Sequential Skylab-3 S-190A Photograph illustrating the Directional Characteristic of Surface Specular Reflection (Sunglint.) (Note: The pattern changes with the angle of view.)

134

NASA JPL SL3
RL 42 SEP 73



25 km

Figure 22. First of Three Sequential Landsat MSS Band 5
Scenes Showing no Change of Pattern with Change in View
Angle. (Note: A change of pattern would provide
evidence of sunglint, see Figures 23 and 24).



10-10074 S. 01



Figure 22. First of Three Sequential Landsat MSS Band 5
Scenes Showing No Change of Pattern with Change
in View Angle.
(Note: A change of pattern would provide evidence
of sunglint, see Figures 23 and 24.)

1724-14470

Landsat-1 MSS Band 5

17 July 1974

1:1,000,000

14 knots 20° (Nantucket Tower)

2.3 meters

Figure 23. Second of Three Sequential Landsat MSS Band 5 Scenes
Showing No Change of Pattern with Change in View Angle.
(Note: A change of pattern would provide evidence of
sunglint, see Figures 22 and 24.)

1724-14472

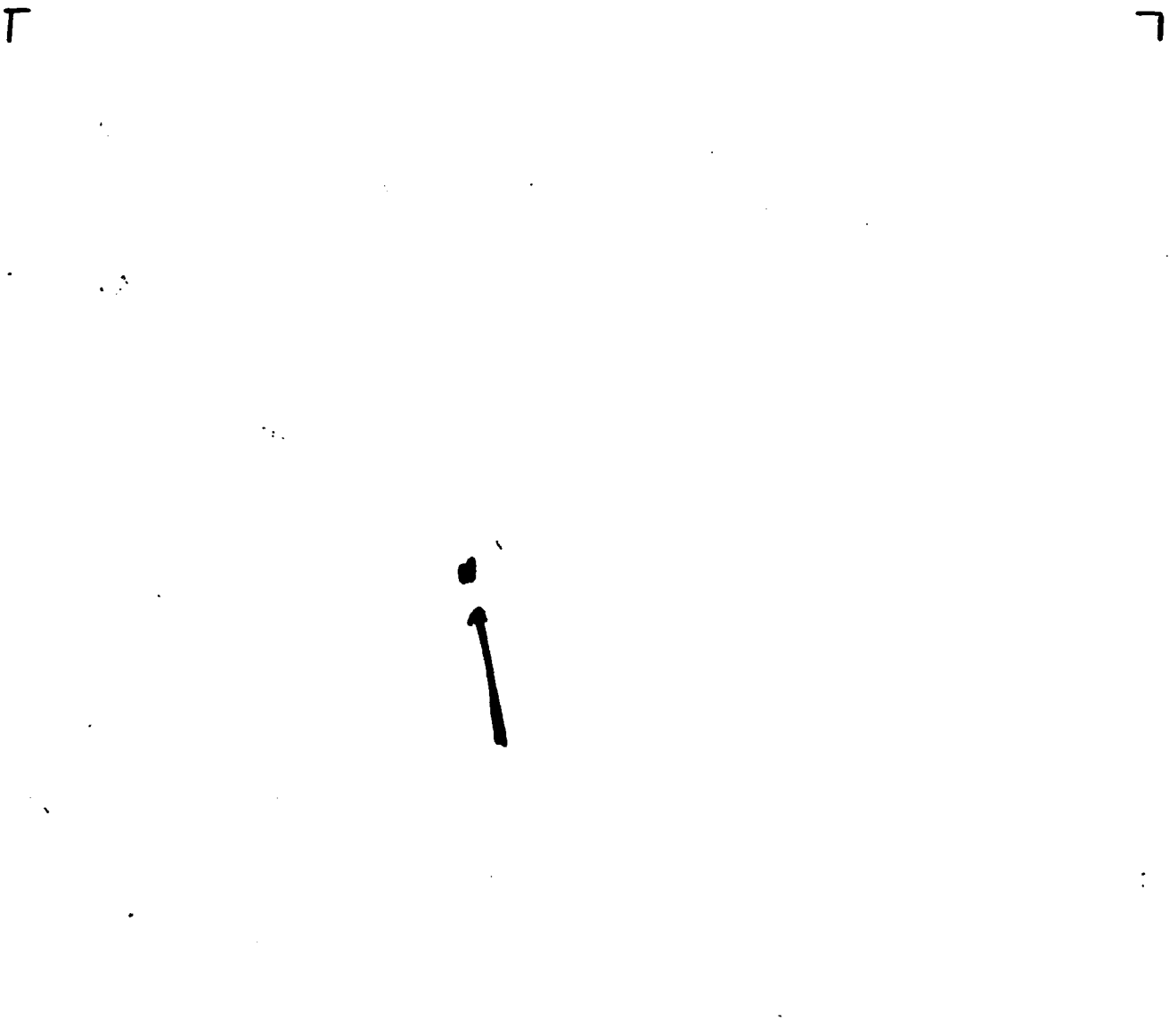
Landsat-1 MSS Band 5

17 July 1974

1:1,000,000

14 knots 20° (Nantucket Tower)

2.3 meters



25 km

**Figure 23. Second of Three Sequential Landsat MSS Band 5
Scenes Showing no Change of Pattern with Change in View Angle.
(Note: A change of pattern would provide evidence of sunglint,
see Figures 22 and 24).**



20-14472 5 01



20-14472 5 01



25 km

The image is a grayscale satellite photograph of a coastal region. A scale bar at the bottom center indicates a distance of 25 km. A north arrow, consisting of a vertical line with an arrowhead pointing upwards, is located in the center-right portion of the image. The image shows a coastline with various land and water features, though the details are somewhat obscured by the grainy quality of the scan. There are some dark, irregular shapes that could be islands or peninsulas. The overall pattern of the land and water appears consistent across the frame, supporting the caption's claim of no change in pattern with changes in view angle.

Figure 24. Third of Three Sequential Landsat MSS Band 5 Scenes Showing no Change of Pattern with Changes in View Angle. (Note: A change of pattern would provide evidence of sunglint, see Figures 22 and 23).

[REDACTED]

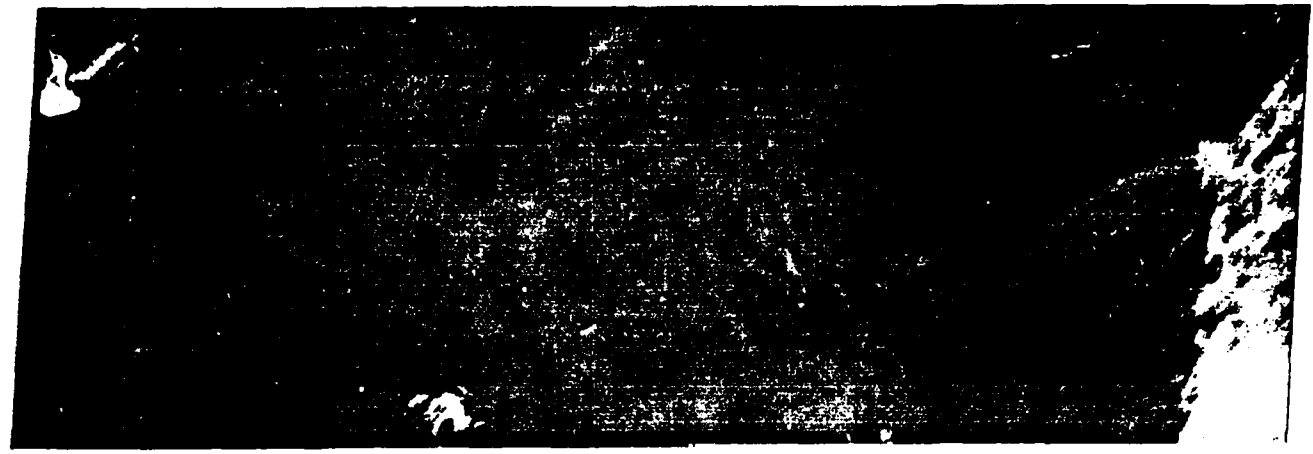
10071-30

10071-30

10070-301

10070-301

10041-301



10071-301

10071-301 10071-301

10071-301

17 JUL 74 C N40-18/10070-50 N N40-18/10070-39 MSS 5 D SUN EL58 RZ117 190-0094-N-1-N-D-2L NACA FPTS F-1724-14475-5 01

10072-00

10071-301

10071-301

10070-301

[REDACTED]

Figure 24. Third of Three Sequential Landsat MSS Band 5 Scenes
Showing No Change of Pattern with Change in View Angle.
(Note: A change of pattern would provide evidence of
sunglint, see Figures 22 and 23.)

1724-14475

Landsat-1 MSS Band 5

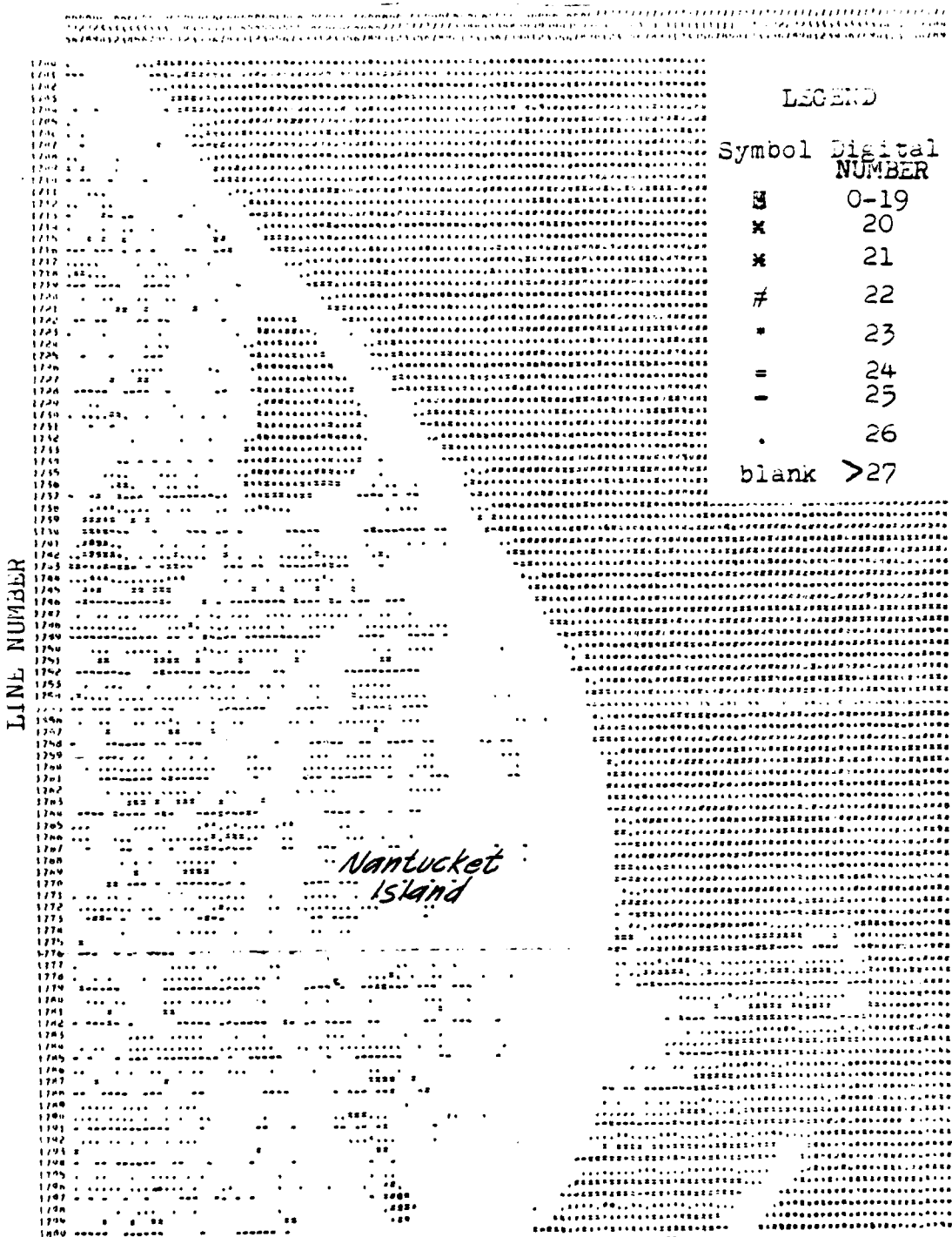
17 July 1974

1:1,000,000

14 knots 20° (Nantucket Tower)

2.3 meters

POINT NUMBER



POINT NUMBER

LINE NUMBER	POINT NUMBER	LEGEND	
		Symbol	Digital Number
1700	1700		
1701	1701		
1702	1702		
1703	1703		
1704	1704		
1705	1705		
1706	1706		
1707	1707		
1708	1708		
1709	1709		
1710	1710		
1711	1711		
1712	1712		
1713	1713		
1714	1714		
1715	1715		
1716	1716		
1717	1717		
1718	1718		
1719	1719		
1720	1720		
1721	1721		
1722	1722		
1723	1723		
1724	1724		
1725	1725		
1726	1726		
1727	1727		
1728	1728		
1729	1729		
1730	1730		
1731	1731		
1732	1732		
1733	1733		
1734	1734		
1735	1735		
1736	1736		
1737	1737		
1738	1738		
1739	1739		
1740	1740		
1741	1741		
1742	1742		
1743	1743		
1744	1744		
1745	1745		
1746	1746		
1747	1747		
1748	1748		
1749	1749		
1750	1750		
1751	1751		
1752	1752		
1753	1753		
1754	1754		
1755	1755		
1756	1756		
1757	1757		
1758	1758		
1759	1759		
1760	1760		
1761	1761		
1762	1762		
1763	1763		
1764	1764		
1765	1765		
1766	1766		
1767	1767		
1768	1768		
1769	1769		
1770	1770		
1771	1771		
1772	1772		
1773	1773		
1774	1774		
1775	1775		
1776	1776		
1777	1777		
1778	1778		
1779	1779		
1780	1780		
1781	1781		
1782	1782		
1783	1783		
1784	1784		
1785	1785		
1786	1786		
1787	1787		
1788	1788		
1789	1789		
1790	1790		
1791	1791		
1792	1792		
1793	1793		
1794	1794		
1795	1795		
1796	1796		
1797	1797		
1798	1798		
1799	1799		
1800	1800		

Figure 26. "Grey-Map" Mss5 Old Man Shoal.

POINT NUMBER

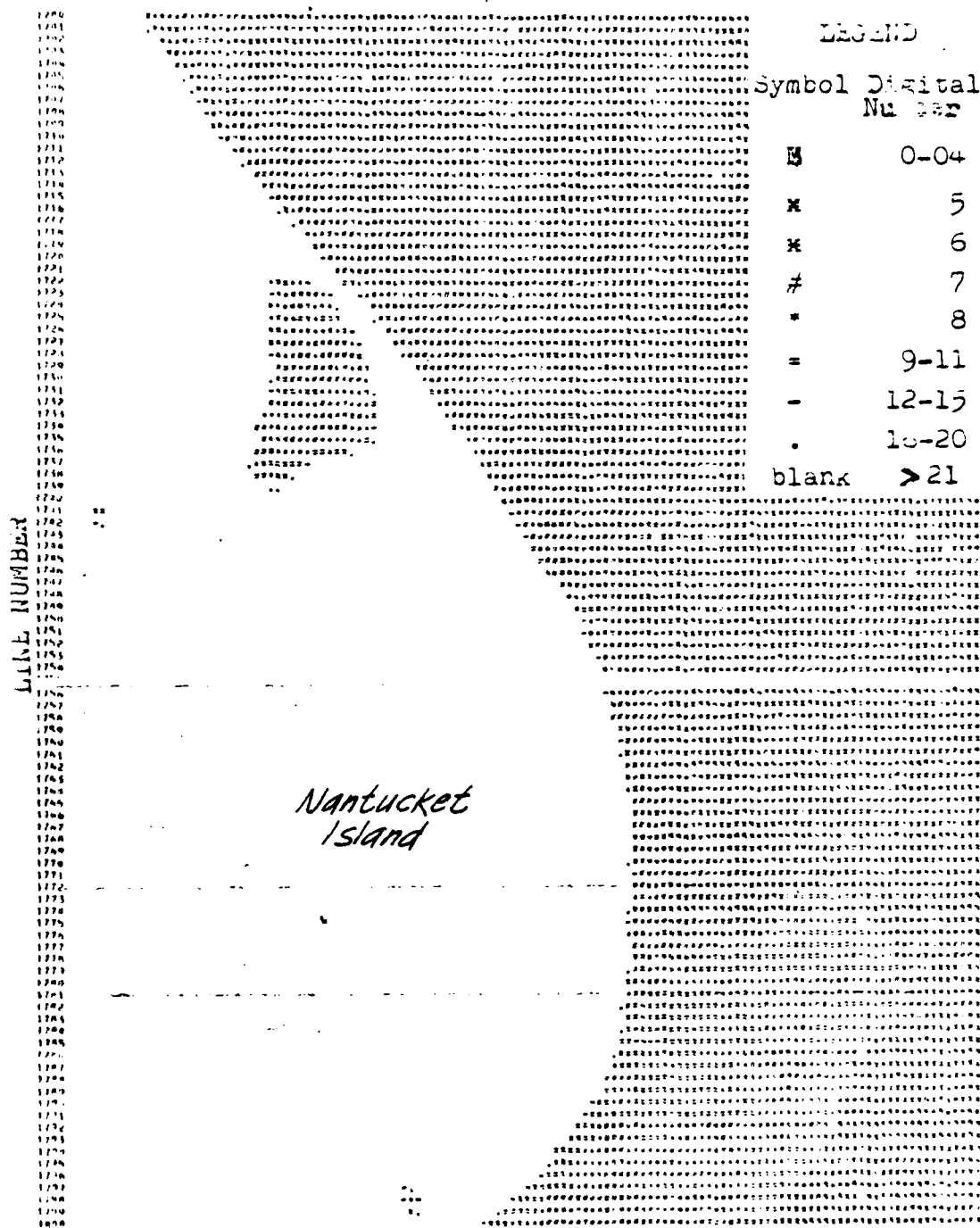


Figure 27. "Grey-Map" MSS6 Old Man Shoal.

POINT NUMBER

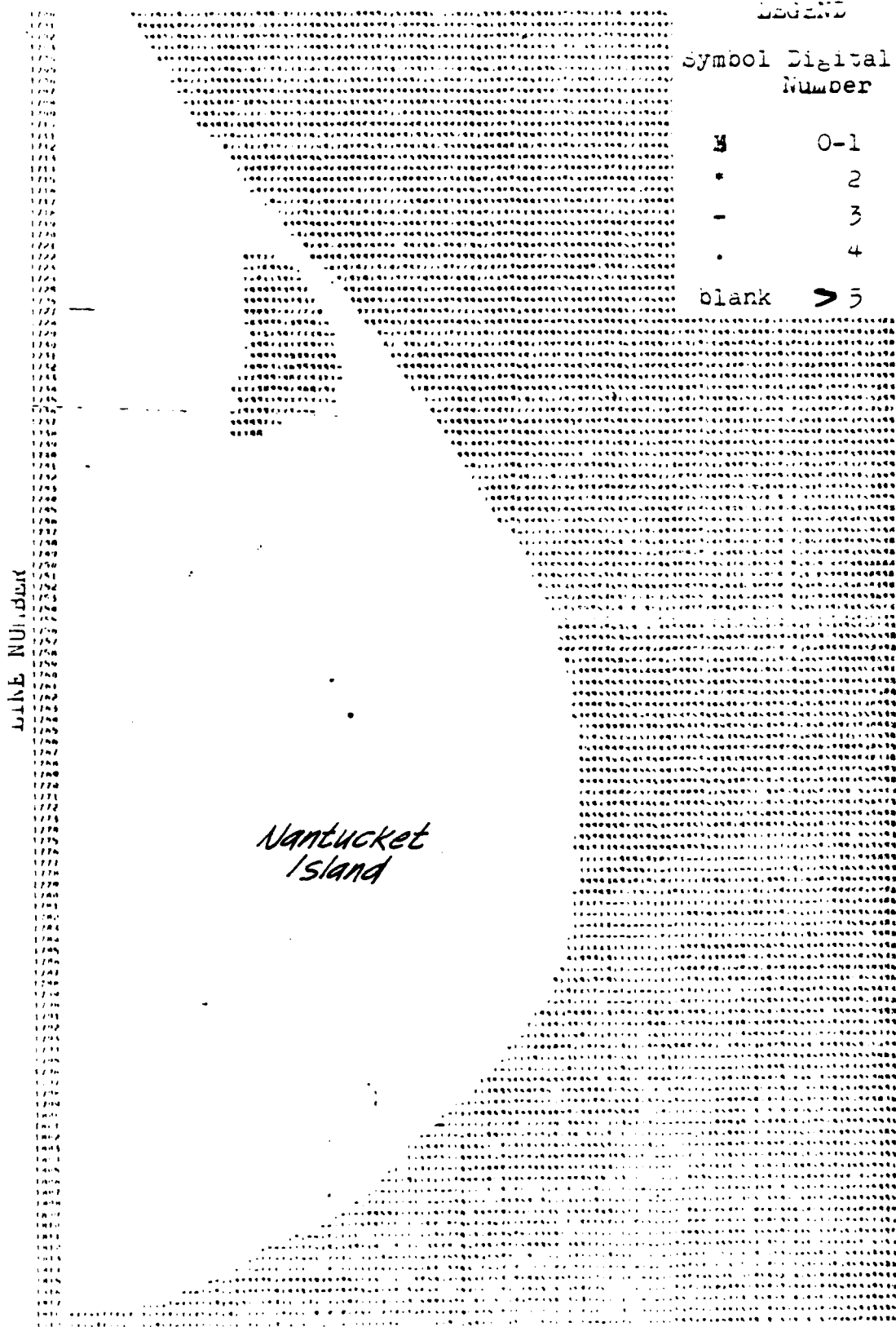


Figure 28. "Grey-Map" MSS7 Old Man Shoal.

Region 5, 10, 11

Internal save
Surface Manifestation

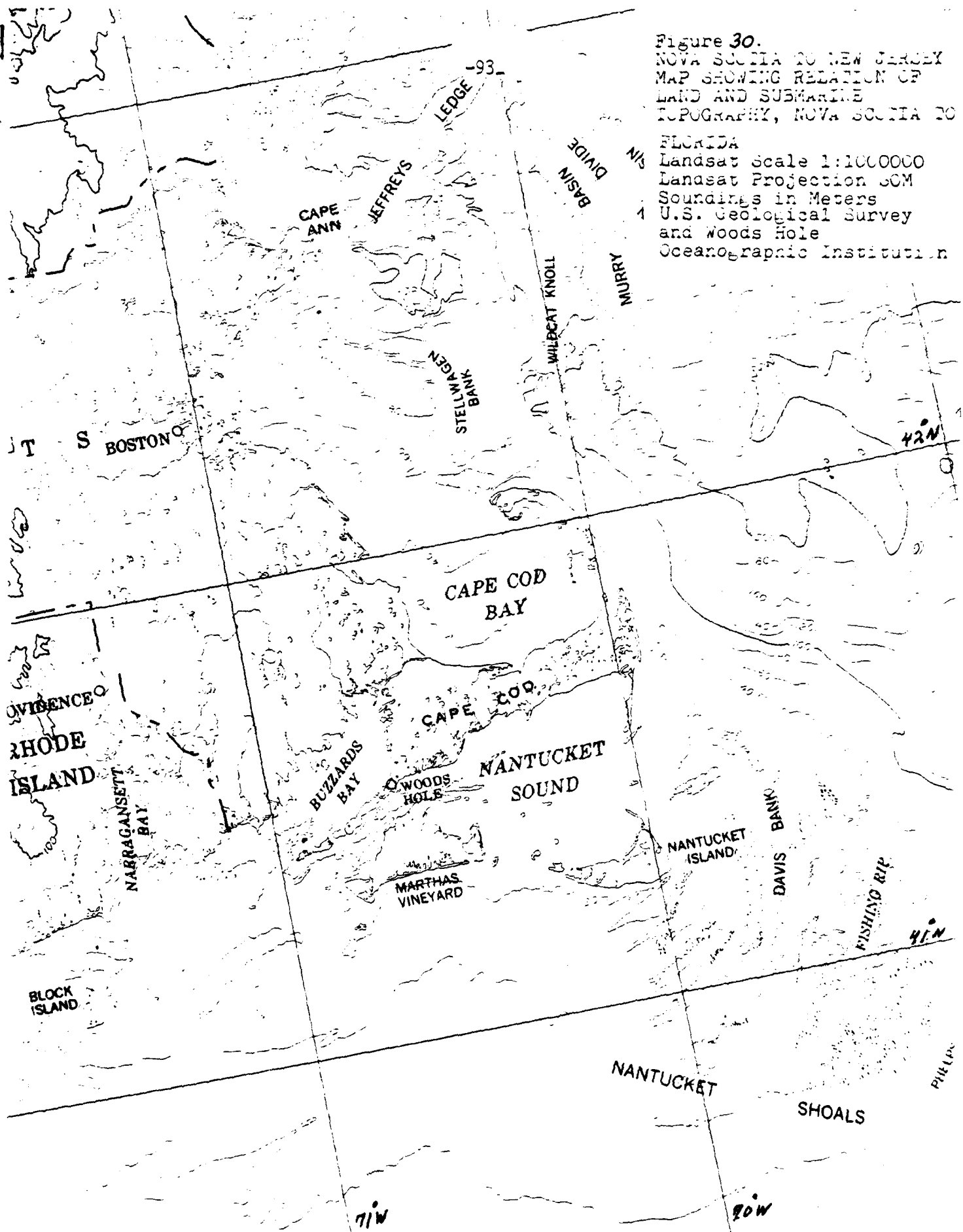
"Grey Water" —

Billingsgate Shoal —
Calibration Area

Internal save —
Surface Manifestation

"Dark Water" —

Figure 30.
NOVA SCOTIA TO NEW JERSEY
MAP SHOWING RELATION OF
LAND AND SUBMARINE
TOPOGRAPHY, NOVA SCOTIA TO
FLORIDA
Landsat Scale 1:1000000
Landsat Projection 30M
Soundings in Meters
U.S. Geological Survey
and Woods Hole
Oceanographic Institution



46 5493

KOE SEMI LOGARITHMIC CHARTS & CO. DIVISION
RENTON, WASHINGTON

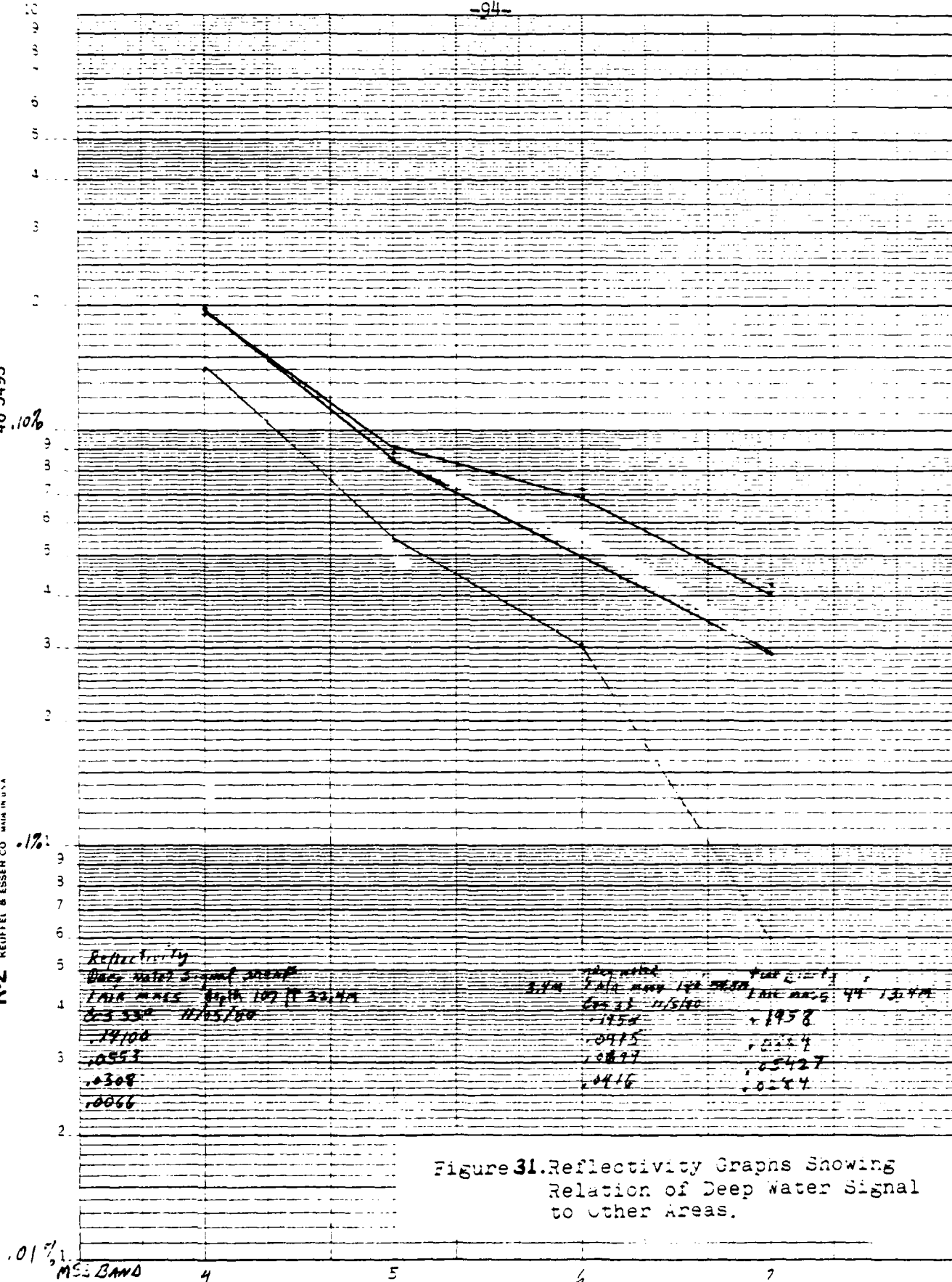


Figure 31. Reflectivity Graphs Showing Relation of Deep Water Signal to Other Areas.

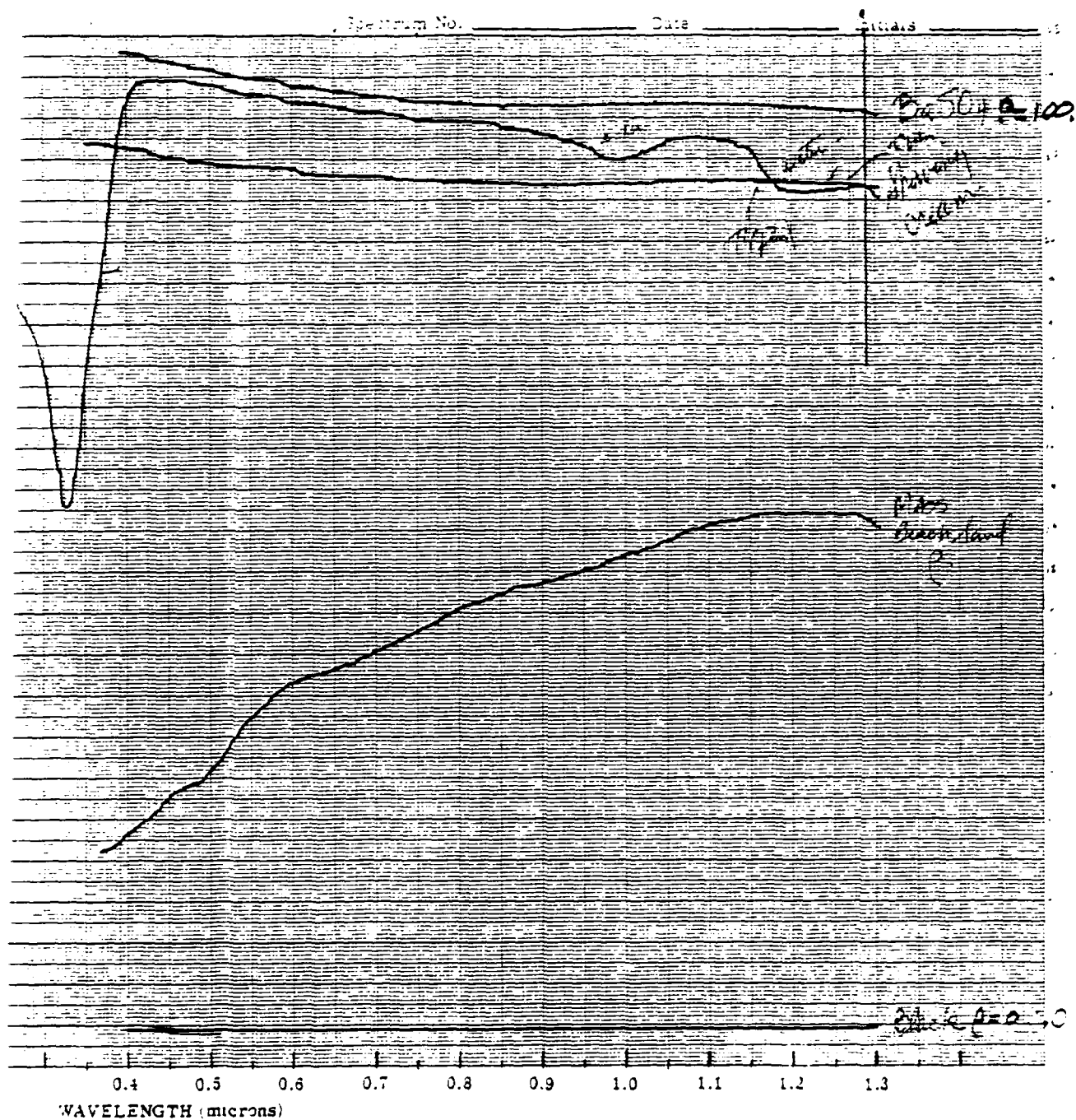
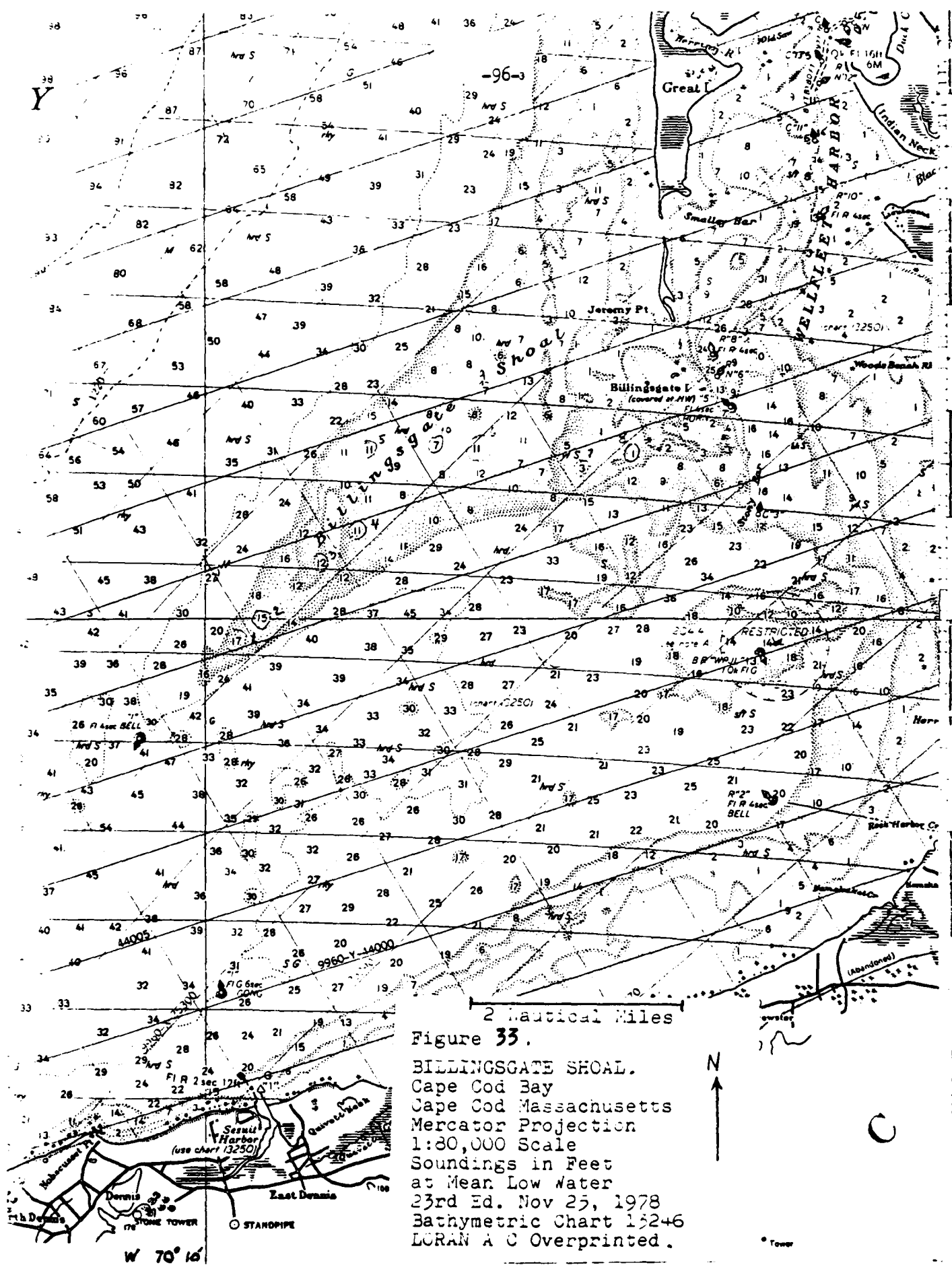


Figure 32. Reflectivity Spectrums of Massachusetts Beach Sand and Simulated Sea Foam.



SCATTER PLOT

N= 11 OUT OF 11 2:MSS4 VS. 1:Z

MSS4

6.7000 +♦

+

5.9200 +

+

5.1400 + ♦

+

4.3600 +

+

3.5800 +

+

2.8000 +

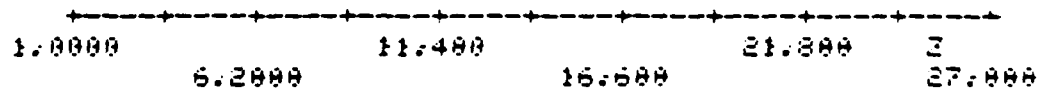


Figure 34. Regression of the Log Digital Number vs. Plotted Depth in MSS Band 4.

SCATTER PLOT

N= 11 BUT OF 11 3:MSS5 VS. 1:Z

MSS5

5.2000 ++

+

4.6400 +

+

4.0800 +

+

3.5200 +

+

2.9600 +

+

2.4000 +

1.0000

6.2000

11.400

16.600

21.800

Z

27.000

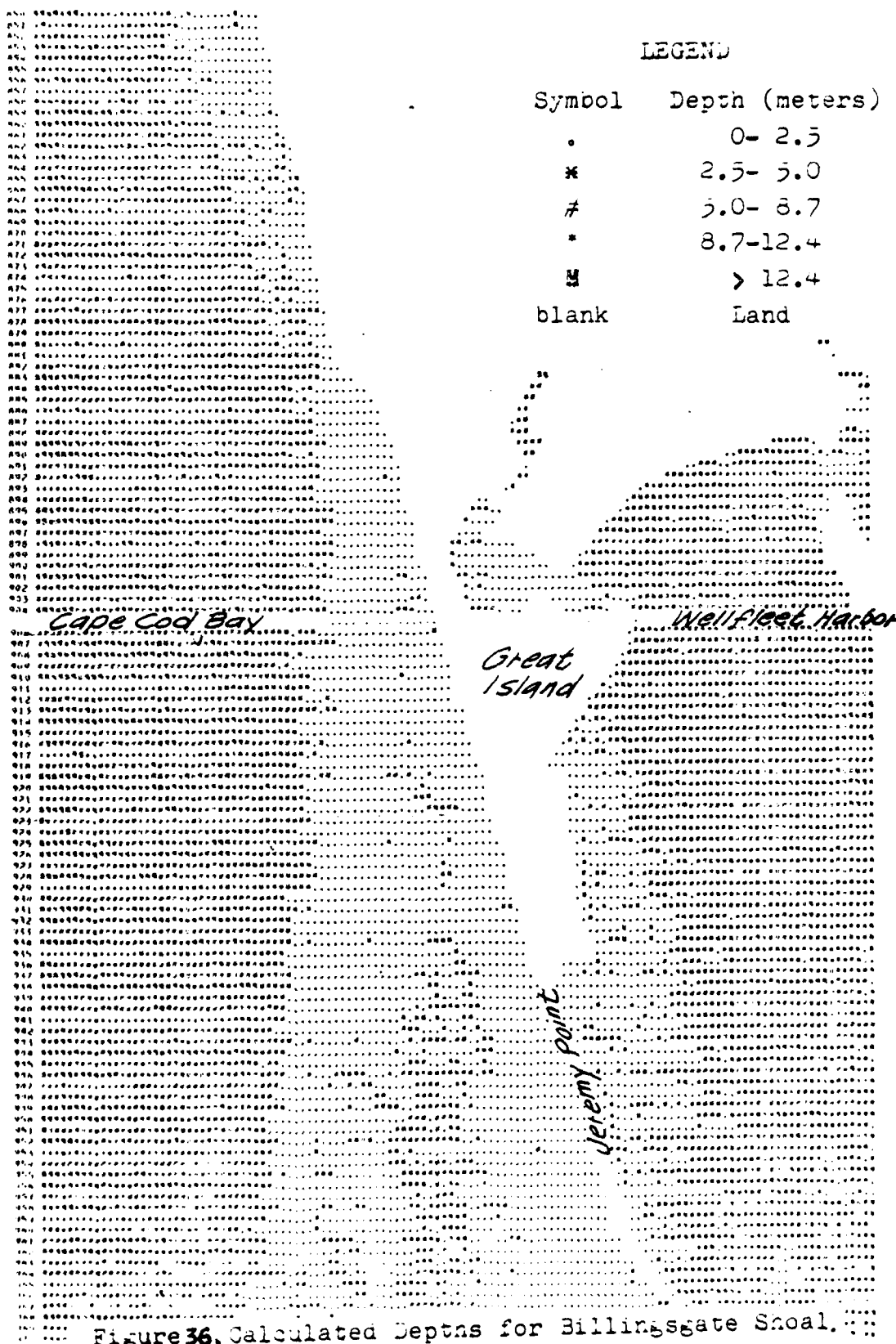
Figure 35. Regression of the Log Digital Number
vs. Plotted Depth in MSS Band 5.

-99-
POINT NUMBER

LEGEND

Symbol	Depth (meters)
.	0- 2.5
*	2.5- 5.0
#	5.0- 8.7
*	8.7-12.4
M	> 12.4
blank	Land

LINE NUMBER



CALIBRATION BILLINGSgate Shoals

Line 934 Point 215 Step 3

Depth 11' 3.7 meters

100%

46 5493

10%

1%

K-E SEMI LOGARITHMIC SCALING & DIVISIONS
REMOVED & RECALCULATED

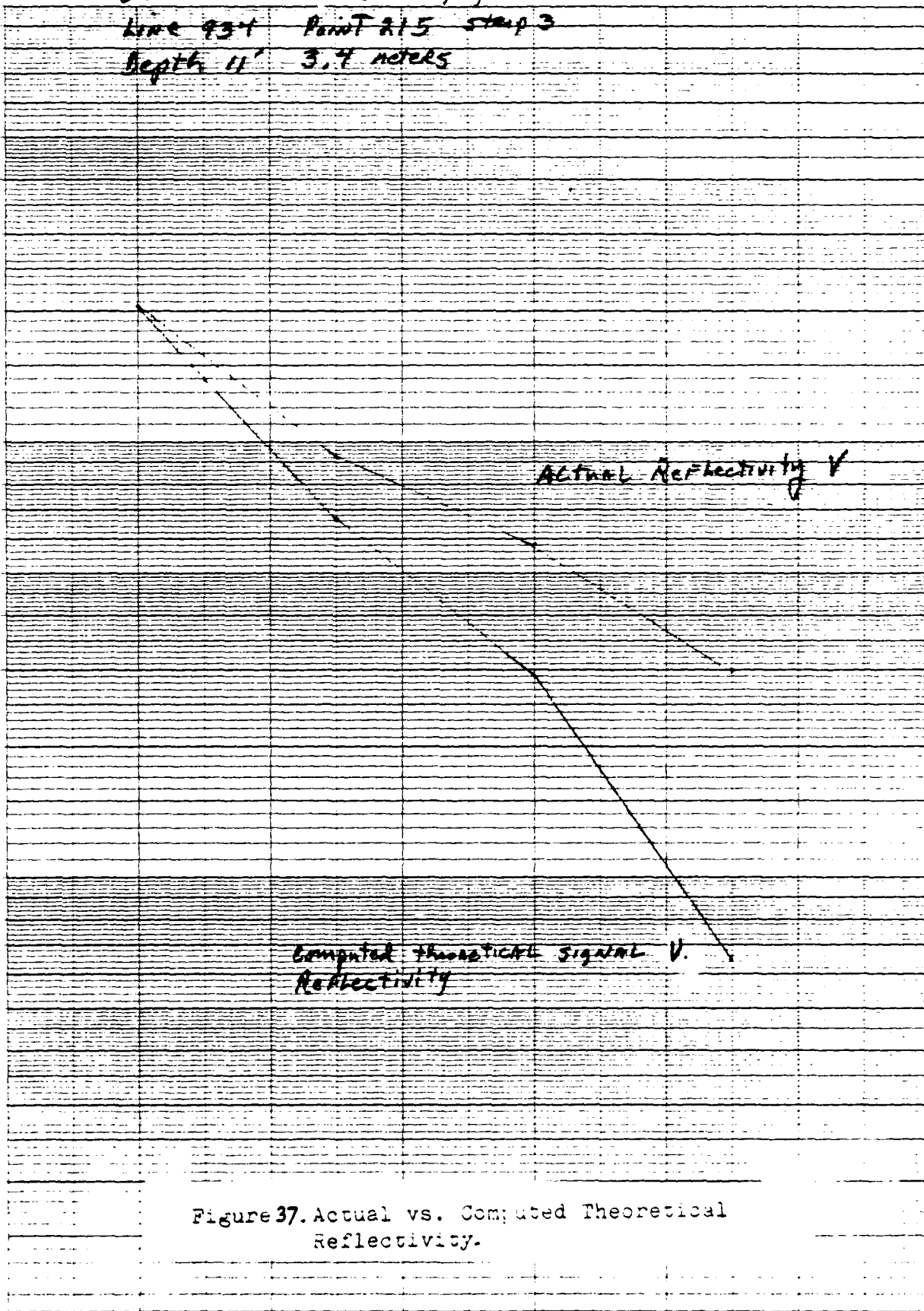


Figure 37. Actual vs. Computed Theoretical Reflectivity.

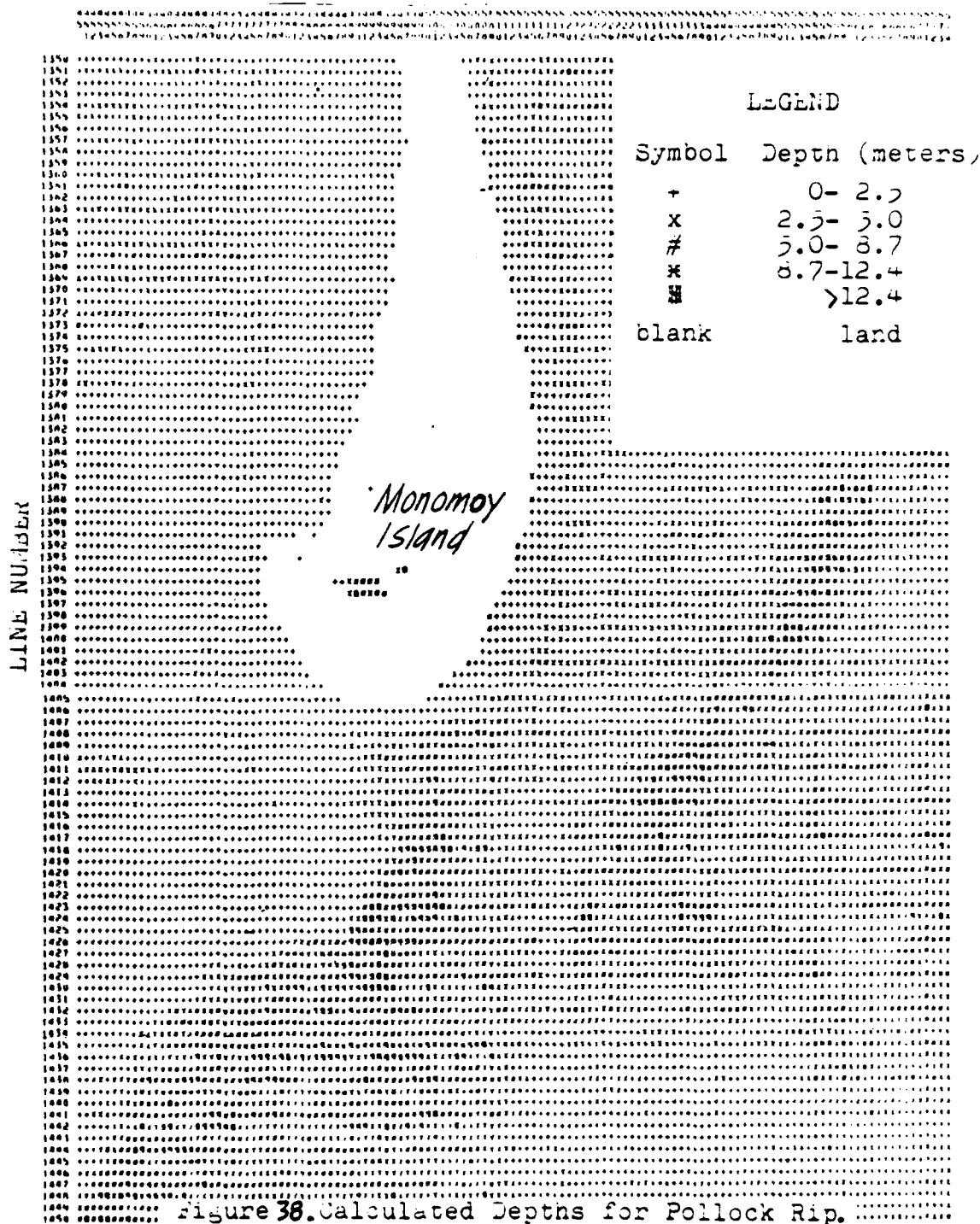
MSS BAND 4

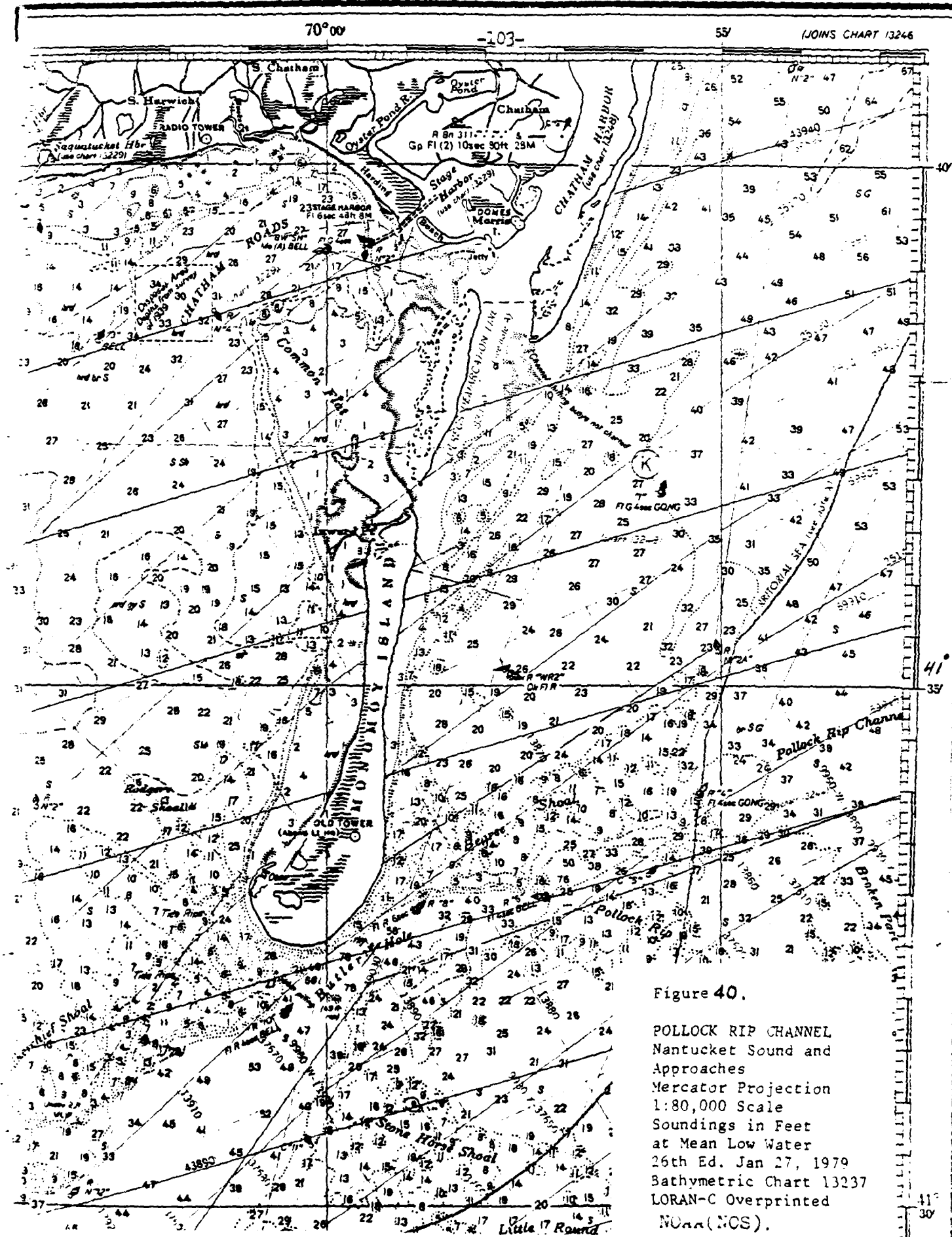
5

6

7

POINT NUMBER





POINT NUMBER

LEGEND

Symbol	Depth (meters)
.	0- 2.5
*	2.5- 5.0
#	5.0- 8.7
*	8.7-12.4
■	>12.4
blank	land

LINE NUMBER

Nantucket
Island

Figure 41. Calculated Depths for Old Man Shoal.

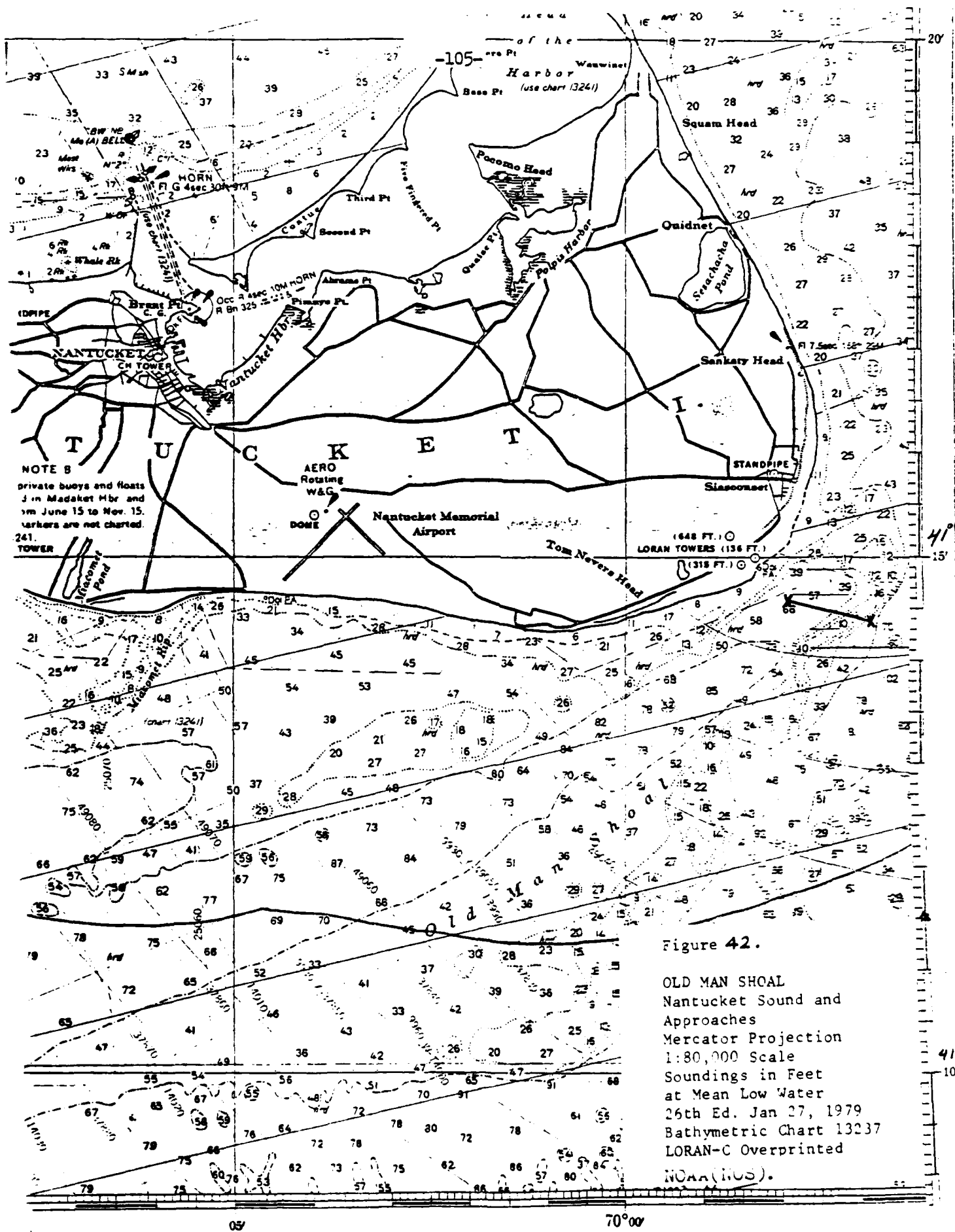


Figure 42.

OLD MAN SHOAL
Nantucket Sound and
Approaches
Mercator Projection
1:80,000 Scale
Soundings in Feet
at Mean Low Water
26th Ed. Jan 27, 1979
Bathymetric Chart 13237
LORAN-C Overprinted
NOAA(NOS).

Figure 43. MSS Band 4 Reflectivity
Actual vs. Computed Theoretical
Relevant to Bottom Profile
by Pixel Position.

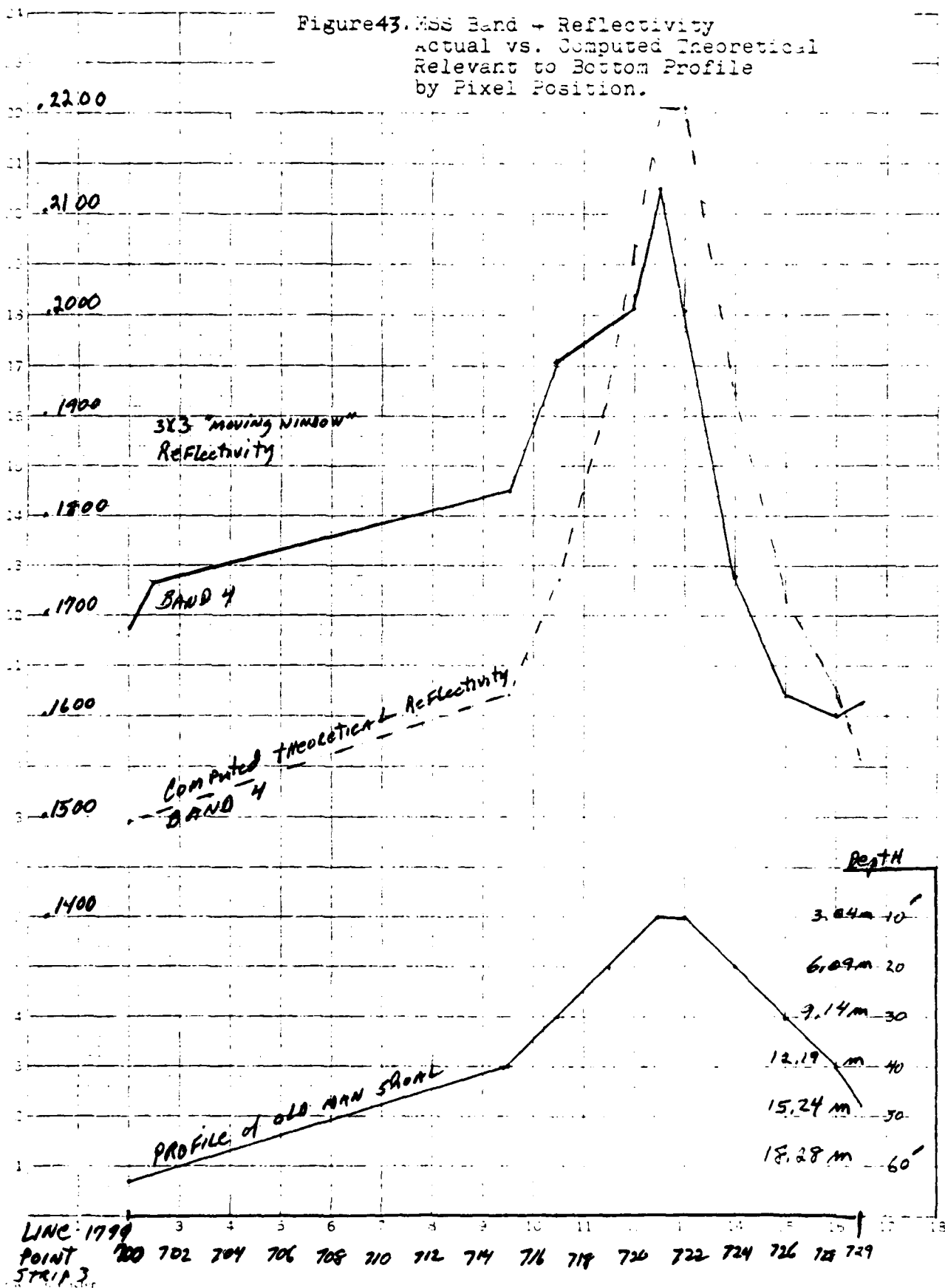


Figure 44. Comparison of Actual vs. Computed Theoretical Signals for Old Man Shoal.

Digital Count 30

28
26
24
22
20
18
16
14
12
10
8
6
4
2

OLD MAN SHOAL
LINE 1799 STRIP 3
POINT 721
Depth 10 Feet

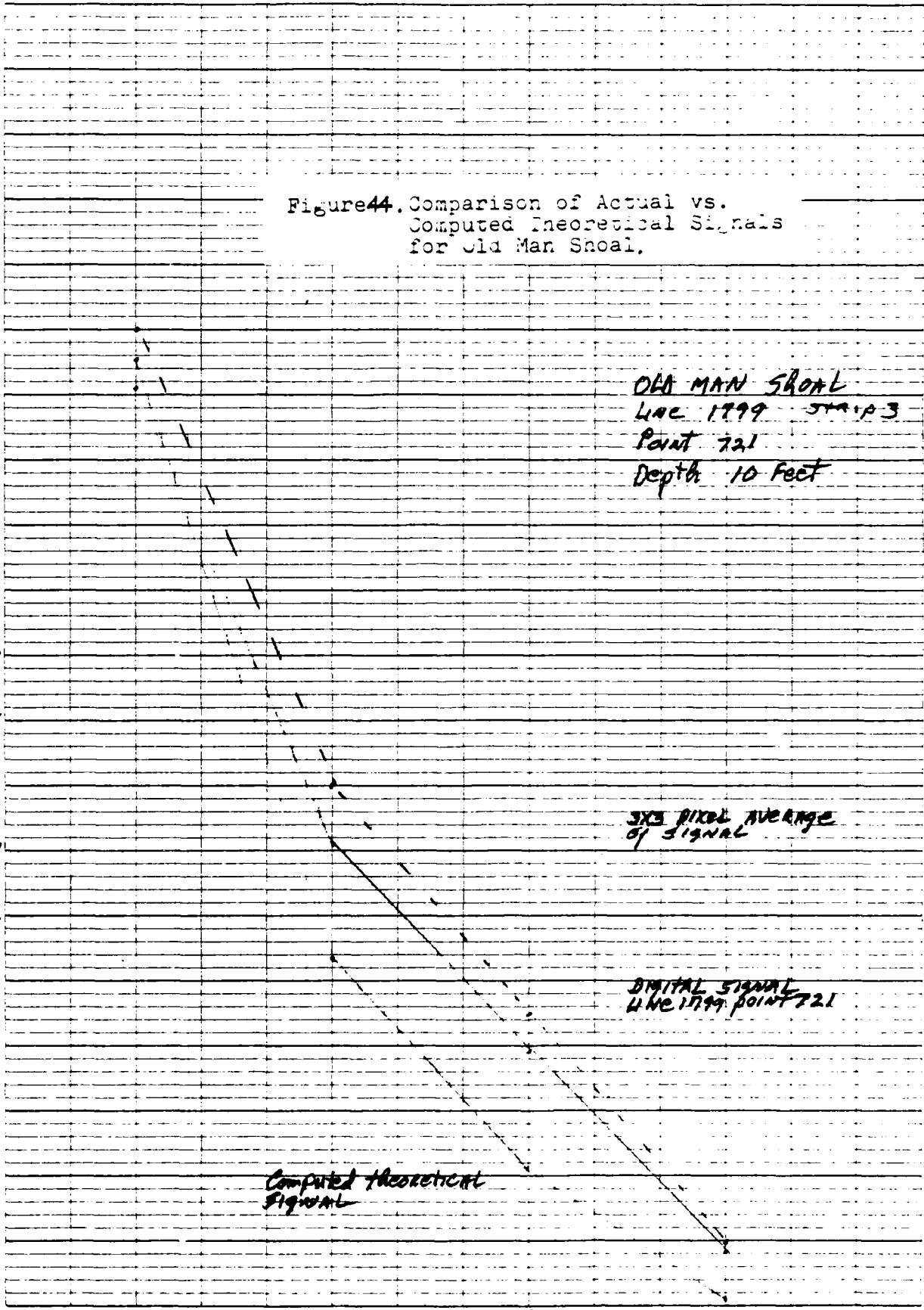
3x3 PIXEL AVERAGE
OF SIGNAL

DIGITAL SIGNAL
LINE 1799 POINT 721

Computed theoretical
SIGNAL

10 Squares to the BAND

4 5 6 7



-108-
Reflectivity $V-V_s$

funnel model

STRIP 3

LINE 1799

Point 721

Depth 10' 3.05m

3x3 pixel average

OLD MAN Shoal

46 5493

100%

10%

K-E SEMI LOGARITHMIC PLOTTER * in Eastman
KODAK SAFETY FILM * MADE IN U.S.A.

Figure 45. Reflectivity $V-V_s$ Old Man Shoal.

M35 4
BAND

5

6

7

Shoals "A" Depth 30' 9.14m
 Line 1789 Port 208 Strip 3

100%

46 5493

10%

Figure 46. Comparison of Actual Reflectivity to Calculated Theoretical Reflectivity for Shoals "A".

K-E SEMI LOGARITHMIC PLOTTER
 NEUFEL & ESSEN CO. MADE IN USA

1%

% Reflectivity

Calculated
 Theoretical
 Reflectivity

Actual Reflectivity

ZERO - -> ZERO

MSS
 BAND

4

5

6

7

Shoals "A" Line 1789 Point 708 Strip 3

V-VS Reflectivity

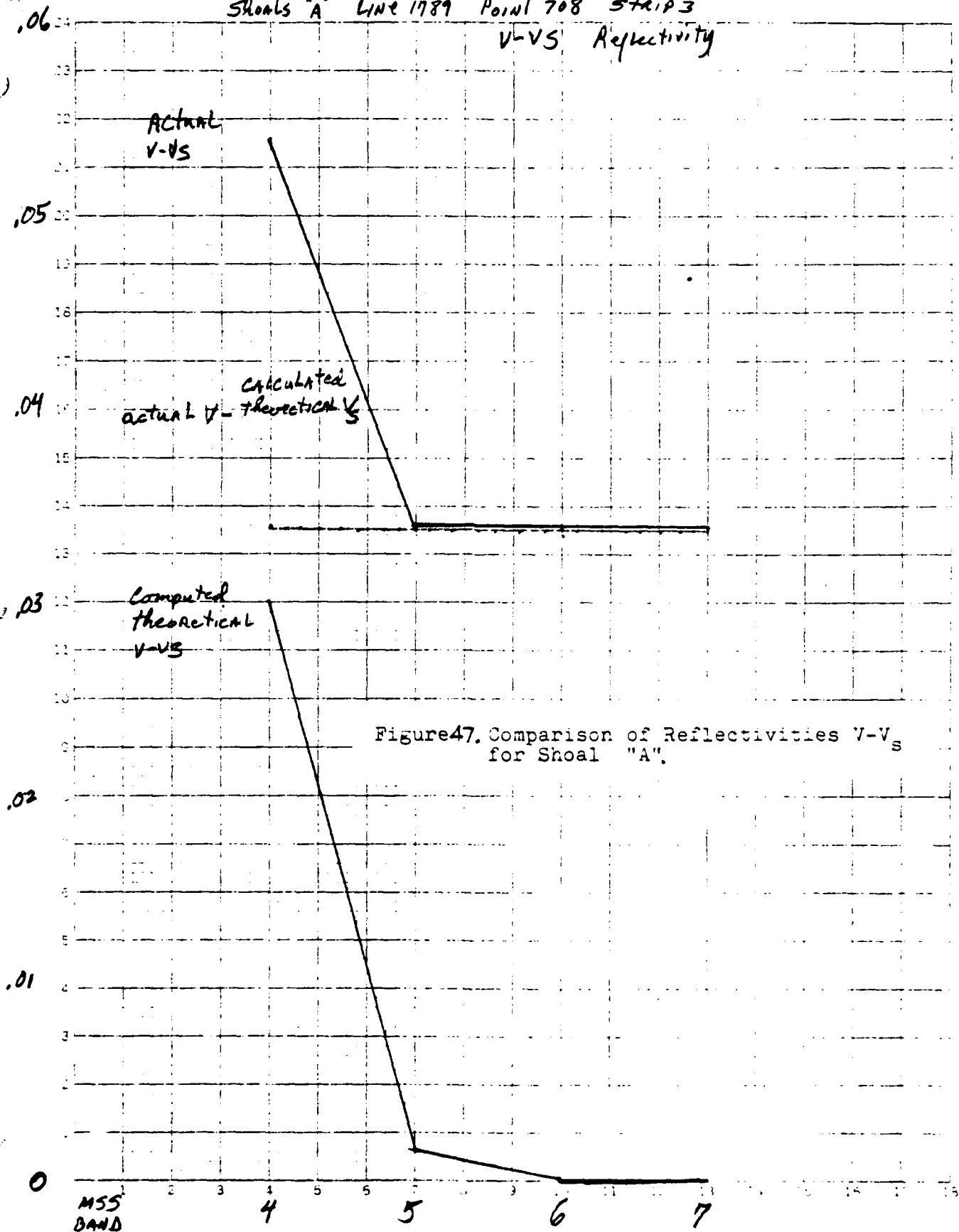


Figure 47. Comparison of Reflectivities V-V_s for Shoal "A".

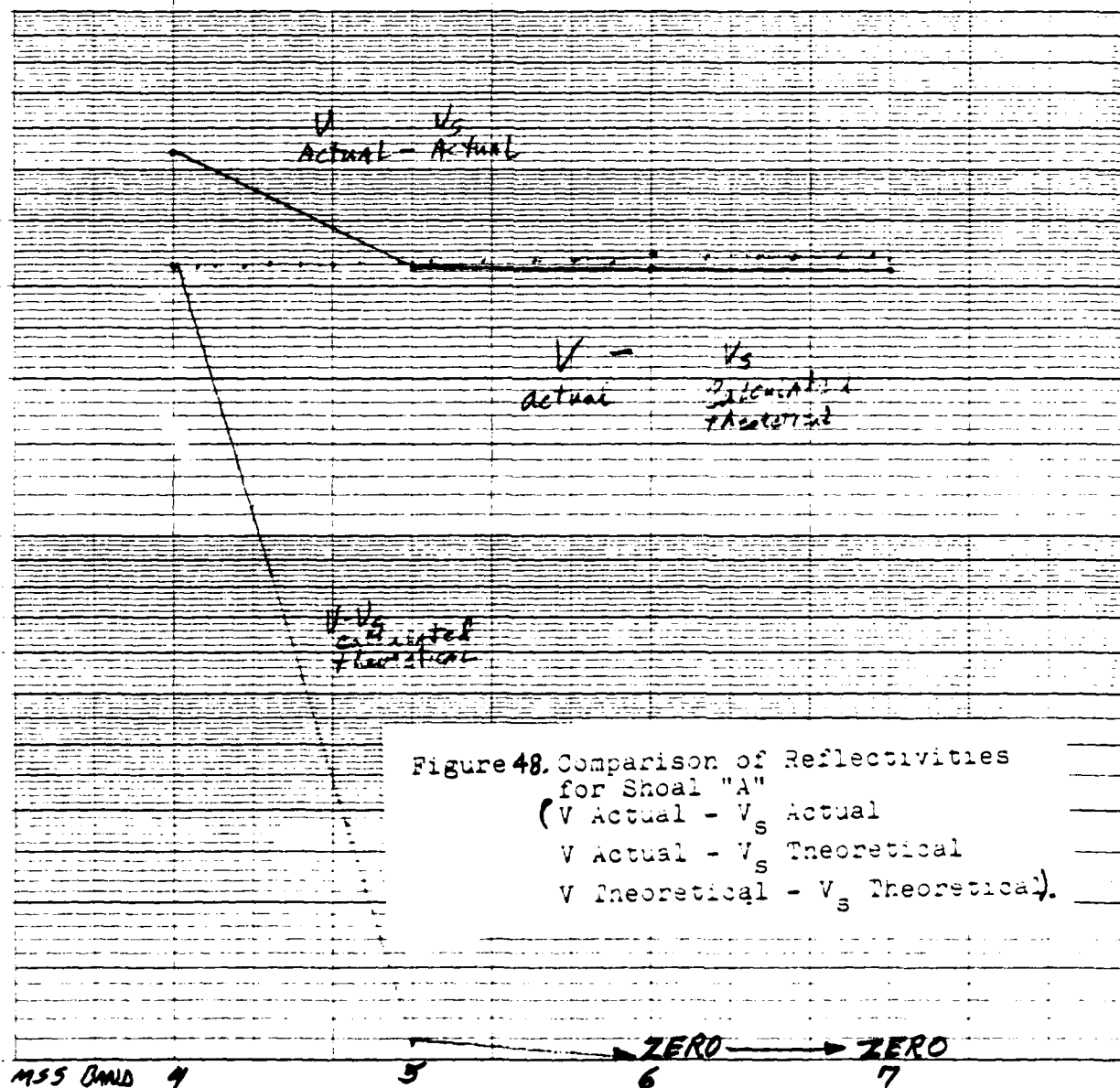
100%

SHOALS "A" Depth 30' -111-
LINE 1789 Point 708 STRIP 3

46.5493

K-E SEMI-LOGARITHMIC PLOTTER A-10 DUBOIS-REY
KEUFFEL & ESSER CO. MADE IN U.S.A.

1%



POINT NUMBER

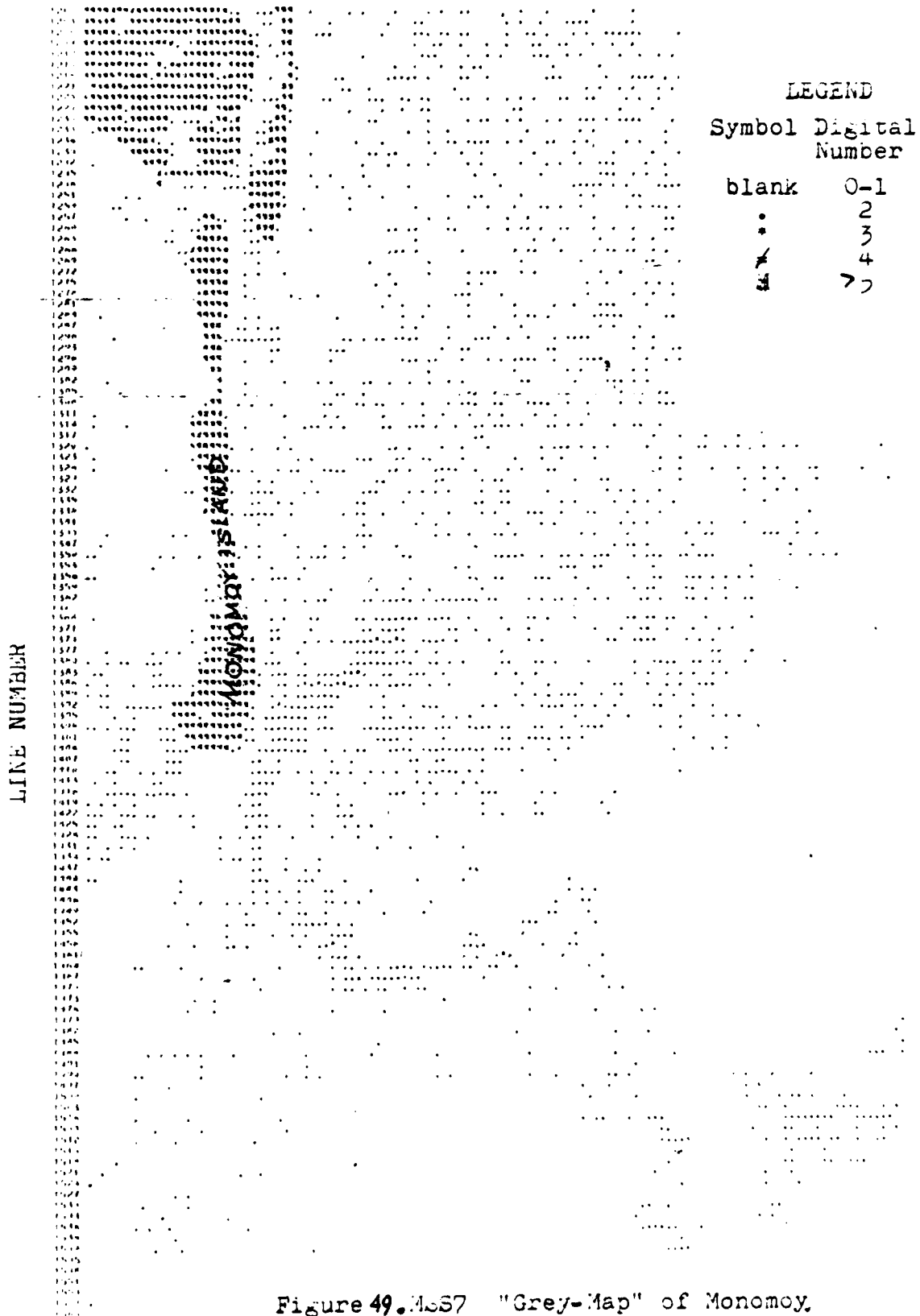
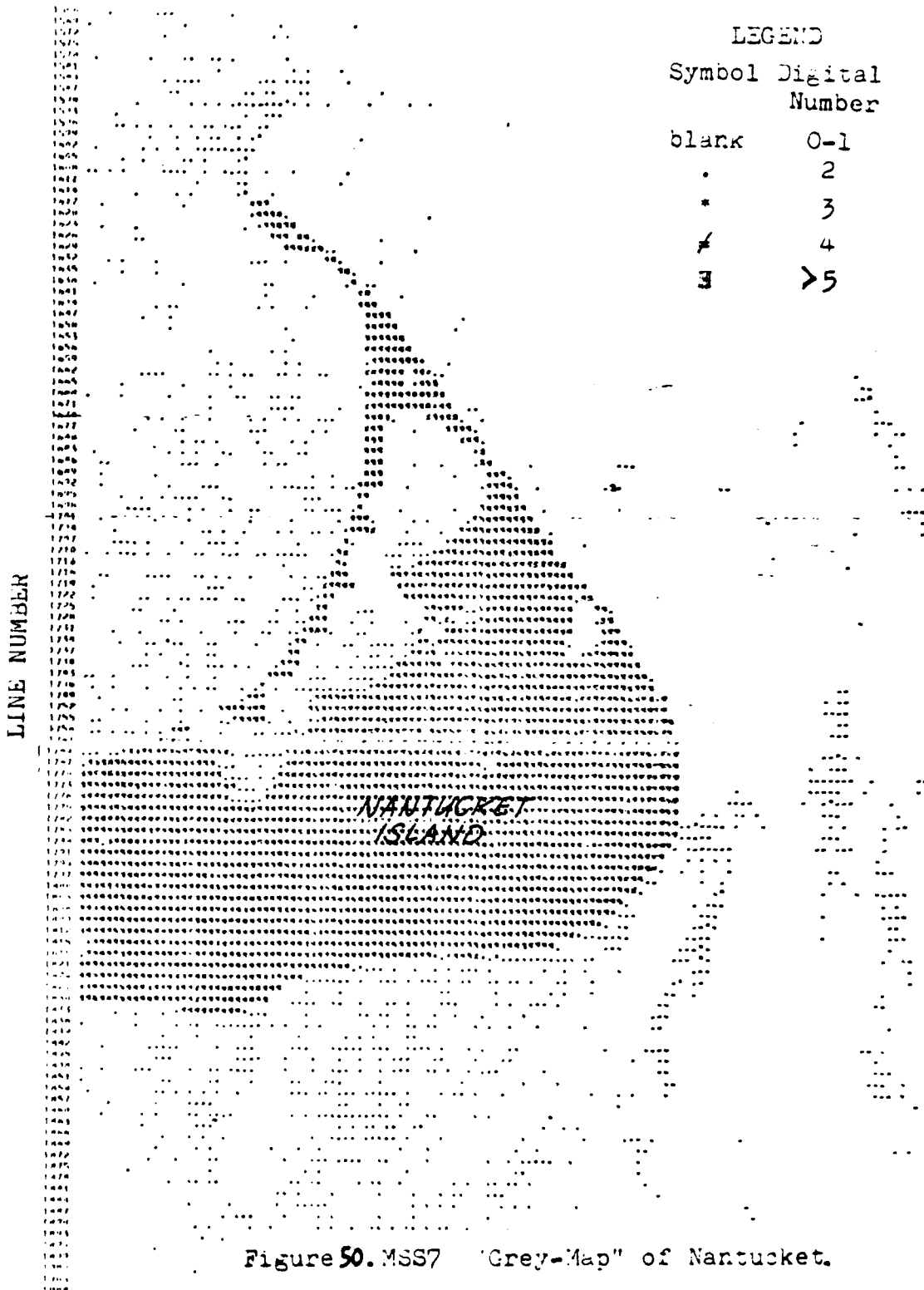


Figure 49. MsB7 "Grey-Map" of Monomoy.

POINT NUMBER



100%

"grey water"

-114-

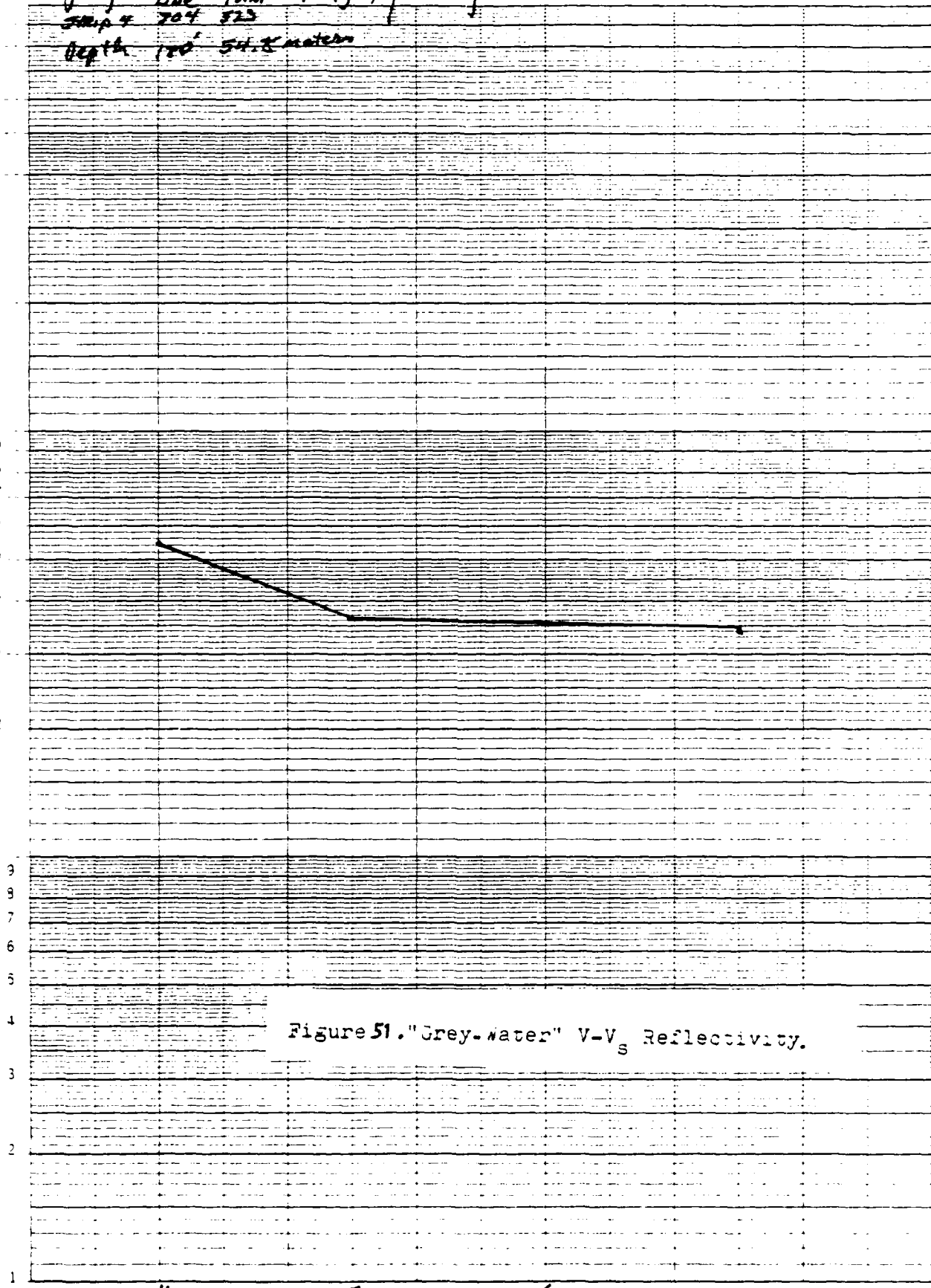
Line Point V-V_s reflectivity
 Strip # 704 523
 Depth 120' 54.8 meters

46 5493

10%

K-E SEMI-LOGARITHMIC PLOTTER & ANALYZER
 KEUFEL & ESSER CO. MADE IN U.S.A.

1%



MSS
 BAND

4

5

6

7

Figure 51. "Grey-water" V-V_s Reflectivity.

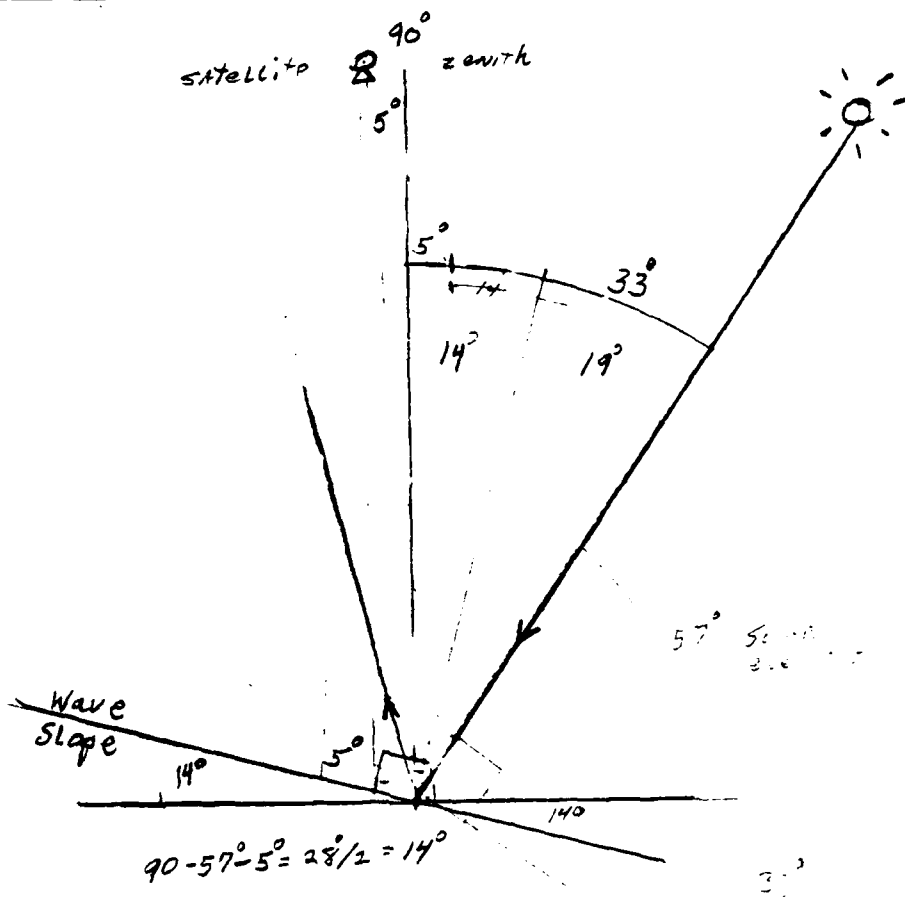


Figure 52. Illustrating Estimate of Wave Slope Necessary for Specular Reflection.

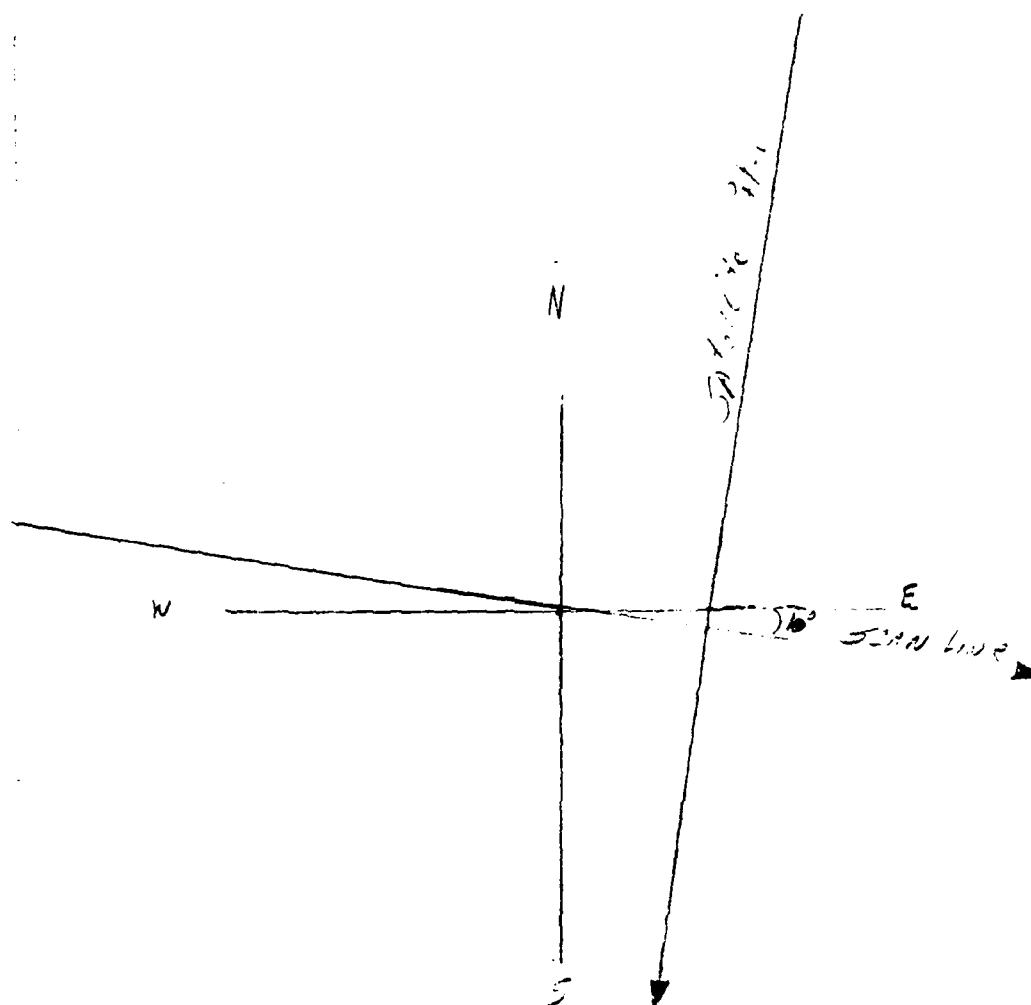


Figure 53, Scan Line Orientation to Geographic Directions.

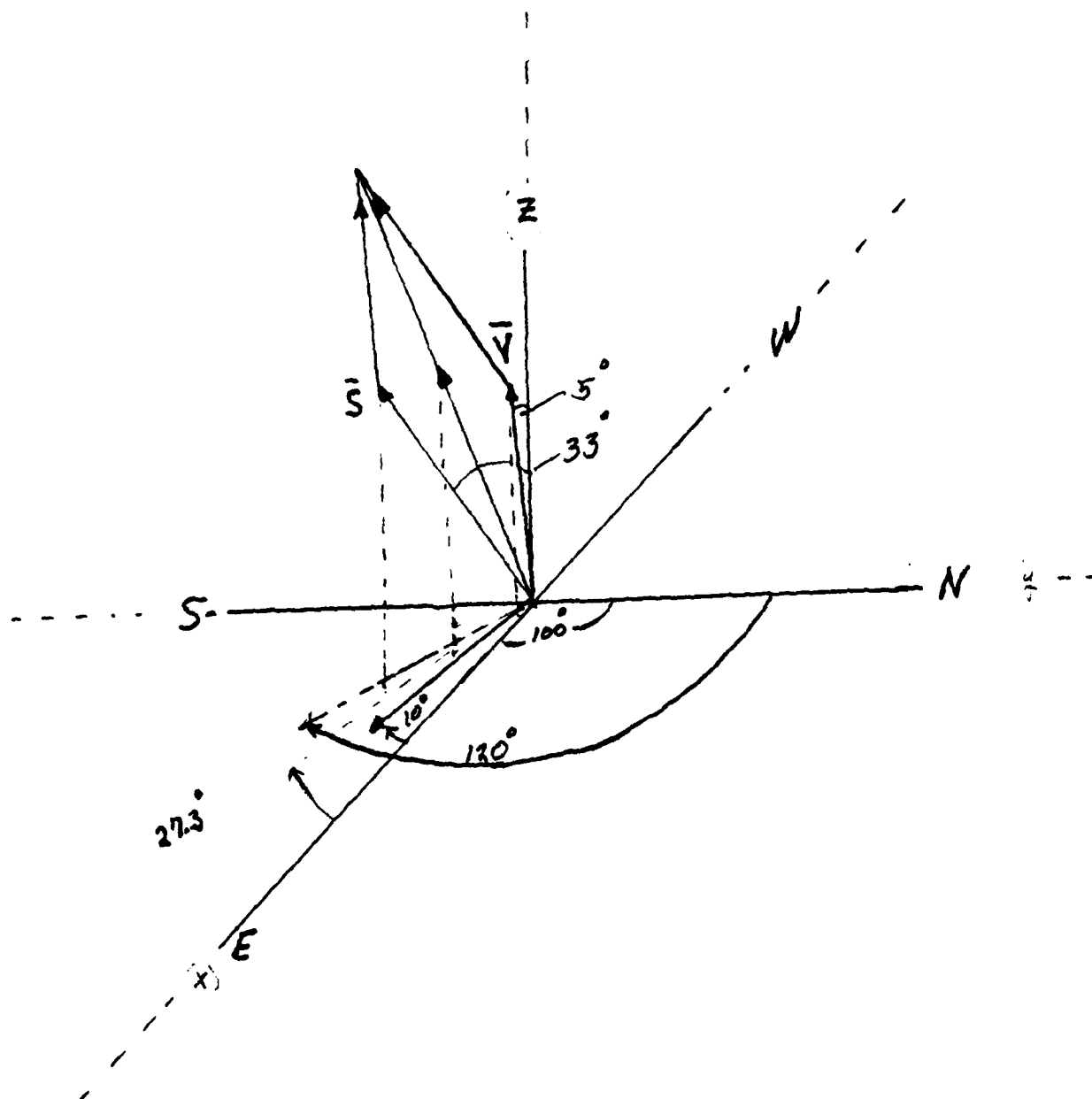


Figure 54. Three Dimensional Illustration of Unit Vector Solution.

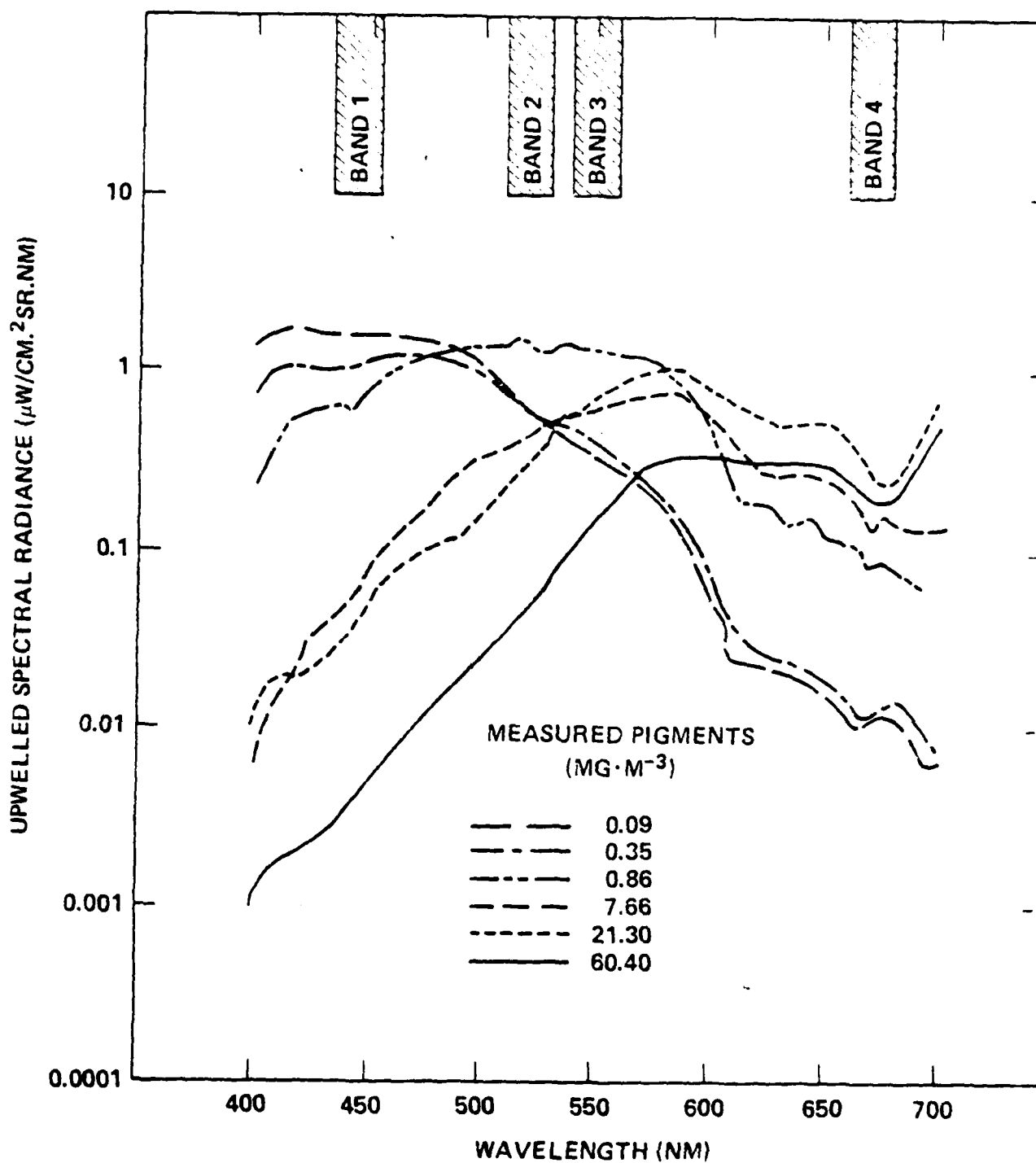


Figure 55. Upwelling Spectral Radiance from Phytoplankton.

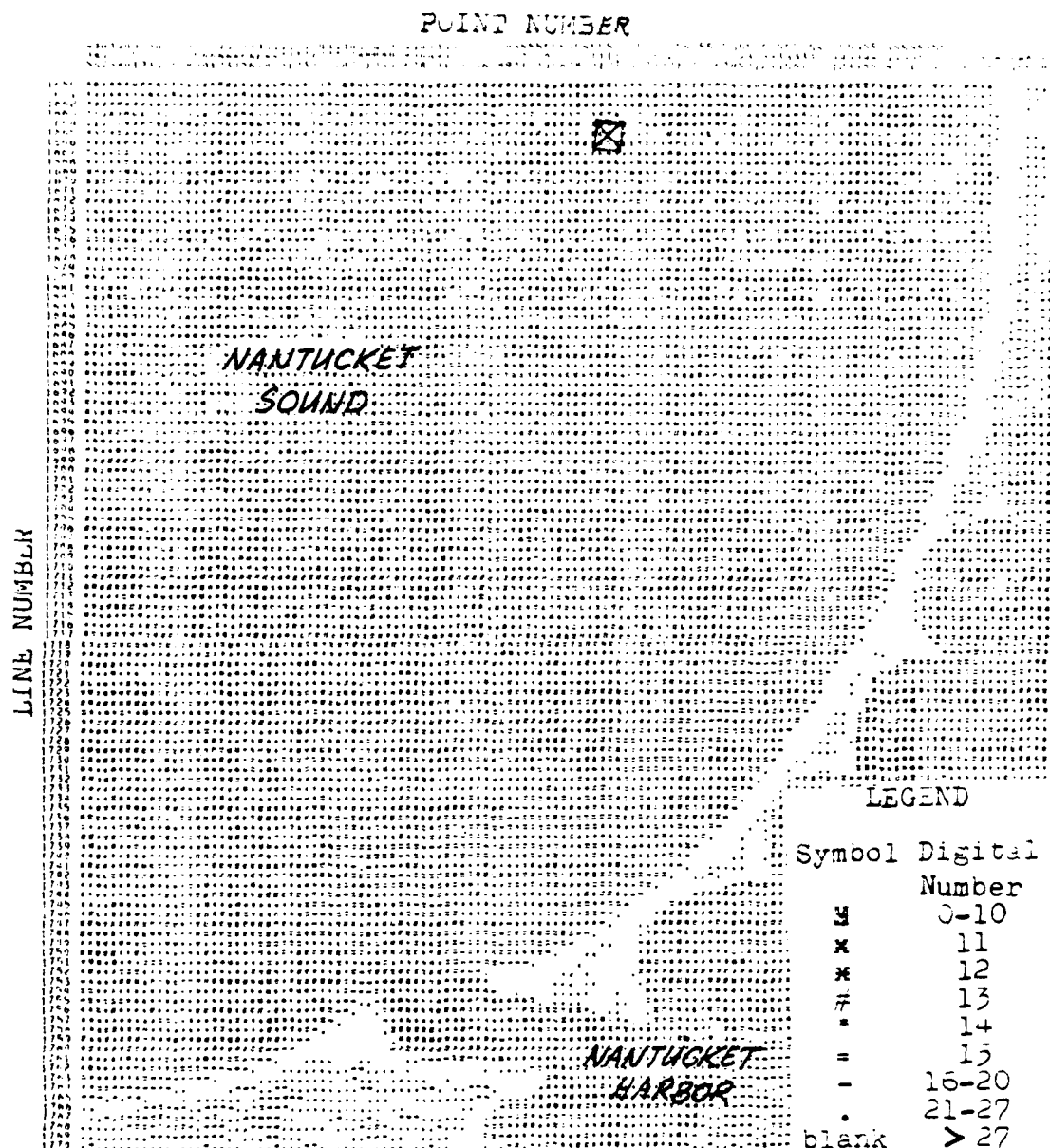


Figure 56. "Grey-Map" MSS, Nantucket Sound.

10%

46 5493

1%

.01%

K-E SEMI LOGARITHMIC PAPER
KEUFFEL & ESSER CO. MADE IN U.S.A.

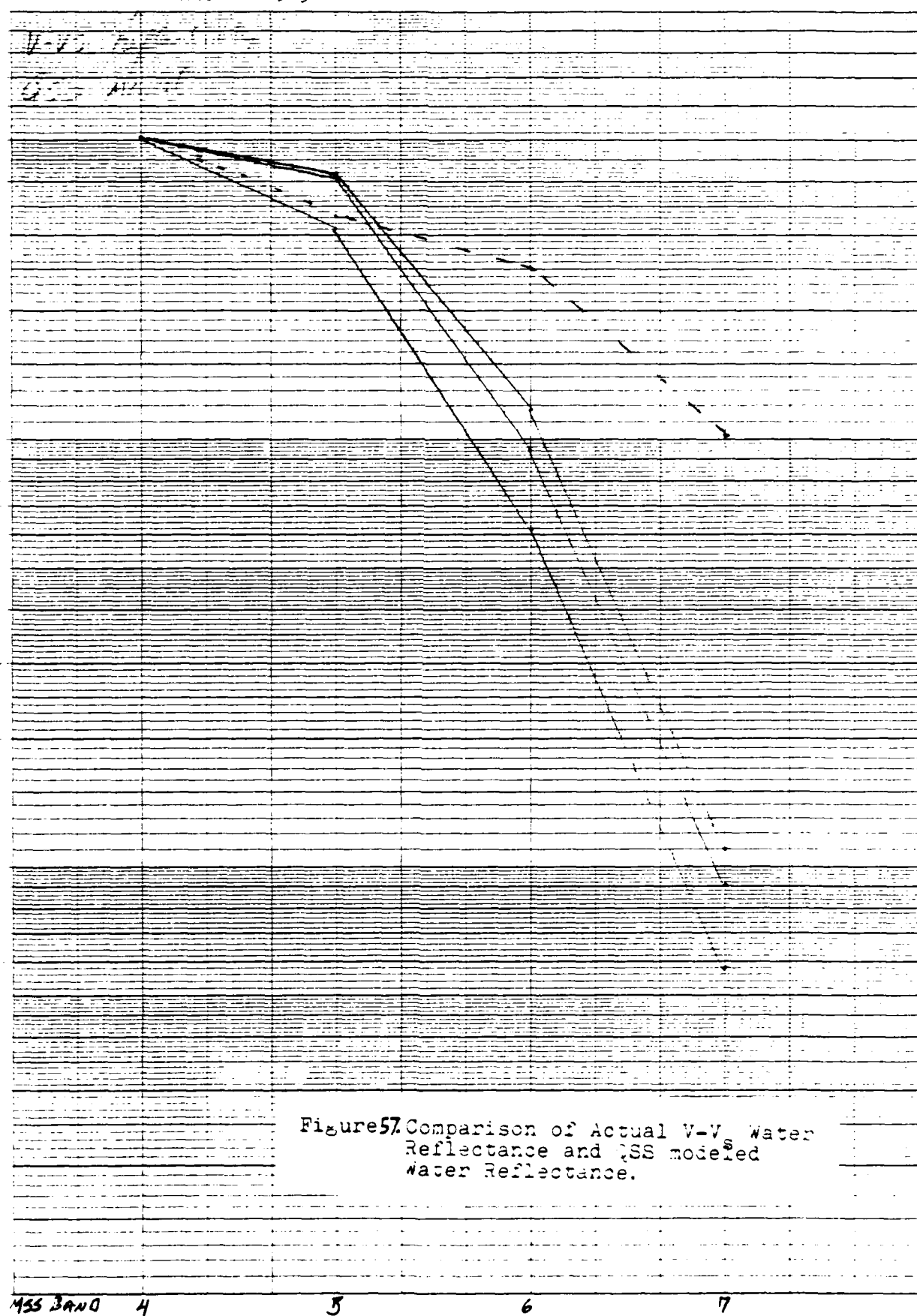
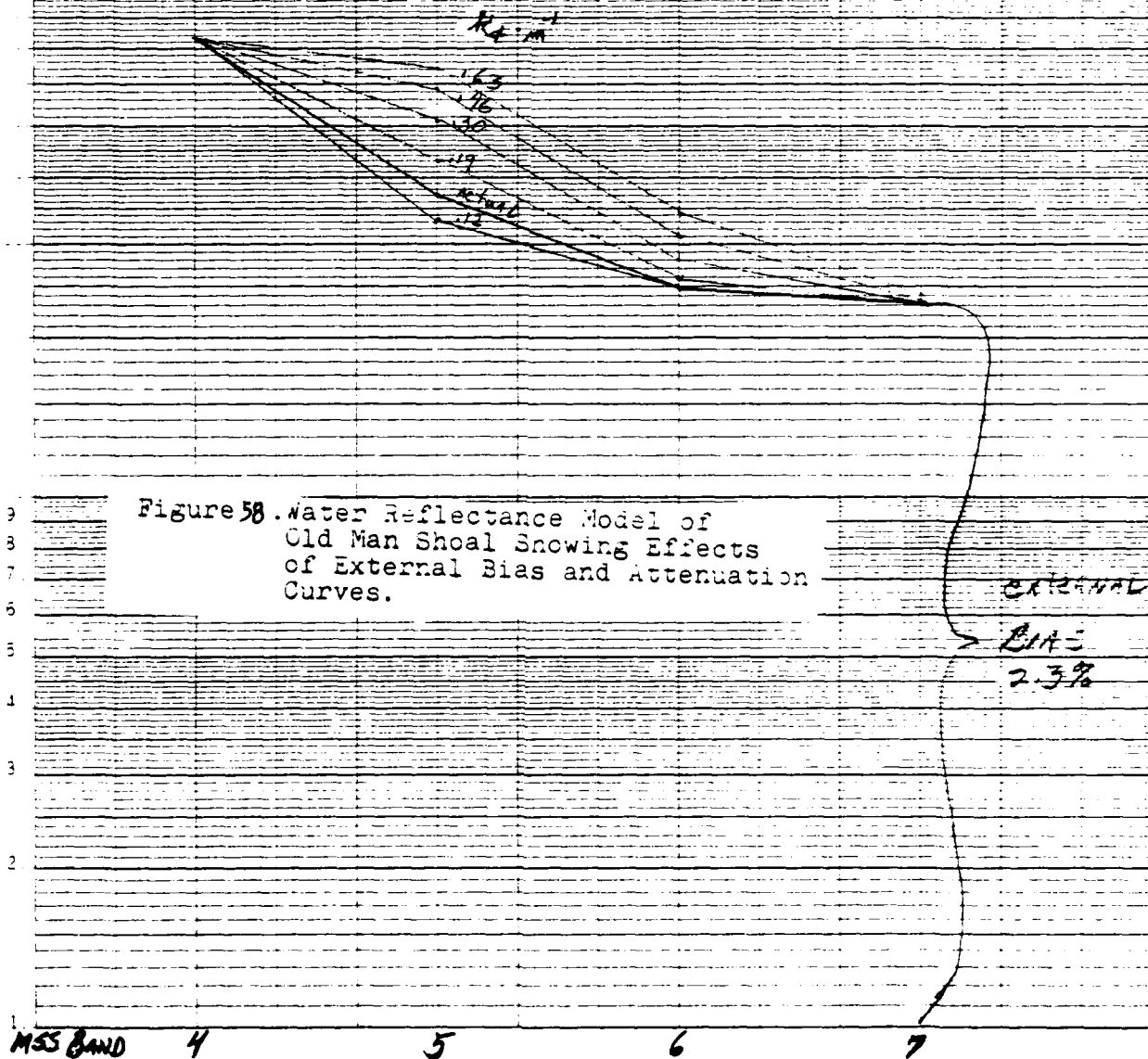


Figure 57. Comparison of Actual V-V Water Reflectance and JSS modeled Water Reflectance.

Reflectivity MSS BAND 4
BAND 5
BAND 6
BAND 7

OLD MAN Shoal QJS Model
LINE 1749 BIAS 2.3% reflectivity V-Vs
Point 221
STOP 2



46 5493

K-E DATA LOGARITHMIC SCALE, 100 DIVISIONS
NEUTEL & ESSER CO. MADE IN U.S.A.

POINT

LEGEND

Symbol	Digital Number
E	0-9
x	10
*	11
#	12
.	13
=	14
-	15
.	16
blank	17

LINE

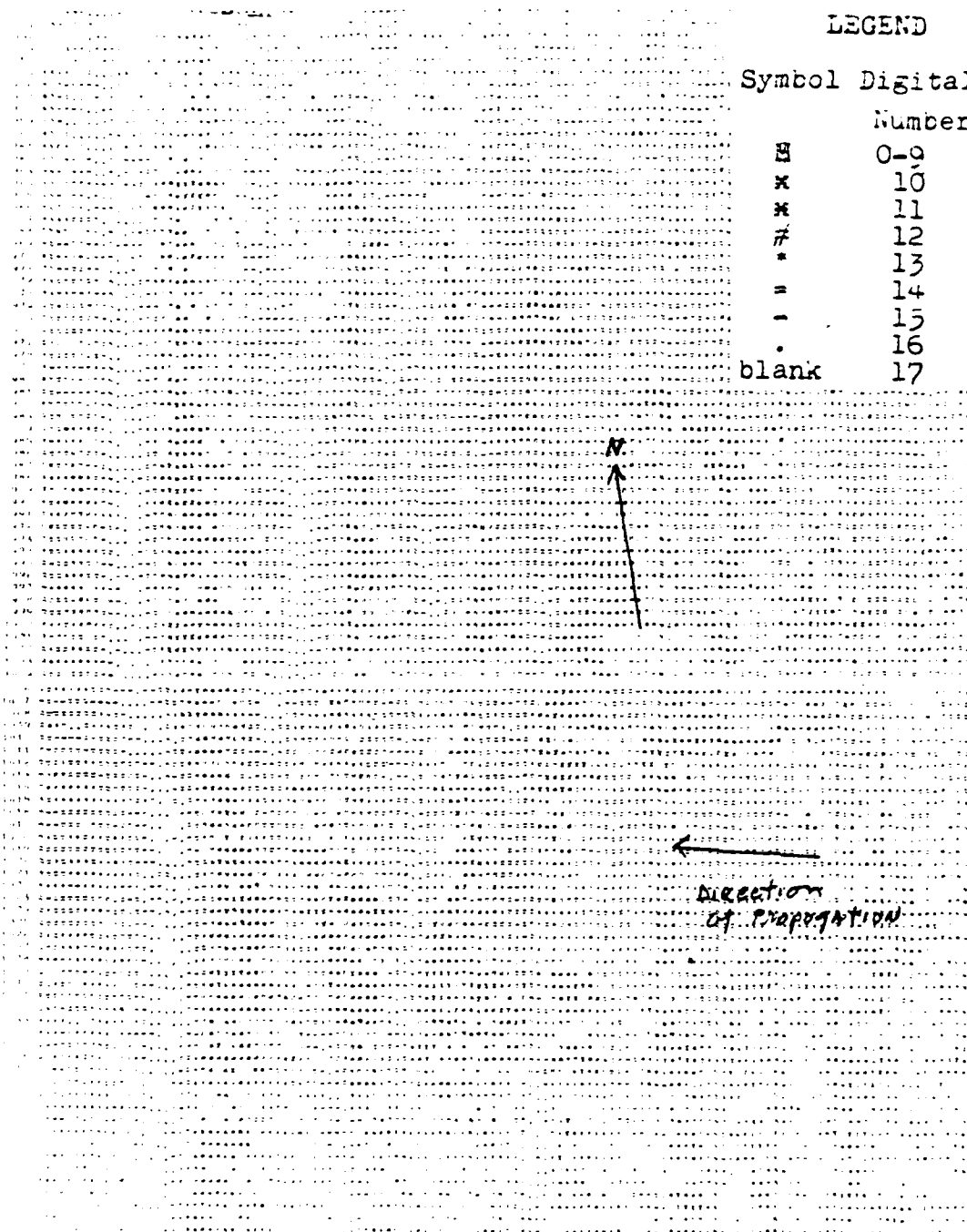


Figure 59. "Grey-Map" MSS5 Surface Manifestation of Internal Waves.

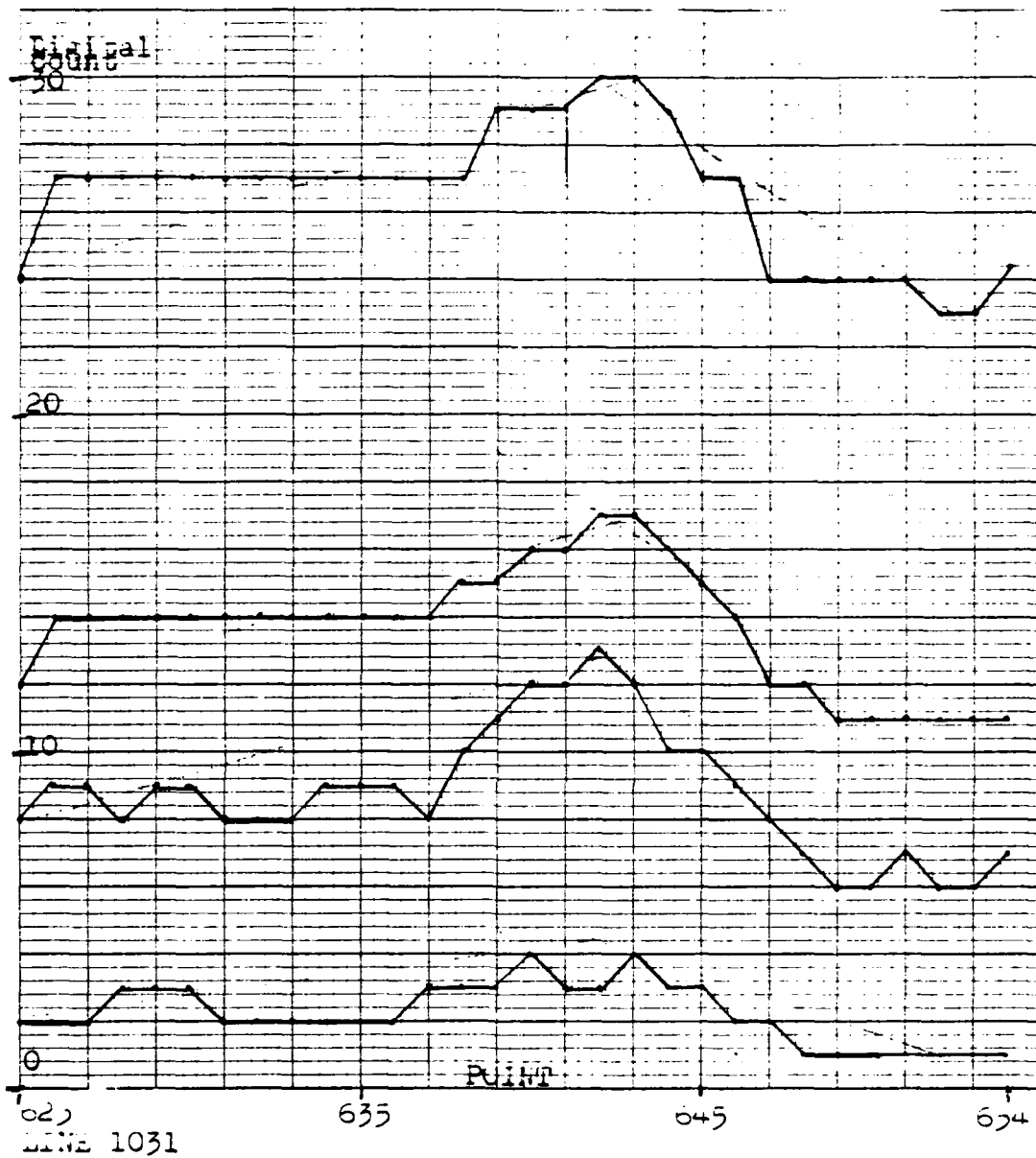


Figure 60 Digital Number in Each MSS Band Across a Surface Manifestation of Internal Wave (Line 1031, Points 625-654).

TABLE 1. CHARACTERISTICS OF IMAGERY UTILIZED IN STUDYING HYDROGRAPHIC FEATURES OFF CAPE COD

SPACECRAFT	LST**	SENSOR	DATE	ELEVATION	AZIMUTH	IMAGE ID	FILM AND BAND	REMARKS
Skylab-3 ERBP (Earth Resources Experiment Package)	1333	S-190A 6-lens camera	12 Sep 73	52°	205°	SI-3-37-131	B&W IR (.7-.8 μ m)	Some cloudiness over Martha's Vineyard, western Cape Cod, and extreme eastern part of South Wellfleet
						SI-3-38-131	B&W IR (.8-.9 μ m)	
						SI-3-39-131	Color IR (.5-.88 μ m)	Ships' wakes clearly visible
						SI-3-40-131	Color (.4-.7 μ m)	
						SI-3-41-131	Panchromatic (.6-.7 μ m)	
Skylab-3	1333	S-190B	12 Sep 73	52°	205°	SI-3-42-132 sequential frames (.5-.6 μ m)	Panchromatic sequential frames (.5-.6 μ m)	Sequence shows evidence of sunlight revealed by change of view angle
						SI-3-42-133 sequential frames (.5-.6 μ m)	Panchromatic sequential frames (.5-.6 μ m)	
						SI-3-42-134 sequential frames (.5-.6 μ m)	Panchromatic sequential frames (.5-.6 μ m)	
						SI-3-86-313	Color (.4-.7 μ m)	
						SI-3-86-314	Color (.4-.7 μ m)	
Landsat-1	0953	MSS	13 Dec 73	21°	154°	1508-14530	4,5,6,67	Partially cloudy southern edge
Landsat-1	0947	MSS	17 July 74	57°	122°	1724-14470	5*	Vivid examples of hydrographic features/"shoal" pattern in all 4 bands, shows "edge" of "shoal" when wind direction is 20°
Landsat-1	0947	MSS	17 July 74	57°	120°	1724-14472	4,5,6,67*	Print shows turbidity along Race Point and estuaries; "shoal" pattern in all 4 bands
Landsat-1	0947	MSS	17 July 74	58°	117°	1724-14475	5*	
Landsat-2	0944	MSS	22 Apr 75	51°	131°	2090-14441	4*	

TABLE 1. (cont.)

SPACECRAFT	LST	SENSOR	DATE	ELEVATION	AZIMUTH	IMAGE ID	FILM AND BAND	REMARKS
Landsat-2	0944	MSS	28 May 75	58°	121°	2126-14440	4*	Shows "edge" of "shoal" feature when wind direction is 330°
Landsat-1	0942	MSS	6 Nov 75	27°	152°	2288-14423	4, 5, 6, 67*	
Landsat-1	0912	MSS	13 May 76	51°	115°	5390-14124	4, 5, 6, 67*	"Shoal" patterns visible in all 4 bands
Landsat-2	0936	MSS	11 Apr 77	45°	128°	2810-14265	4, 5, 6, 67*	Con-trail and shadow visible
Landsat-3	0943	MSS	9 Mar 78	35°	139°	30004-14435	4, 5, 6, 67*	Calm - no wind - no "shoal" patterns. Shows breach of Monomoy Island
Landsat-2	0927	MSS	21 Oct 78	31°	145°	21368-14275	4, 5, 6, 67*	"Shoal" patterns reappear
Landsat-3	0943	RBV	9 Mar 78	35°	139°	30004-14435	A, B, C, 6D (.505 μ m to .750 μ m)	Camera affects visual - mottled in D&R
Landsat-3	0943	RBV	15 Apr 78	49°	132°	30041-14433	A, B, C, 6D (.505 μ m to .750 μ m)	"flare effect" in C on lower edges, resolution increased to 40 meters
Landsat-3	0944	RBV	19 Aug 78	51°	129°	30167-14444	A, B, C, 6D (.505 μ m to .750 μ m)	
Seasat-A Synthetic Aperture Radar	0743	Microwave	27 Aug 78	---	---	Rev 808	23.5 cm. (1-Band)	Shows "shoal" pattern also visible in microwave

* Wave lengths of Landsat MSS bands are as follows: band 4, .5-.6 μ m; band 5, .6-.7 μ m; band 6, .7-.8 μ m; and band 7, .8-1.1 μ m)

** Local Standard Time

TABLE 2. SELECTED WEATHER DATA FOR DATES OF IMAGE ACQUISITION
(see Table 1)

Date	Lat N	Long W	Local Time	Direction	Speed	Visibility N. Miles	SWELL		Direction	WIND WAVES	
							Period In Seconds	Height In Meters		Period In Seconds	Height In Meters
12 Sep 73	40.50N 41.40.3 41.17	069.40W 069.57 070.06	1330	300 ESE 260	4 kn 4 kn 12 kn	5-10 8 12	5	0.6	310	5	0.9 Nantucket Lightship Chatham Coast Guard Nantucket Tower
13 Dec 73	40.50 41.40.3 41.17	069.40 069.57 070.06	0953	010 00	2 kn calm 00 kn	5-10 15 12	calm 00	00	020	5	0.6 Nantucket Lightship Chatham Coast Guard Nantucket Tower
17 Jul 74	40.50 41.40.3 41.17	069.40 069.57 070.06	0947	330 NNW 20	3 kn 10 kn 14 kn	5-10 10 12	calm 00	00	330	5	0.6 Nantucket Lightship Chatham Coast Guard Nantucket Tower
22 Apr 75	40.30 41.40.3 41.17	069.28 069.57 070.06	0944	270 WSW 360	18 kn 10 kn 13 kn	25 10 12	05	1.5	230	5	2.1 Nantucket Lightship Chatham Coast Guard Nantucket Tower
28 May 75	41.40.3 41.17	069.57 070.06	0944	130 WSW 330	8 kn 6 kn 15 kn	25 5-10 12	05	0.6	140	5	0.6 Nantucket Lightship Chatham Coast Guard Nantucket Tower
6 Nov 75	41.40.3 41.17	069.57 070.06	0942	030 NNE 00	8 kn 5 kn 0 kn	25 10 15	00	00	020	5	0.9 Nantucket Lightship Chatham Coast Guard Nantucket Tower
13 May 76	40.30 41.40.3 41.17	069.28 069.57 070.06	0912	320 W 280	12 kn 12 kn 6 kn	25 10 15	00	00	280	5	0.9 Nantucket Lightship Chatham Coast Guard Nantucket Tower
11 Apr 77	40.30 41.40.3 41.17	069.28 069.57 070.06	0926	090 E 00	10 kn 10 kn 0 kn	25 06 15	00	00	050	5	0.6 Nantucket Lightship Chatham Coast Guard Nantucket Tower
9 Mar 78	40.30 41.40.3 41.17	069.28 069.57 070.06	0943	320 WNW 00	2 kn 2 kn 0 kn	25 or more 10 25	---	---	270	5	0.3 Nantucket Lightship Chatham Coast Guard Nantucket Tower
15 Apr 78	40.30 41.40.3 41.17	069.28 069.57 070.06	0943	040 NW 310	24 kn 20 kn 10 kn	2 to 5 10 15	5	1.5	010	5	1.5 Nantucket Lightship Chatham Coast Guard Nantucket Tower
19 Aug 78	40.30 41.40.3 41.17	069.28 069.57 070.06	0944	180 NNE 360	4 kn 10 kn 10 kn	5 to 10 10 10	---	---	080	4	0.6 Nantucket Lightship Chatham Coast Guard Nantucket Tower
21 Oct 78	40.50 41.40.3 41.17	069.50 069.57 070.06	0927	300 WSW 00	6 kn 12 kn 0 kn	5 to 10 08 15	02	0.6	350	5	0.3 Nantucket Lightship Chatham Coast Guard Nantucket Tower
27 Aug 78	40.30 41.40.3 41.17	069.28 069.57 070.06	0714	260 WSW 10	12 kn 10 kn 8 kn	25 8 15	5	0.6	100	5	0.6 Nantucket Lightship Chatham Coast Guard Nantucket Tower
Jan 5, 6, 8 7, 78 Feb 5, 6, 8 7, 78	40.50 Blizzards	069.50	Variable	Variable	10 kn 80 kn peak	5 to 10	Variable	1.2-2.4	Variable	Variable	3.3 Peak Wave Height 5.6 meters Nantucket Lightship

TABLE 3. TIDAL SUMMARY FOR NANTUCKET ON DATES OF
IMAGERY ACQUISITION (See Table 1)

Date	LST**		Height in Feet Above Mean Low Tide
13 Dec 73	0953	Flood	4.9 (1.5 m)
17 Jul 74	0947	Ebb	7.6 (2.3 m)
22 Apr 75	0944	Ebb	7.1 (2.2 m)
28 May 75	0944	Flood	4.4 (1.3 m)
6 Nov 76	0942	Flood	6.3 (1.9 m)
13 May 76	0912	Ebb	6.4 (1.9 m)
11 Apr 77	0926	Flood	2.5 (0.8 m)
9 Mar 78	1104	Flood	7.8 (2.4 m)
15 Apr 78	0943	Ebb	6.3 (1.9 m)
19 Aug 78	0944	Flood	9.3 (2.8 m)

* Time of tides calculated from Observatory Station Data, Boston,
Massachusetts

** Local Standard Time

TABLE 4. TIDAL CURRENT DATA AT POLLOCK RIP CHANNEL ON DATES OF IMAGE ACQUISITION
(see Table 1)

Date	LSW**	Direction	Current	Wind Speed*	Direction	
13 Dec 73	0953	012°	true	0.7 kn	subdued feature	00 kn 00° transparencies
17 Jul 74	0947	125°	true	0.6 kn	bright feature	14 kn 330° print printed dark
22 Apr 75	0944	157°	true	0.7 kn	subdued feature	13 kn 00° print printed dark
28 May 75	0944	358°	true	0.8 kn	bright feature	15 kn 330° print printed dark
6 Nov 75	0942	011°	true	0.8 kn	bright feature	00 kn 00° print printed light
13 May 76	0912	205°	true	0.6 kn	subdued feature	06 kn 280° print printed dark
11 Apr 77	0926	221°	true	0.8 kn	subdued feature	00 kn 00° print printed dark

* Tidal current data Pollock Rip Channel measured by NOAA

** Local Standard Time

TABLE 5. PERCENTAGE OF INCREASED RADIANCE COMPARED TO
SOLAR IRRADIANCE

Landsat MSS Band	$V-V_s(L)$ Radiance $\text{mw/cm}^2\text{sr}$	% $(V-V_s)$ Radiance (L)	(E_0) Irradiance $\text{mw/cm}^2\text{sr}$	% (E_0) Irradiance
4	.0848242	22.430	8.1099	22.777
5	.0811401	21.455	7.5669	21.252
6	.0710987	18.800	6.4588	18.140
7	.1411167	37.315	13.470	37.831
	<hr/>	<hr/>	<hr/>	<hr/>
Total:	.3781797	100	35.6056	100

TABLE 6. SLOPE OF DIGITAL NUMBER TO LINEAR PIXEL POSITION
FOR SURFACE MANIFESTATIONS OF INTERNAL WAVE

Landsat MSS Band	Westward Slope	Eastward Slope
4	35°	20°
5	31°	16°
6	34°	16°
7	20°	10°

REFERENCES CITED

- Anonymous, "Blizzard '78", Boston Sunday Globe (a special 24 page section), pp. 2-24, Sunday, 19 February 1978.
- Anonymous, Landsat Newsletter, No. 15, National Aeronautics and Space Administration (NASA), Goddard Space Flight Center, Mission Utilization Office, Greenbelt, Maryland, p. 2, 1 June 1977.
- Anonymous, Ye Ancient Wrecke 1626, Loss of the Sparrow-Hawk in 1626, Alfred Mudge and Son, Boston, Massachusetts, p. 41, 1865.
- Apel, J.R., Charnell, R.L., and Blackwell, R.J., "Ocean Internal Waves off the North American and African Coasts from ERTS-1," Proceedings of 9th Symposium on Remote Sensing of the Environment, Atlantic Oceanographic and Meteorological Laboratories, National Oceanic Atmospheric Administration (NOAA), Miami, Florida, pp. 1345-1351, 1975.
- Apel, J.R., Byrne, M.H., Proni, J.R., and Sellers, R., "A Study of Oceanic Internal Waves using Satellite Imagery and Ship Data," Remote Sensing of the Environment, Vol. 5, American Elsevier Publishing Company, Inc. New York, New York, pp. 125-135, 1976.
- Bothner, M.H., Parmenter, C.M., and Milliman, J.D., Temporal and Spatical Variations in Suspended Matter in Continental Shelf and Slope Waters off the Northeastern United States: Georges Bank and Vicinity (preliminary copy), U.S. Geological Survey and Woods Hole Oceanographic Institution, Woods Hole, Massachusetts, p. 50, 1980.
- Brown, W.L., Polcyn, F.C., Sillman, A.N., and Stewart, S.R., Water Depth Measurement by Wave Refraction and Multispectral Techniques, Report No. 31650-31-T, Willow Run Laboratories, Willow Run, Michigan, p. 43, 1971.
- Bush, Donna, NOAA, National Marine Fisheries Service, Narragansett, Rhode Island, Personal Communication, 22 October 1979.
- Chance, J.E., Professor of Mathematics, Pan American University, Eidenberg, Texas, Personal Communication, 7 February 1980.
- Colvocoresses, A.P., U.S. Geological Survey, Memorandum for Record, Subj: Radiometric Discrepancies in Landsat-2 Tapes and Images (EC-52, Landsat), p. 2, 18 May 1977.

- Cowell, R.N., Brewster, W., Landis, G.W., Langley, P., Morgan, J., Rinker, J., Robinson, J.M., and Sorem, A.L., "Basic Matter and Energy Relationships in Remote Reconnaissance," Photogrammetric Engineering, Vol. 29, pp. 761-799, 1963.
- Cox, C.S. and Munk, W.H., "Measurement of the Roughness of the Sea Surface from Photographs of the Sun's Glitter," Journal of Optical Society of American, Vol. 44, pp. 838-850, 1954.
- Cramer, S.D., Jr. (Vice Admiral), "Challenges," Proceedings 41st Annual American Society of Photogrammetry, pp. 9-14, March 1975.
- Dawson, James, "Ancient Charts and Modern Mariners," Marine Geodesy, Vol. 4, No. 2, Crane, Russack, and Company Inc., pp. 113-119, 1980.
- Denoyer, John, M., U.S. Geological Survey, Letter to Rick Scudder, Office of Environmental Control, p. 3, 25 November 1979.
- Doak, E.L., Lyzenga, D.R., and Polcyn, F.C., Remote Bathymetry by Landsat in the Chagos Archipelago, Environmental Research Institute of Michigan (ERIM), Interim Technical Report 135900-1-T, Ann Arbor, Michigan, p. 41, April 1979.
- Duntley, S.Q., Austin, R.W., Wilson, W.H., Edgerton, C.F., Moran, S.E., Ocean Color Analysis (final technical report to Naval Research Laboratory (NRL) and NOAA), University of California, San Diego, Scripps Institute of Oceanography Visibility Laboratory, San Diego, California, p. 73, 1974.
- Francis, Keith and Reed, Charles, Bottom Reflectance Variations and their Contribution to Water Depth (Calculations), Class Project Eastern Michigan University, Geography 505, ERIM, Ann Arbor, Michigan, p. 53, 1979.
- Fricke, Peter and Maiolo, John, "Public Knowledge and Perceptions of the Effects of the Argo Merchant Oil Spill," In the Wake of the Argo Merchant (Proceedings of a symposium held January 11-13, 1978), Center for Management Studies, University of Rhode Island, p. 181, August 1978.
- Gordon, H.R., "Simple Calculation of the Diffuse Reflectance of the Ocean," Applied Optics, Vol. 12, No. 12, pp. 2803-2804, December 1973.
- Green, Arthur (Captain), Listing of Shipwreck File for Cape Cod Area, Defense Mapping Agency Hydrographic/Topographic Center (DMAHTC), Washington, D.C., 1979.

- Gutman, A.L., Goetz, M.J., Brown, F.D., Lentowski, J.F., and Tiffney, W.N., Nantucket Shoreline Survey an Analysis of Nantucket Shoreline Erosion and Accretion Trends since 1846, Massachusetts Institute of Technology (MIT) Sea Grant College Report, MITSG 79-7, Cambridge, Massachusetts, p. 51, 1979.
- Hammack, J.C., "Landsat Goes to Sea," Photogrammetric Engineering and Remote Sensing, Vol. 43, No. 6, pp. 683-691, 1977.
- Hovis, W.A., NOAA, National Environmental Satellite Service (NESS), Washington, D.C., "NIMBUS-7 Coastal Zone Color Scanner: System Description and Initial Imagery" (Submitted to Science for publication), p. 14 and Personal Communication, 21 March 1980.
- Jerlov, N.G., Marine Optics, Elsevier Publishing Company, Amsterdam, Netherlands, p. 231, 1976.
- LaFond, E.C., and Cox, C.S., "Internal Waves (Part 1)," The Sea (Hill, M.N., ed.), Vol. 1, Interscience, New York, New York, pp. 731-763, 1962.
- Leonard, J.E., Fisher, J.J. (and other contributing authors), Coastal Geology and Geomorphology of Cape Cod; An Aerial and Ground View. (Geology of Southeastern New England, A Guidebook for Field Trips to the Boston Area and Vicinity, Barry Cameron, ed.), Science Press, Princeton, New Jersey, pp. 224-264, 1976.
- Limeburner, Richard, Physical Oceanographer, Woods Hole, Massachusetts, Personal Communication, 27 September 1979.
- Lyzenga, D.R., Research Scientist, Applications Division, ERIM, Ann Arbor, Michigan, Personal Communication, 20 May 1980.
- Lyzenga, D.R., and Polcyn, F.C., Techniques for the Extraction of Water Depth Information from Landsat Digital Data, ERIM, Final Report No. 129900-1-F, Ann Arbor, Michigan, p. 57, March 1979.
- Maul, G.A., and Gordon, H.R., "On the Use of Earth Resources Technology Satellite (Landsat-1)," Optical Oceanography, Remote Sensing of the Environment, Vol. 4, pp. 95-128, 1975.
- McCave, I.N., "Sand Waves in the North Sea off the Coast of Holland," Marine Geology, Vol. 10, pp. 199-225, 1971.
- Melham, Thomas, "Cape Cod's Circle of Seasons," National Geographic, Vol. 148, No. 1, Washington, D.C., pp. 40-65, July 1975.
- Milgram, J.H., Being Prepared for Future Argo Merchants, MIT Sea Grant Program Report No. MITSG 77-10, Cambridge, Massachusetts, pp. 15-27, April 1977.

- Naval Environmental Prediction Research Facility (NEPRF), Environmental Phenomena and Effects, Vol. 2, Navy Tactical Applications Guide, Defense Meteorological Satellite Program (DMSP), Monterey, California, p. 159, 1979.
- Neumann, Gerhard, and Pierson, Willard, Jr., Principles of Physical Oceanography, Prentis-Hall Inc., Englewood Cliffs, New Jersey, p. 295, 1966.
- Oldale, R.N., Friedman, J.D., and Williams, R.S., Jr., "Changes in Coastal Morphology of Monomoy Island, Cape Cod, Massachusetts," Geological Survey Research 1971, U.S. Geological Survey Professional Paper 750-B, pp. B101-B107, 1971.
- Olson, C.E., Jr., "The Energy Flow Profile in Remote Sensing," Proceedings of 2nd SRSE, 1st Rept. 4864-3-X, pp. 187-199, 1962.
- Onysko, Steven, Chatham Bars Inlet (A Review of the Historical Migration of the Inlet and Proposed Alternatives for Navigation Improvement), U.S. Army Corps of Engineers, New England Division, Massachusetts, 1978.
- Phaneuf, Wayne, "Coast Resorts Race to Rebuild in Time for Tourist Onslaught," Boston Daily News, p. 6, Monday, 6 March 1978.
- Polcyn, F.C., NASA/Cousteau Ocean Bathymetry Experiment, ERIM, Report No. 118500-1-F, Ann Arbor, Michigan, p. 127, 1976.
- Polcyn, F.C., Lyzenga, D.R., and Tanis, F.J., Demonstration of Satellite Bathymetric Mapping, ERIM, Report No. 122200-1-F, Ann Arbor, Michigan, p. 43, January 1977.
- Portney, John, U.S. National Park Service, Cape Cod National Seashore, South Wellfleet, Massachusetts, Personal Communication, 28 September 1979.
- Rea, D.K., Class notes and Personal Communication from AOS405, Survey of Geological Oceanography, University of Michigan, Ann Arbor, Michigan, 18 October 1979.
- Ryder, Robert, Cape Cod Fisherman and boat owner, Chatham, Massachusetts, Personal Communication (also interview for National Geographic article, see Melham, 1975), 25 September 1979.
- Sawyer, C. and Apel, J.R., Satellite Images of Ocean Internal Wave Signatures, Atlantic Oceanographic and Meteorological Laboratories, Miami, Florida, Published by NOAA, Environmental Research Laboratories (ERL), p. 17, September 1976.
- Shepard, F.P., Trefethen, J.M., and Cohee, G.V., "Origin of Georges Bank," Geological Society of America Bulletin, Vol. 45, pp. 281-302, 1934.

Short, N.M., Lowman, P.D., Jr., Freden, S.C., Finch, W.A., Jr., Mission to Earth: Landsat Views the World, NASA SP-360, U.S. Government Printing Office, Washington, D.C., p. 459, 1976.

Shuchman, R.A., Research Scientist, Radar and Optics Division, ERIM, Personal Communication, 1980.

Stewart, H.B., Jr., and Jordan, G.F., "Underwater Sand Ridges on Georges Shoal," Papers in Marine Geology, Shepard Commemorative Volume (R.L. Miller, ed.), MacMillian Company, New York, New York, pp. 102-114, 1964.

Strahler, A.N., A Geologist's View of Cape Cod, American Museum of Natural History, the National History Press, Garden City, New Jersey, p. 115, 1966.

Swift, D.J.P., "Sand Ridges of Nantucket: Relation of Topography to Flow," (a proposal for study), NOAA, Atlantic Marine Geophysical Laboratories, Miami, Florida, p. 8, 11 December 1978.

Taranik, J.V., Characteristics of the Landsat Multispectral Data System, U.S. Department of Interior, Geological Survey, Open File Report 78-187, Souix Falls, South Dakota, p. 76, January 1978.

Tisdall, Tracey and El-Baz, Farouk, "Analysis of Water Color as Seen in Orbital and Aerial Photographs of Cape Cod, Nantucket, and Martha's Vineyard, Massachusetts," Apollo-Soyuz Test Project, Vol. II (Farouk El-Baz and D.M. Warner, eds.), NASA SP-412, pp. 531-543, December 1979.

Turner, R.E., "Radiative Transfer on Real Atmospheres," ERIM Report No. 190100-24-T, Ann Arbor, Michigan, p. 107, 1974.

U.S. Defense Mapping Agency Hydrographic/Topographic Center, "Sea State," American Practical Navigator, Vol. 1 (Bowditch), Pub. No. 9, p. 1386, 1977.

_____, "Internal Waves," American Practical Navigator, Vol. 1 (Bowditch), Pub. No. 9, p. 1386, 1977.

Williams, R.S., Jr., "Delineation of Recent Changes in the Coastline of Monomoy Island, Cape Cod, Massachusetts with Landsat-3 Images (MSS and RBV)," Proceedings of American Society of Photogrammetry 45th Annual Meeting, Vol. 1, Washington, D.C., pp. 290-291, 18-24 March 1979.

Wolfe, W.L., and Zissis, G.L., eds., The Infrared Handbook, ERIM (for the Office of Naval Research), Department of the Navy, U.S. Government Printing Office, Washington, D.C., p. 1711, 1978.

AD-A102 343

DEFENSE MAPPING AGENCY HYDROGRAPHIC/ TOPOGRAPHIC CENT--ETC F/G 8/10
INTERPRETATION OF HYDROGRAPHIC FEATURES SEEN IN THE WATERS OFF --ETC(U)
MAY 81 C L REED

UNCLASSIFIED

NL

3 OF 3

AD-A
102 343



END
DATE
FILMED
8-81
DTIC

Wright, D.R., Physical Oceanographer, National Marine Fisheries Service,
Woods Hole, Massachusetts, Personal Communication, 22 October 1979.

**NU
DATE
ILME**